UNIVERSITY OF CALIFORNIA

SANTA CRUZ

**INVESTIGATING THE CELLULAR PRION PROTEIN'S METAL DRIVEN *CIS* INTERACTION**

A dissertation submitted in partial satisfaction
of the requirements for the degree of

DOCTOR OF PHILOSOPHY

in
CHEMISTRY
by

**Kathleen A. Markham**

December 2018

The Dissertation of Kathleen A. Markham
is approved:

_____
Professor Theodore Holman, Chair

_____
Professor Glenn Millhauser, Advisor

_____
Professor Michael Stone

_____
Lori Kletzer
Vice Provost and Dean of Graduate Studies

**TABLE OF CONTENTS**

**TABLE OF FIGURES**

## TABLES

**Abstract**

Investigating the Cellular Prion Protein's Metal Driven *cis* Interaction

Kathleen A. Markham

The cellular prion protein ($PrP^C$) undergoes an N-C interdomain interaction upon the addition of endogenous metal ligands. Studies demonstrated that the octarepeat domain coordinates copper or zinc, which elicits this interdomain contact termed *cis* interaction. What is unclear is if physiologically relevant N-terminal segments are assisting in $PrP^C$'s *cis* interaction. These N-terminal segments have been shown to play a potentially significant role in the function and regulation of the cellular prion protein. While full knockdown of $PrP^C$ in mice is relatively benign, the deletion of an internal 21 amino acid stretch, known as ΔCR, produces neonatal lethal toxicity. The polybasic tail, $_{23}KKRPKPGGW_{31}$, has been shown to associate with ionotropic membrane receptors and is essential for ΔCR toxicity. Through the use of $^{15}N$-$^{1}H$ HSQC NMR, LC-MS/MS, and electrophysiology studies, our findings indicated that both the polybasic tail and central region are essential components in assisting the *cis* interaction. Additionally, elimination of the positive charge on the polybasic tail reduces the measured *cis* interaction, which indicates that the cis interaction is partially assisted through electrostatics. Furthermore, $^{113}Cd$, $^{2}J_{NH}$, and $^{15}N$-$^{1}H$ HSQC NMR were employed to investigate $PrP^C$'s octarepeat domain when complexed with diamagnetic metal ions. These results provided detailed information about the

coordination sphere for $Zn^{2+}$ that had been previously lacking. Multi-dimensional NMR findings showed that $Cd^{2+}$ induced a *cis* interaction and that coordination was localized to the most distal epsilon nitrogen on the histidine imidazole ring within the octarepeat domain. $^{113}Cd$ NMR was able to successfully measure $PrP^C$'s *cis* interaction and any weakened interactions resulting from pathological mutations. Together, these results demonstrate that physiologically relevant segments of $PrP^C$ participate in the *cis* interaction and misregulation could lead to toxicity. Additionally, we have demonstrated that $Cd^{2+}$ via $^{113}Cd$ NMR is a viable surrogate for measuring $Zn^{2+}$'s driven *cis* interaction

For Dr. Daniel Hostetter

The driving force behind me going to graduate school

**Acknowledgements**

Joining the Millhauser lab was one the best decisions I have made in my scientific career. The Millhauser lab trained me to be a skillful and independent scientist. Glenn provided the lab members with the foundation to write and present motivated and articulate scientific information. Additionally, Glenn encouraged diving into the literature and coming up with ideas and explanations of our own. This helped me grow as an independently thinking scientist.

Ted Holman and Michael Stone, my dissertation committee, have been a constant source of advice since before entering graduate school. Whenever, I had questions about new ideas, my committee was always available to discuss. Thank you for the ever-present availability and willingness.

Jack Lee has been one of the most helpful and truest friends in my graduate school career. Jack has been answering my constant questions about how to use the NMR instruments, how to process data, analyze data, and how to troubleshoot my experiments. Jack took the time to teach me how to do liquid nitrogen and helium fills, which provided me a deeper understanding of how the NMR instruments worked. He even went on adventures to UC Berkeley and SFSU to help me use their instruments. Thank you for all of the help and the valuable friendship. I could not have completed my graduate studies without your vital help.

Pervious members of the lab Eric Evans, Jill Miller, Alex McDonald and Rafael Palomino were the pillars of the Millhauser lab when I joined. I would not have been able to start or run a single instrument without their help. The HPLC columns would still not be shut down if it were not for these people. Alex McDonald not

only helped me in Millhauser lab but later, became a collaborator (with the Harris) for the remainder of my PhD. Eric Evans and I walked through the process of learning how to assign a protein, and he was the expert in all things EPR and PrP. Rafael Palomino mentored me in my rotation and was easy going, always willing to help, attitude. Finally, Jill Miller, one of my closer friends in the early years of graduate school, was always someone I could talk to.

The undergraduates, interns, and rotation students have all been valuable pieces of my graduate career. They taught me how to mentor other students and train future scientists. A special shout to my two undergraduates Kaitlyn Vain who is now a graduate student here at UCSC, and Richard Linsley who helped me establish the cadmium NMR studies. You two were the best undergraduates.

The current Millhauser lab members helped me during stressful scientific times and were also valued friends. Graham Roseman, I will forever know you as my crazy little brother. I always enjoyed our scientific arguments, and the arguments that were not scientific. Valerie Chen was always there for any issue and she always had a nugget of information for you. Thank you for teaching me mass spectrometry and how to raise kittens. If something was ever broken, if I needed to remember my license plate number, or if I needed a tool I would call Kevin Schilling in a heartbeat. Rachel Olfield brought an extra piece of soul to the lab that was not there before, and I am incredibly lucky to call her my friend. I believe in that each and every one is an extremely talented of scientist. Thank you so much for putting up with me and helping me grow as a scientist and person.

My friends and family have been the biggest support system throughout this journey. They were there for every single up and down possible. My friends

constantly cheered me on and were never upset when I would spend my weekends researching instead of hanging out. My parents were the most supportive of all. My parents never once asked if this was something I really needed to be doing and trusted in my belief and passion. Thank you to my family and friends, without you, I would not have gotten to this point.

*The Co-authors Dr. Alex McDonald and Dr. Bei Wu performed and wrote all research from LC-MS/MS and electrophysiology results in chapter 2, respectively. The Co-authors Professor David Harris and Professor Glenn Millhauser listed directed and supervised the research that forms the basis of this dissertation for chapter 2. Where Co-Author Professor Glenn Millhauser directed and supervised all works present in this dissertation.*

# Chapter 1
# Introduction

## The History and Pathophysiology of Prion Diseases

### Creutzfeldt-Jakob Disease

Prion diseases are a class of fatal neurodegenerative diseases that affect all mammals, including humans. The study of prion diseases, more technically known as the Transmissible Spongiform Encephalopathies (TSEs), has a rich history dating back well over one hundred years. One of the first human cases of a prion disease was documented by Dr. Hans Gerhard Creutzfeldt in 1920 and involved his patient Bertha Elschker. The neurologist, Alfons Maria Jakob, was also engaged in the study of nervous system ailments and noticed the striking similarities between the symptoms of some of his patients and those of Bertha Elschker. Together, these patients displayed a variety of symptoms including dementia, psychiatric and behavioral issues, myoclonus (involuntary twitching), and ataxia (paralysis and loss of coordination). Using postmortem histological methods, Creutzfeldt and Jakob each noted that the brain matter of these patients had substantial neuronal degradation, neuronal swelling, and proliferation of astrocytes. Collectively, the information derived from the study of these patients lead to the discovery of a new neurodegenerative ailment, now known as Creutzfeldt-Jakob disease (CJD).

### Death by Cannibalism, Kuru

It is now well established that a variety of mammals, beyond humans, may also develop prion diseases. The link between animal and human prion diseases emerged from the study of Kuru, a fatal malady identified in the early 1900s that spread rapidly among the Fore people of Papua New Guinea. The first report of Kuru by a western physician was from Australian colonist Vincent Zigas in the 1950's. Yet, it wasn't until the early 1960's that extensive research by Australian Michael Alpers and American Daniel Carleton Gajdusek demonstrated that Kuru was a result of handling or ingesting brain tissue, a common practice that came from the Fore tradition of cannibalism.

The Fore people practiced cannibalism where they ate their deceased ancestors. Although the practice is commonly referred to as ritualized, the Fore people consumed their dead to harness nutrition, rather than for religious practice. The belief was that by ingesting their ancestor's remains, they would absorb the life force that was normally consumed by local vegetation when bodies were otherwise buried in the ground. The gallbladder was the only organ the Fore people avoided, because it was believed to make the meat taste sour. Additionally, special attention was given to the brain, which was prepared by stuffing tissue into bamboos cylinders and steamed. The women and children prepared and ate the deceased ancestors, while the men believed that participation would weaken them as warriors. This was because they needed their strength to fight the neighboring tribes that they believed had cursed them with a disease they called Kuru.

**Figure 1: Child with Kuru in the Southern Fore Tribe Women and children were the primary population to contract Kuru. Symptoms of Kuru included shaking, ataxia, and tremors were common symptoms.**

Medical literature reporting a neurological disease that primarily afflicted women and children prompted Alpers to investigate the cause of Kuru (Figure 1). Alpers hypothesized that because only the women and children ate tissues from their deceased, the source of Kuru was from ingestion of an infectious agent. He collected biological samples from Kuru infected patients and sent them to virologist Daniel Carleton Gajdusek for analysis. These results demonstrated nothing unusual about the blood, urine, or cerebrospinal fluid. However, Gajdusek reported that the Kuru infected brain tissue had massive neurodegeneration and vacuolization of the

neutrophil in the grey matter (Figure 2). Additionally, the lack of immune response and inflammation in these samples indicated that Kuru was neither bacteria nor viral infection

Scrapie, a prion disease found in sheep, had strikingly similar pathologies to Kuru. Despite documentation of scrapie dating back to the 1750's, detailed research information about pathophysiology was limited. What was known from a detailed study was that Scrapie was transmissible among sheep. Alpers hypothesized that the same infectivity seen with scrapie also applied to Kuru.

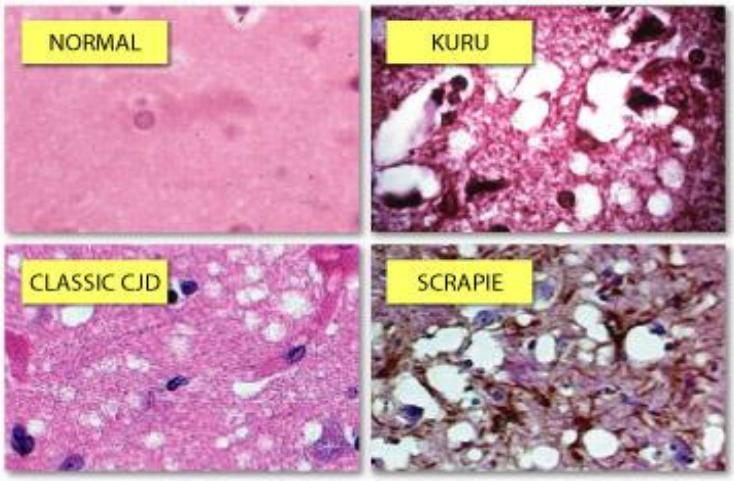


**Figure 2. Post Mortem Histopathology of Brain Tissue of Prion Diseases. Brain slices from CJD, Kuru, and scrapie individuals/animals. Kuru, classic CJD, and Scrapie are characterized by extensive vacuolization of the neutrophil in the grey matter.**

In order to determine if the transmissible infection originated from cannibalism, Alpers needed brain matter from a Kuru infected patient. To this end, Alpers convinced the parents of a Kuru infected child, Kigea, to allow him to autopsy their child's body and collect the diseased tissue. Using the autopsied brain matter, Alpers had Gajdusek inoculate chimpanzees to determine the infectivity of Kuru. Two years

after inoculation, the chimpanzees suffered neurodegeneration such as vacuolization of neutrophil which was consistent with Kuru, which indicated that this disease was transmissible. These studies confirmed that ingestion of Kuru infected brain matter was responsible for the spread of the disease.

Gajdusek published his study in 1966, where he confirmed that Kuru had both the longest incubation period of any reported human disease and was transmissible. Additionally, a connection among Kuru, scrapie, and CJD was established when studies confirmed the infectivity of all three diseases. Because of their similar pathologies and infectivity, these diseases were termed transmissible spongiform encephalopathies (TSEs).

## "Mad Cow" Disease

In Britain during the 1980's, the world saw a TSE emerge that crossed the species barrier. Bovine spongiform encephalopathy (BSE) infected approximately one million cattle before the source of the infection was identified. The infectious particle was found to originate from bone meal, sourced from contaminated slaughterhouse remains. In a horrifying twist, the infected meat from the cattle contaminated the food supply in Britain, where it then transmitted to humans. The human prion disease resulting from ingestion of BSE contaminated meat was determined to be a variant version of Creutzfeldt-Jakob disease (vCJD). This outbreak of "mad cow disease" pulled prion diseases out of the annals of scientific curiosity, and into the realms of geopolitical catastrophe.

## The Discovery of the Prion Protein

The connection among Kuru, Scrapie, and CJD had been established, but, the causative agent of these diseases remained enigmatic. That is, until in 1982, when scientist Stanley Prusiner demonstrated that a protein was the infectious particle in the transmissible spongiform encephalopathies (1). In his studies, Prusiner ruled out bacteria and nucleic acid (1–3) as the causal agent. Prusiner reported that the only way to effectively break down the scrapie aggregates was by denaturation in urea, which implied a protein composition (2, 3). Prior to this study, a protein had never been implicated as the infectious agent in a disease. The protein responsible was named Prion by Prusiner for proteinaceous infectious particle. Furthermore, the prion protein was identified as an endogenous protein that was primarily localized to the Central Nervous System (CNS) (1, 4, 5). Prusiner hypothesized from his studies that endogenous cellular prion protein would convert into a toxic isoform, scrapie, thus resulting in neurodegeneration.

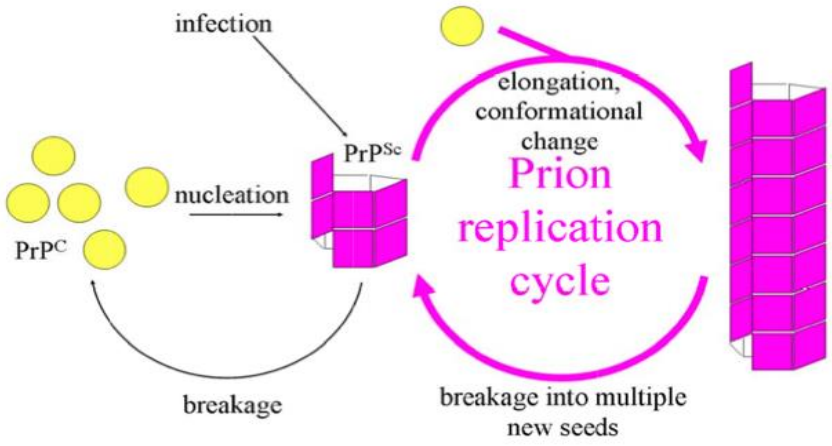


**Figure 3: The "Protein Only" Hypothesis and the Prion Protein Replication Cycle. $PrP^{C}$ is required from prion disease toxicity. In yellow is helical native folded $PrP^{C}$ and in magenta is beta-sheet rich toxic $PrP^{SC}$. $PrP^{SC}$ requires $PrP^{C}$ to dock onto and covert to $PrP^{SC}$ as a template(6).**

The method of conversion of the prion protein into its toxic scrapie isoform was explained with the "protein only" hypothesis. The "protein only" hypothesis postulates that prion diseases arise when the helical cellular prion protein ($PrP^{C}$) converted into a beta sheet rich scrapie isoform ($PrP^{SC}$)(7). The mechanism proposed that a healthy protein was converted into its toxic isoform through $PrP^{SC}$ docking onto $PrP^{C}$ thus initiating a conversion in a autocatalytic fashion (Figure 3)(7). The initial source of $PrP^{SC}$ for conversion could occur via infectious, genetic, or sporadic avenues.

A neurodegenerative disease caused by the misfolding of a protein was the first to be identified. While the "protein only" hypothesis explained a potential

mechanism for how prion diseases arose spontaneously, it did not ascribe a function for endogenous $PrP^C$. Having a precise function for the cellular prion protein is sure to provide insight into prion disease pathogenesis

Characterization of the Prion Protein

The molecular features of $PrP^C$ provide a foundation for deciphering its physiological function. Studies found that the PRNP gene encodes for $PrP^C$ on chromosome 20 in humans. Once expressed, $PrP^C$ is concentrated primarily at the pre- and post-synaptic membranes of the CNS (8, 9). Structurally, $PrP^C$ starts as a 253 amino acid protein, which after post translational modification, results in mature PrP(23-231). Figure 4 highlights significant regions along the prion protein's C- and N-terminal domains. The structured C-terminal domain (residues 126-230) is glycophosphatidylinositol (GPI) anchored to the plasma membrane. This globular domain is comprised of three alpha helices, two short beta strands, and a disulfide bond linking helices α 2 and α 3. Furthermore, helices α2 and α3 have variable glycosylation sites at asparagine residues 181 and 197. The N-terminus (residues 23-125), is a primarily flexible domain that encompasses the metal-binding octarepeat (OR) domain, polybasic tail, and hydrophobic central region.

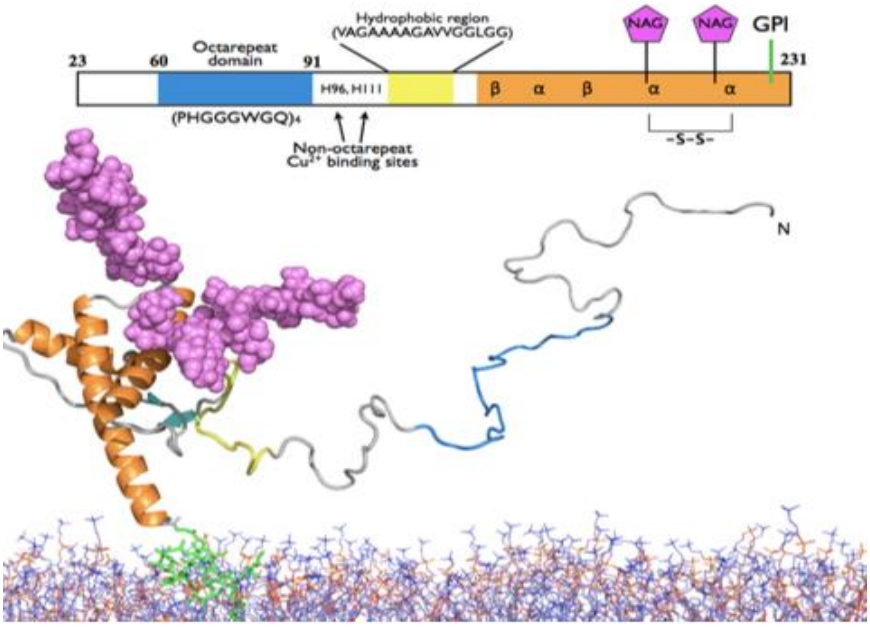


**Figure 4: Model of Linear and 3D diagram of $PrP^C$. $PrP^C$ is GPI anchored (green) to the plasma membrane. Globular C-terminal domain (orange) with glycans (pink), and disulfide bond connecting helices 2 and 3 (black). N-terminal domain has the octarepeat in blue, hydrophobic domain in yellow, and non-octarepeat copper binding sites labeled. All colors in 3D model correlate with linear schematic of $PrP^C$ (10).**

$PrP^C$ studies showed that the N-terminal domain coordinates physiological relevant divalent metal ions in *vivo*. The OR domain, 60-$(PHGGGWGQ)_4$-90 (shown in blue figure 4), can coordinate either $Cu^{2+}$or $Zn^{2+}$ through histidine side chains (11–14). A single $Zn^{2+}$ can coordinate through OR histidine side chains with a ~200μM dissociation constant (15). However, $Cu^{2+}$ binds to $PrP^C$ in a multicomponent fashion that relies heavily on metal ion concentration and pH of encompassing environment (13, 16).

Low $Cu^{2+}$ occupancy results in the highest affinity binding modality with a dissociation constant of 0.1 nM. This binding modality coordinates a single $Cu^{2+}$ through all four histidine side chains of the OR (Figure 5A)(16). With a dissociation constant of 10 μM, the lowest affinity binding modality is when $Cu^{2+}$ is at its maximal occupancy, which coordinates four $Cu^{2+}$ through a single histidine side chain in the OR(Figure 5B)(16) (PUSHIE2014).

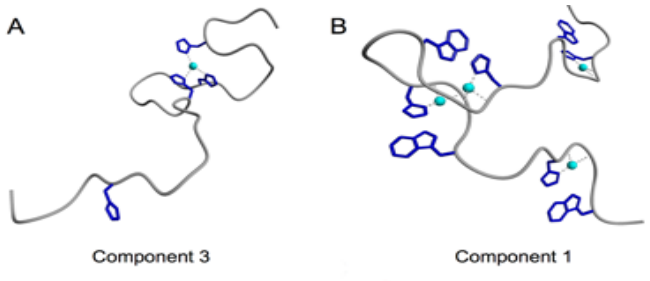


**Figure 5: Copper Coordination of the Octarepeat Domain Histidine residues imidazole side chains (dark blue) and copper ions (light blue) in the octarepeat domain. A.) Component 3 is the highest affinity where a single copper coordinates the octarepeat histidines nitrogens on the imidazole side chains. B.) Component 1 binding has the lowest affinity where each imidazole side chain can coordination a single copper, resulting in the OR loading up 4 ions. (16).**

Studies show that $PrP^C$ modulates physiologically relevant metal ion concentrations, which is suggestive of a role in neuronal metal ion homeostasis. Through x-ray fluorescence imaging maps, Pushie et al measured if $PrP^C$ expression levels alter metal ion concentrations as well as localization in the brain(17).

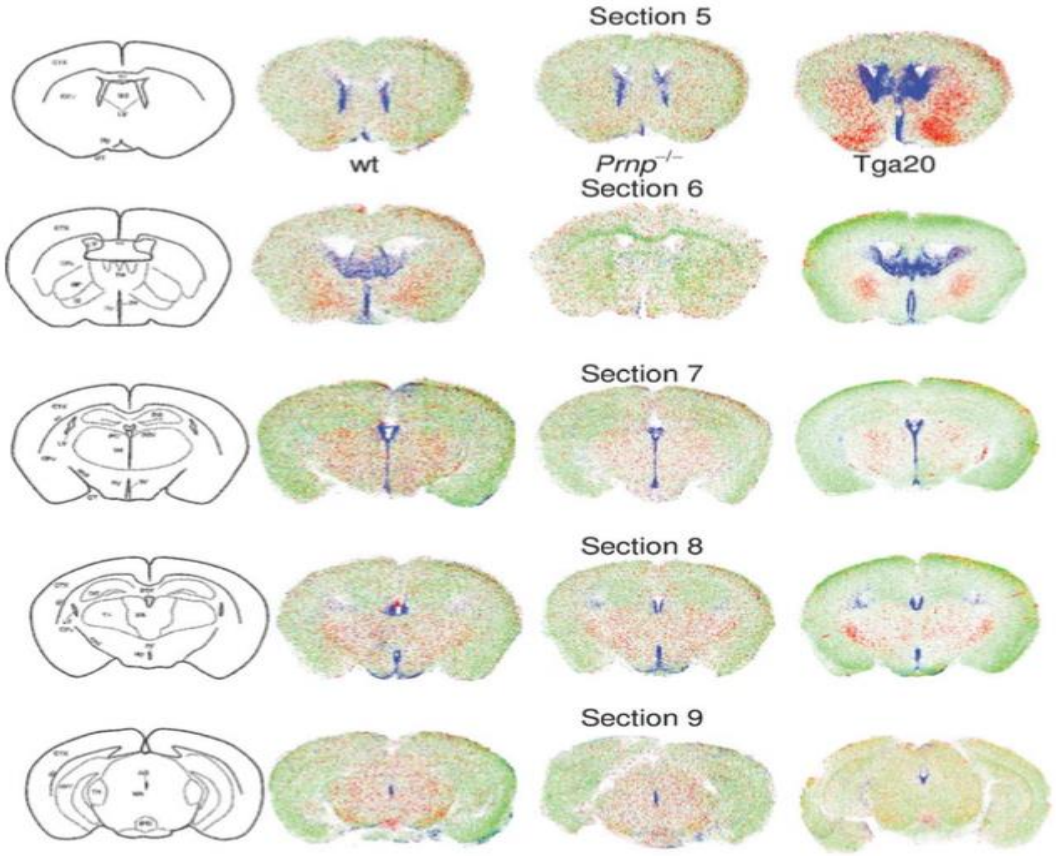


**Figure 6: $PrP^C$ Regulates Metal Ion Concentrations in the Brain X-ray fluorescence imaging maps of brains from anterior (5) to most posterior (9). Left is wild-type, middle is Prnp-/- null and to the right is Tga 20 $PrP^C$ overexpression mice. Fe (red), Cu (blue), and Zn (green) fluorescence are indicated. (17)**

These results show that Prnp-/- mouse brain slices exhibited a decrease in Cu (blue) concentrations in the periventricular region in respect to $PrP^C$ wild-type and overexpression. Zn (green) and Fe (red) local concentrations showed a decrease in the hippocampal region when compared $PrP^C$ wild-type and overexpression (17). Moreover, there was a decrease of Fe in the thalamus of Prnp-/- brain slices.

Although Fe does not directly coordinate to $PrP^C$ as seen with Cu and Zn, this study demonstrates that the prion protein levels alter Fe concentrations (17). Conversely, the opposite affect is seen for $PrP^C$ over expression, which is indicative of prion protein expression modulating neuronal metal ion concentrations.

Metal Driven cis Interaction

Studies by Spevacek et al demonstrated that global changes in the prion protein upon the addition of divalent zinc might be a part of a signaling process regulated by $PrP^C$ (18). Historically, study of the cellular prion protein assumed the N-terminal and C-terminal domains were non-interacting. However, there was a lack of biophysical evidence for mature full-length prion protein in the presence and absence of endogenous metal ions. Through $^{1}H$-$^{15}N$ HSQC NMR, Spevacek et al identified that upon the addition of $Zn^{2+}$ there was a decrease in C-terminal cross-peak intensity. These results indicated that the chemical dynamics localized around that amino acid were being affected (18) by the addition of $Zn^{2+}$.

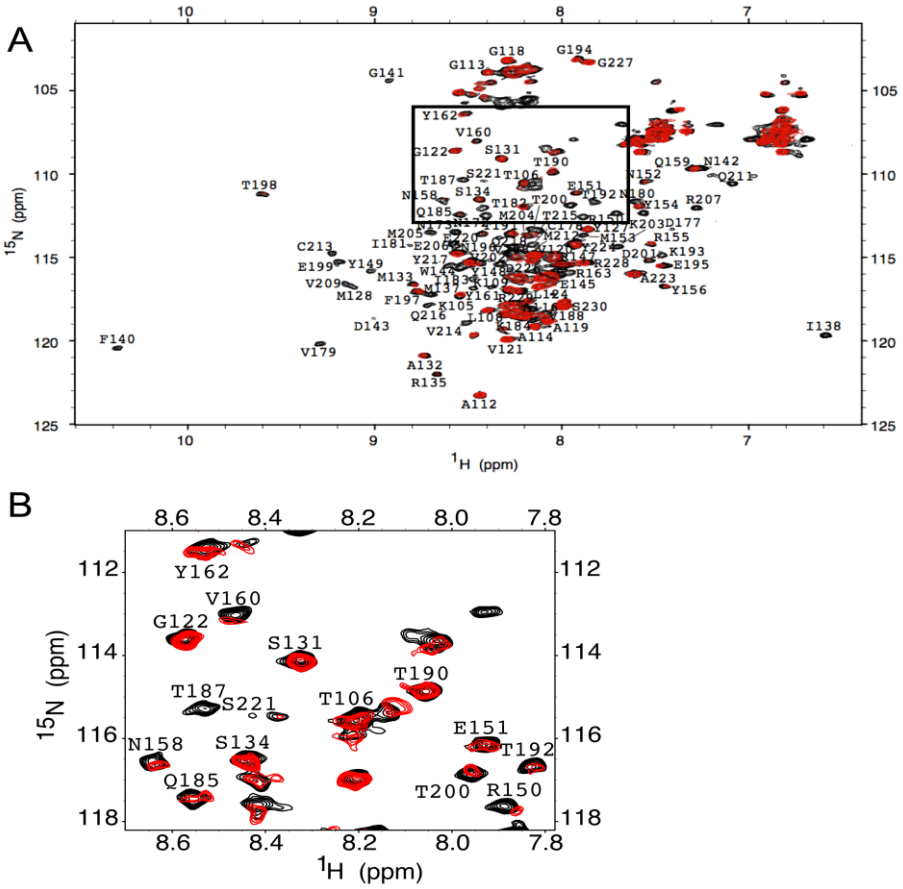


**Figure 7. $^{1}$H-$^{15}$N HSQC NMR spectra of wild-type MoPrP's cis Interaction In black is full length wild-type PrPC and red is in the presence of 3 equivalents of $ZnCl_2$. Upon the addition of $Zn^{2+}$, there is a loss of intensity in cross-peaks corresponding to C-terminal domain residues, which indicates intermediate exchange. B. Zoom in on a section highlighting C-terminal cross-peaks of the box indicated in A.(18)**

When mapped onto the protein, the affected C-terminal residues are localized to a well-defined negatively charged cleft on the N-terminal ends of helices α2 and α3 (Figure 9). These results were validated with a C-terminal PrP construct (90-230), which confirmed that $Zn^{2+}$ induces a *cis* interaction and the effects seen are not from direct coordination of helices α2 and α3 (18). From these results, Spevacek

hypothesized that addition of $Zn^{2+}$ to the OR drove an N-C terminal contact, also referred to as the *cis* interaction (18).

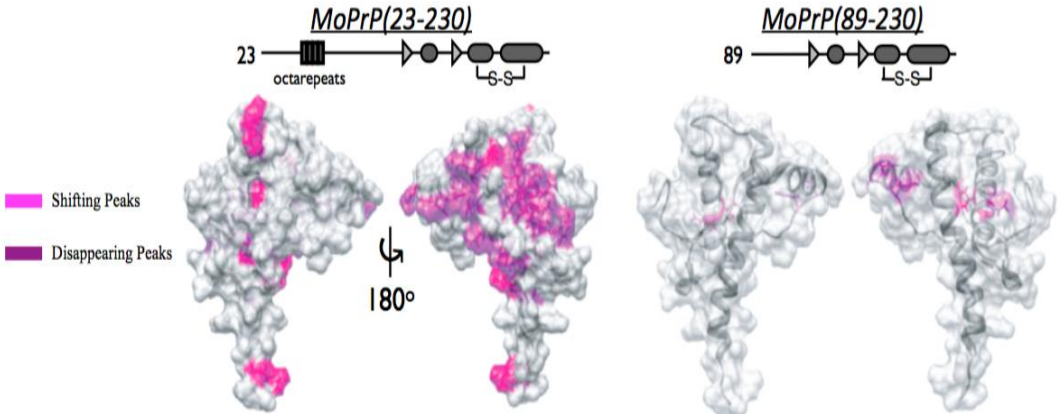


**Figure 8. $Zn^{2+}$-driven cis Interaction Localized to Negatively Charged Surface Patch on C-terminus PDB: 1XYX surface diagram for C-terminal wild-type MoPrP and the C-terminal construct MoPrP(91-230), lacking the $Zn^{2+}$ binding N-terminal octarepeat domain respectively. Residues labeled in purple indicated broadening of cross-peaks and residues labeled in pink are significantly shifted cross-peaks (18)**

DEER EPR was employed to further assess if the N terminus was making direct contact with the C-terminal domain. (23). DEER EPR is capable of measuring macromolecular distance measurements through site directed spin labels (SDSL), which can assess conformational distributions of the N and C terminal domain. An addition of an SDSL to the N-terminus and C-terminus would allow for accurate measurements of conformational changes resulting from the addition of $Zn^{2+}$. The N-terminal SDSL (R1) was conjugated to a cysteine incorporated near the OR domain. However, in an effort to avoid non-native disulfide linkages, SDSL (K1) was attached through an unnatural amino acid incorporated on the C-terminal domain(18). When

$Zn^{2+}$ was added to $PrP^{C}$, there was a sharpening of distance distributions that resulted from the spin labels coming into close contact. Coupled with the $^{1}H$-$^{15}N$ HQSC NMR studies, these results that indicated that $Zn^{2+}$drives an N to C- terminal *cis* interaction.

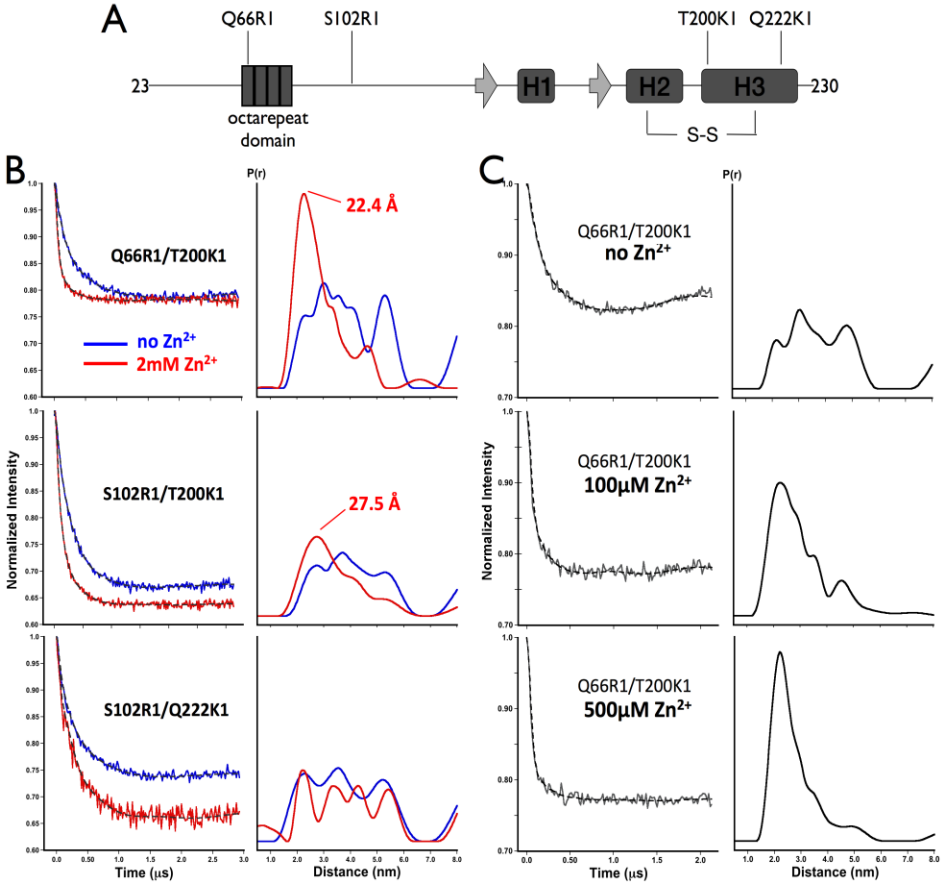


**Figure 9. DEER Measured Inter-Domain Distances of SDSL's Upon the Addition of $Zn^{2+}$. A. linear representation of MoPrP and locations of SDSL for the N-terminus and C-terminus B. Background-corrected dipolar evolution spectra and distance upon the addition of $Zn^{2+}$ (red) and without the addition of $Zn^{2+}$ (blue) C. Distance distributions for MoPrP Q66R1/T200K1 in the presence of increasing concentrations of $Zn^{2+}$ (0, 100, and 500uM)(18).**

The majority of disease-associated mutations reside on helices α2 and α3, where they confer a decrease in negative charge. Spevacek et al hypothesized that the negative surface potential was essential for the *cis* interaction to occur, and that these mutations could weaken that interdomain contact (18). Notable pathological mutations, D177N and E199K (mouse numbering) showed a return in cross-peak intensity on the N-terminal ends of helices α2 and α3 with respect to wild-type (figure 10). These results indicated that the N-C terminal contact may be of physiological importance and that toxicity could be due to pathological mutations that weakening this cis interaction.

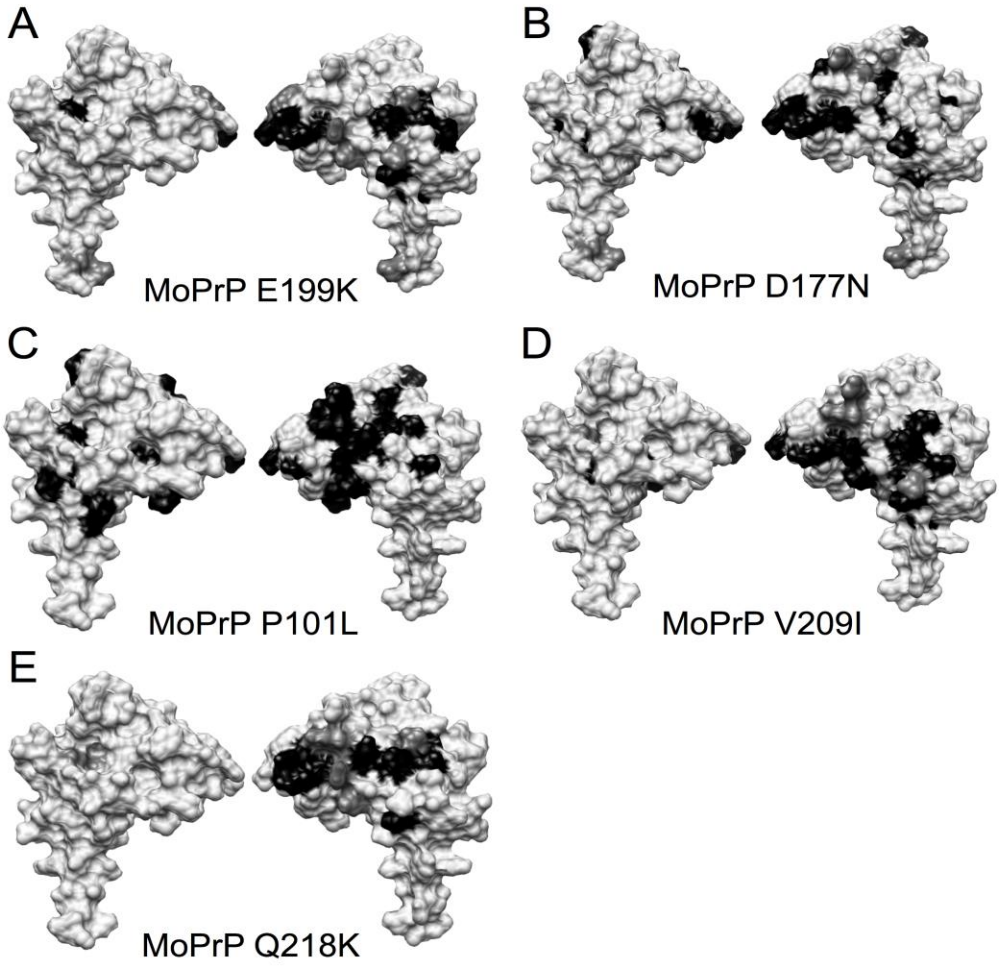


**Figure10. Disease Conferring C-Terminal Mutations Weaken $Zn^{2+}$- driven cis Interaction PDB: 1XYX Surface representation of the C-terminal domain for each mutation tested. Residues labeled in black indicate broadening of cross-peaks and dark grey is shifting of cross-peaks. pathogenic mutants (A-D), and the dominant negative mutant (E)(18).**

Through four-pulse double electron-electron resonance (DEER) EPR spectroscopy and $^{1}H$-$^{15}N$ HSQC NMR spectroscopy, it was demonstrated that addition of $Zn^{2+}$ to the OR segment drives an interdomain interaction, termed the *cis* interaction(18).

Where $PrP^{C}$'s cis interaction could participate in signaling processes that regulate neuronal ion homeostasis, and disruption of that interaction could lead to toxicity.

Prion Protein's N-terminal Toxicity

Cellular assays and animal studies provided intriguing insight into how $PrP^{C}$ might induce toxicity. Deletion of the gene encoding for the entirety of $PrP^{C}$ in mice as well as for the N-terminal domain was exhibited to be relatively benign. However, deletions located central to the protein resulted in toxicity without scrapie inoculation(19–25).

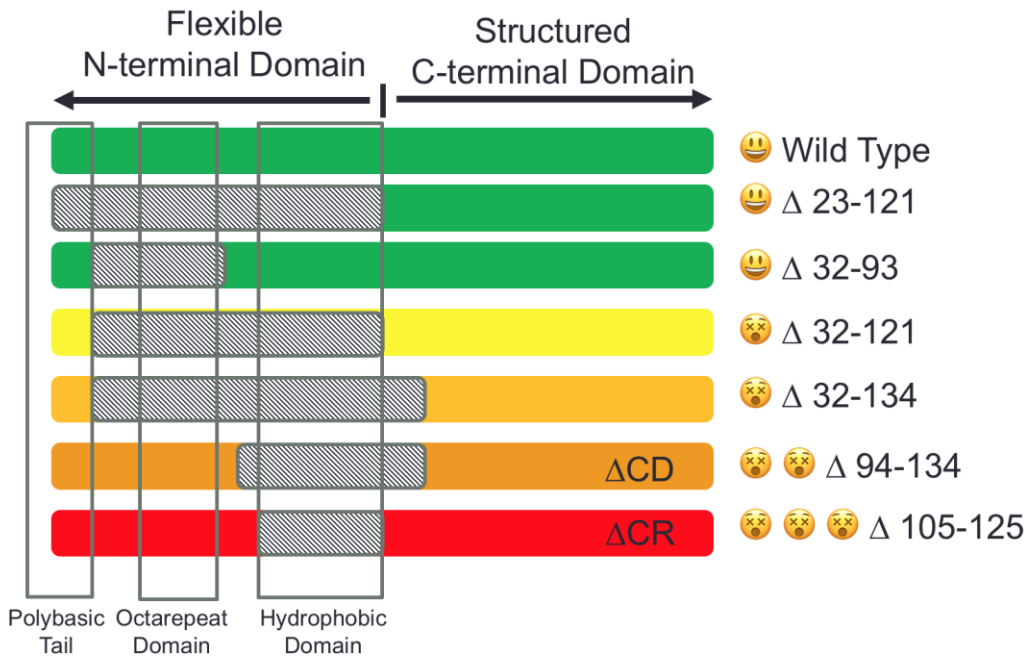


**Figure 11 Prion Deletion Mutations Cause Toxicity. Wild-type, Δ23-121, and Δ32-93 MoPrP(23-230) are well tolerated in mice (indicated in green). Once the deletions extend into the hydrophobic region, toxicity occurs only when in the presence of the first 10 amino acids. Δ32-121, Δ32-134, Δ94-134, and Δ105-125**

**are toxic (yellow to red with red being the most toxic). Adaptation of figure from(26)**

Figure 11 Is a selection of N-terminal deletion mutations studied by various labs, where toxicity increases as you narrow in on the central region(24, 27, 28). Mice expressing these toxic deletions displayed cerebellar neurodegradation and neonatal lethality prior to scrapie inoculation(29). Furthermore, these mice did not display any accumulation of $PrP^{SC}$. The most toxic deletion was a 21 amino acid stretch encompassing the hydrophobic central region (mouse residues 105-125), termed ΔCR. Interestingly, neuronal cells, cultured brain slices, and transgenic mice all expressing ΔCR displayed spontaneous ionic currents(24, 30–32). These currents were measure using electrophysiology experiments and indicated a phenotype consistent with aberrant $PrP^{C}$ activity that involved the transport ions into the cell. Importantly, it was discovered that retaining the poly basic tail (residues 23-31) was essential for the toxicity of these internal deletions (Figure 11)(33, 34).

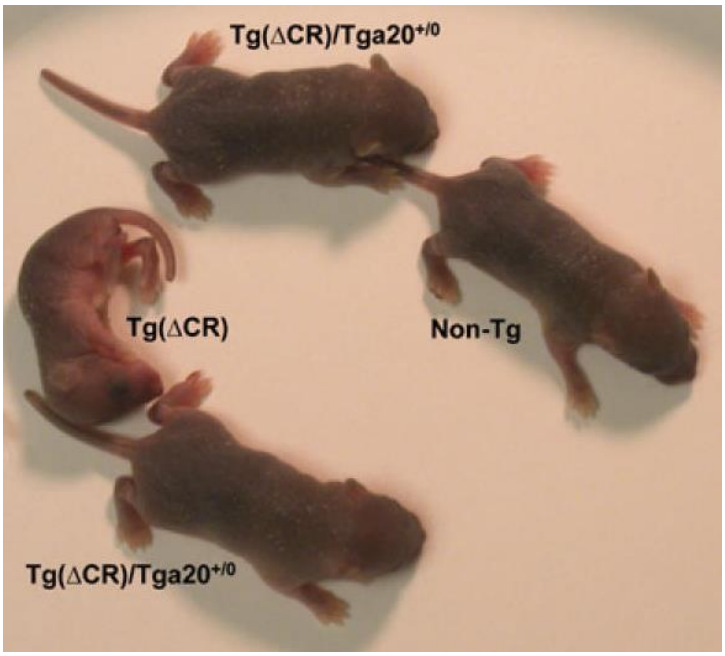


**Figure 12: Transgenic Mice expressing ΔCR non-transgenic and transgenic mice at 3 days of age. Transgenic mice expressing ΔCR on a Prnp 0/0 background suffer from neurotoxicity. Where mice expressing ΔCR and co-overexpressing wild-type show similar phenotype to non-transgenic mice(24).**

The polybasic extreme N-terminus, $_{23}$KKRPKPGGW$_{31}$ is a highly conserved region, which has significant implications in eliciting the prion protein's function. Scientific evidence has shown that deletion of the polybasic extreme N-terminus dramatically stalls prion disease progress (25). Furthermore, this segment is essential for transport of divalent metal ions through AMPA receptors(4, 35, 36). Together, along with the polybasic tail being paramount for ΔCR toxicity, this information implies that deletion of the central region may lead to unregulated interactions between $PrP^C$ and ionotropic membrane receptors (28, 37, 38).

Investigations into a physiological role yielded a new hypothesis where the N-terminal "effector" domain carried out the function $PrP^C$ and misregulation by the C-

terminal "regulator" domain resulted in toxicity (39).This hypothesis suggested that toxic ligands to the C-terminal domain disrupted the regulation of the N-terminus whose job it was to elicit $PrP^{C}$'s function. (39, 40). In support of this hypothesis, a toxic monoclonal antibody, POM 1, was shown to directly over lap the same C-terminal cleft as the *cis* interaction and display similar neurotoxicity to $PrP^{SC}$ (41, 42). Additionally, monoclonal antibodies that target the N-terminal domain or elimination of the entire N-terminus rescues these observed toxic effects (41, 43). The resulting hypothesis is that toxic C-terminal ligands block $PrP^{C}$'s ability to regulate the N-terminal domain's interactions by disruption of the *cis* interaction, which results in neurotoxicity(39, 44).

Specific Aims

This dissertation research aims at furthering our understanding of the regions influencing $PrP^{C}$'s *cis* interaction. Recent works have identified that ΔCR and the polybasic extreme N-terminal domain also participate in physiologically relevant roles. With this new information, we aimed to characterize the role that these domains played in the regulation of $PrP^{C}$'s *cis* interaction. Chapter 2 describes how $Cu^{2+}$'s-driven *cis* interaction is influenced by N-terminal deletions, and charge mutations, using $^{1}H$-$^{15}N$ HSQC NMR spectroscopy, LC-MS/MS, and electrophysiology. Before this work, $PrP^{C}$'s *cis* interaction was postulated to only require the OR domain's coordination of divalent metal ions (45, 46). The data

reported in this dissertation demonstrates that the polybasic extreme N-terminus and central region play pivotal roles in $PrP^{C}$'s $Cu^{2+}$-driven *cis* interaction. This has never been reported before and adds complexity to how $PrP^{C}$ may be regulated. Furthermore, any misregulation of the N-terminal domain could lead to toxicity.

Substantial information $Cu^{2+}$'s coordination environment exists from the use of EPR, however, because $Zn^{2+}$ is diamagnetic, there is a deficiency spectroscopic methods for studying the metal ions perspective (45, 47). Previous studies have reported $^{113}Cd$ as a successful surrogate for $Zn^{2+}$ proteins because of their similar ionic radii, favor towards nitrogen ligands, and are $d^{10}$ metal ions(48, 49). Chapter 3 discusses how $Cd^{2+}$ can serve as a $Zn^{2+}$ surrogate for $^{113}Cd$ NMR spectroscopy and provide information about $PrP^{C}$'s coordination sphere. In this dissertation, we explored $^{113}Cd$ as a surrogate for $Zn^{2+}$ in an effort to measure $PrP^{C}$'s *cis* interaction from the metal ion perspective. The experiments done have isolated cadmium to the most distal nitrogen of the histidine side chain in the OR. We have successfully measured $^{113}Cd$ chemical shift resonances difference between wild-type and OR peptide, which are consistent with a *cis* interaction. Furthermore, we have demonstrated that pathological mutations that are proven to have a weakened *cis* interaction also have an altered $Cd^{2+}$ chemical shift difference in respect to wild-type. Collectively, these results provide a foundation for studying $Zn^{2+}$'s metal coordination environment with spectroscopic methods, which has yet to be done. Finally, Chapter 4 concludes and summarizes all the results found in this dissertation.

References


1. Prusiner, S. 1982. Novel proteinaceous infectious particles cause scrapie. Science (80). 216: 136–144.

2. Prusiner, S.B., D.F. Groth, D.C. Bolton, S.B. Kent, and L.E. Hood. 1984. Purification and structural studies of a major scrapie prion protein. Cell. 38: 127–134.

3. McKinley, M.P., D.C. Bolton, and S.B. Prusiner. 1983. A protease-resistant protein is a structural component of the Scrapie prion. Cell. 35: 57–62.

4. Watt, N.T., H.H. Griffiths, and N.M. Hooper. 2013. Neuronal zinc regulation and the prion protein. Prion. 7: 203–8.

5. Watt, N.T., D.R. Taylor, T.L. Kerrigan, H.H. Griffiths, J. V Rushworth, I.J. Whitehouse, and N.M. Hooper. 2012. Prion protein facilitates uptake of zinc into neuronal cells. Nat. Commun. 3: 1134.

6. Joannamasel. 2010. PrPsc induces conformational change in PrPc. English Wikapedia.

7. Laurent, M. 1996. Prion diseases and the ' protein only ' hypothesis : a theoretical dynamic study.

8. Kretzschmar, H.A., T. Tings, A. Madlung, A. Giese, and J. Herms. 2000. Function of PrP(C) as a copper-binding protein at the synapse. Arch. Virol. Suppl. : 239–49.

9. Vassallo, N., and J. Herms. 2003. Cellular prion protein function in copper homeostasis and redox signalling at the synapse. J. Neurochem. 86: 538–44.

10. Evans, E.G.B., M.J. Pushie, K.A. Markham, H.-W. Lee, and G.L. Millhauser. 2016. Interaction between Prion Protein's Copper-Bound Octarepeat Domain and a Charged C-Terminal Pocket Suggests a Mechanism for N-Terminal Regulation. Structure. 24: 1057–67.

11. Donne, D.G., J.H. Viles, D. Groth, I. Mehlhorn, T.L. James, F.E. Cohen, S.B. Prusiner, P.E. Wright, and H.J. Dyson. 1997. Structure of the recombinant full-length hamster prion protein PrP(29-231): the N terminus is highly flexible. Proc. Natl. Acad. Sci. U. S. A. 94: 13452–7.

12. Brown, L.R., and D.A. Harris. 2003. Copper and zinc cause delivery of the prion protein from the plasma membrane to a subset of early endosomes and the Golgi. J. Neurochem. 87: 353–63.

13. Walter, E.D., D.J. Stevens, M.P. Visconte, and G.L. Millhauser. 2007. The prion protein is a combined zinc and copper binding protein: Zn2+ alters the distribution of Cu2+ coordination modes. J. Am. Chem. Soc. 129: 15440–15441.

14. Evans, E.G.B., and G.L. Millhauser. 2017. Copper- and Zinc-Promoted Interdomain Structure in the Prion Protein: A Mechanism for Autoinhibition of the Neurotoxic N-Terminus. In: Progress in molecular biology and translational science. . pp. 35–56.

15. Walter, E.D., D.J. Stevens, M.P. Visconte, and G.L. Millhauser. 2007. The prion protein is a combined zinc and copper binding protein: Zn2+ alters the distribution of Cu2+ coordination modes. J. Am. Chem. Soc. 129: 15440–1.

16. Walter, E.D., D.J. Stevens, A.R. Spevacek, M.P. Visconte, A. Dei Rossi, and G.L. Millhauser. 2009. Copper binding extrinsic to the octarepeat region in the prion protein. Curr. Protein Pept. Sci. 10: 529–35.

17. Pushie, M.J., I.J. Pickering, G.R. Martin, S. Tsutsui, F.R. Jirik, and G.N. George. 2011. Prion protein expression level alters regional copper, iron and zinc content in the mouse brain. Metallomics. 3: 206.

18. Spevacek, A.R., E.G.B. Evans, J.L. Miller, H.C. Meyer, J.G. Pelton, and G.L. Millhauser. 2013. Zinc drives a tertiary fold in the prion protein with familial disease mutation sites at the interface. Structure.

19. Weissmann, C., M. Fischer, A. Raeber, H. Büeler, A. Sailer, D. Shmerling, T. Rülicke, S. Brandner, and A. Aguzzi. 1998. The use of transgenic mice in the investigation of transmissible spongiform encephalopathies. Rev. Sci. Tech. 17: 278–90.

20. Brandner, S., S. Isenmann, A. Raeber, M. Fischer, A. Sailer, Y. Kobayashi, S. Marino, C. Weissmann, and A. Aguzzi. 1996. Normal host prion protein necessary for scrapie-induced neurotoxicity. Nature. 379: 339–343.

21. Büeler, H., M. Fischer, Y. Lang, H. Bluethmann, H.P. Lipp, S.J. DeArmond, S.B. Prusiner, M. Aguet, and C. Weissmann. 1992. Normal development and behaviour of mice lacking the neuronal cell-surface PrP protein. Nature. 356: 577–82.

22. Weissmann, C., H. Büeler, M. Fischer, A. Sailer, A. Aguzzi, and M. Aguet. 1994. PrP-

deficient mice are resistant to scrapie. Ann. N. Y. Acad. Sci. 724: 235–40.

23. Baumann, F., M. Tolnay, C. Brabeck, J. Pahnke, U. Kloz, H.H. Niemann, M. Heikenwalder, T. Rülicke, A. Bürkle, and A. Aguzzi. 2007. Lethal recessive myelin toxicity of prion protein lacking its central domain. EMBO J.

24. Li, A., H.M. Christensen, L.R. Stewart, K.A. Roth, R. Chiesa, and D.A. Harris. 2007. Neonatal lethality in transgenic mice expressing prion protein with a deletion of residues 105–125. EMBO J. 26: 548–558.

25. Hegyi, I., D. Shmerling, A. Cozzio, J. Götz, T. Blättler, C. Von Mering, S. Brandner, E. Flechsig, T. Rülicke, M.B. Fischer, C. Hangartner, C. Weissmann, and A. Aguzzi. Expression of amino-terminally truncated PrP in the mouse leading to ataxia and specific cerebellar lesions. doi.org.

26. McDonald, A.J., J.P. Dibble, E.G.B. Evans, and G.L. Millhauser. 2014. A new paradigm for enzymatic control of α-cleavage and ß-cleavage of the prion protein. J. Biol. Chem. 289: 803–13.

27. Solomon, I.H., J.E. Huettner, and D.A. Harris. 2010. Neurotoxic mutants of the prion protein induce spontaneous ionic currents in cultured cells. J. Biol. Chem. 285: 26719–26726.

28. Biasini, E., J.A. Turnbaugh, T. Massignan, P. Veglianese, G. Forloni, V. Bonetto, R. Chiesa, and D.A. Harris. 2012. The toxicity of a mutant prion protein is cell-autonomous, and can be suppressed by wild-type prion protein on adjacent cells. PLoS One.

29. Li, A., H.M. Christensen, L.R. Stewart, K.A. Roth, R. Chiesa, and D.A. Harris. 2007. Neonatal lethality in transgenic mice expressing prion protein with a deletion of residues 105–125. EMBO J. 26: 548–558.

30. Solomon, I.H., N. Khatri, E. Biasini, T. Massignan, J.E. Huettner, and D.A. Harris. 2011. An N-terminal polybasic domain and cell surface localization are required for mutant prion protein toxicity. J. Biol. Chem. 286: 14724–14736.

31. Solomon, I.H., E. Biasini, and D.A. Harris. Ion channels induced by the prion protein Mediators of neurotoxicity. Prion. 61: 40–45.

32. Turnbaugh, J.A., U. Unterberger, P. Saa, T. Massignan, B.R. Fluharty, F.P. Bowman, M.B. Miller, S. Supattapone, E. Biasini, and D.A. Harris. 2012. The N-Terminal, Polybasic

Region of PrPC Dictates the Efficiency of Prion Propagation by Binding to PrPSc. J. Neurosci.

33. Westergard, L., J.A. Turnbaugh, and D.A. Harris. 2011. A nine amino acid domain is essential for mutant prion protein toxicity. J. Neurosci. 31: 14005–17.

34. Turnbaugh, J.A., L. Westergard, U. Unterberger, E. Biasini, and D.A. Harris. 2011. The N-terminal, polybasic region is critical for prion protein neuroprotective activity. PLoS One. 6: e25675.

35. Watt, N.T., and N.M. Hooper. 2003. The prion protein and neuronal zinc homeostasis. Trends Biochem. Sci. 28: 406–10.

36. Watt, N.T., D.R. Taylor, T.L. Kerrigan, H.H. Griffiths, J. V. Rushworth, I.J. Whitehouse, and N.M. Hooper. 2012. Prion protein facilitates uptake of zinc into neuronal cells. Nat. Commun. 3: 1134.

37. Solomon, I.H., N. Khatri, E. Biasini, T. Massignan, J.E. Huettner, and D.A. Harris. 2011. An N-terminal Polybasic Domain and Cell Surface Localization Are Required for Mutant Prion Protein Toxicity .

38. Turnbaugh, J. a, U. Unterberger, P. Saá, T. Massignan, B.R. Fluharty, F.P. Bowman, M.B. Miller, S. Supattapone, E. Biasini, and D. a Harris. 2012. The N-terminal, polybasic region of PrP(C) dictates the efficiency of prion propagation by binding to PrP(Sc). J. Neurosci. 32: 8817–30.

39. McDonald, A.J., B. Wu, and D.A. Harris. 2017. An inter-domain regulatory mechanism controls toxic activities of PrP $^{C}$. Prion. : 1–10.

40. Wu, B., A.J. McDonald, K. Markham, C.B. Rich, K.P. McHugh, J. Tatzelt, D.W. Colby, G.L. Millhauser, and D.A. Harris. 2017. The N-terminus of the prion protein is a toxic effector regulated by the C-terminus. Elife. 6.

41. Sonati, T., R.R. Reimann, J. Falsig, P.K. Baral, T. O'Connor, S. Hornemann, S. Yaganoglu, B. Li, U.S. Herrmann, B. Wieland, M. Swayampakula, M.H. Rahman, D. Das, N. Kav, R. Riek, P.P. Liberski, M.N.G. James, and A. Aguzzi. 2013. The toxicity of antiprion antibodies is mediated by the flexible tail of the prion protein. Nature. 501: 102–6.

42. Polymenidou, M., R. Moos, M. Scott, C. Sigurdson, Y. Shi, B. Yajima, I. Hafner-Bratkovič, R. Jerala, S. Hornemann, K. Wuthrich, A. Bellon, M. Vey, G. Garen, M.N.G. James, N. Kav, and A. Aguzzi. 2008. The POM Monoclonals: A Comprehensive Set of

Antibodies to Non-Overlapping Prion Protein Epitopes. PLoS One. 3: e3872.

43. Evans, E.G.B., and G.L. Millhauser. 2017. Copper- and Zinc-Promoted Interdomain Structure in the Prion Protein: A Mechanism for Autoinhibition of the Neurotoxic N-Terminus. . pp. 35–56.

44. Wu, B., A.J. Mcdonald, K. Markham, C.B. Rich, K.P. Mchugh, J. Rg Tatzelt, D.W. Colby, G.L. Millhauser, and D.A. Harris. 2017. The N-terminus of the prion protein is a toxic effector regulated by the C-terminus.

45. Spevacek, A.R., E.G.B. Evans, J.L. Miller, H.C. Meyer, J.G. Pelton, and G.L. Millhauser. 2013. Zinc drives a tertiary fold in the prion protein with familial disease mutation sites at the interface. Structure. 21: 236–246.

46. Evans, E.G.B., M.J. Pushie, K.A. Markham, H.-W. Lee, and G.L. Millhauser. 2016. Interaction between Prion Protein's Copper-Bound Octarepeat Domain and a Charged C-Terminal Pocket Suggests a Mechanism for N-Terminal Regulation. Structure. 24: 1057–67.

47. Evans, E.G.B., M.J. Pushie, K.A. Markham, H.-W. Lee, and G.L. Millhauser. 2016. Interaction between Prion Protein's Copper-Bound Octarepeat Domain and a Charged C-Terminal Pocket Suggests a Mechanism for N-Terminal Regulation. Structure. 24: 1057–1067.

48. Armitage, I.M., T. Drakenberg, and B. Reilly. 2013. Use of (113)Cd NMR to probe the native metal binding sites in metalloproteins: an overview. Met. Ions Life Sci.

49. Cotton FA, W.G. 1988. Advanced Inorganic Chemistry: A Comprehensive Text. New York: Wiley.

# CHAPTER 2
# ALTERED DOMAIN STRUCTURE OF THE PRION PROTEIN CAUSED BY $Cu^{2+}$ BINDING AND FUNCTIONALLY RELEVANT MUTATIONS: ALANYSIS BY CHEMICAL CROSS-LINKING AND NMR

Alex J. McDonald[1,4], Deborah R. Leon[1,2,4], Kathleen A. Markham[3,4], Bei Wu[1], Kevin Schilling[3], Jake Pushie, Catherine E. Costello[1,2,*], Glenn L. Millhauser[3,*], and David A. Harris[1,5,*]

[1]Department of Biochemistry and [2]Center for Biomedical Mass Spectrometry, Boston University School of Medicine, Boston, MA 02118 USA
[3]Department of Chemistry and Biochemistry, University of California, Santa Cruz, Santa Cruz, CA 95064 USA
[4]These authors contributed equally
[5]Lead Contact

## INTRODUCTION

Prion diseases, or transmissible spongiform encephalopathies, are caused by the conversion of a normal, cellular protein, $PrP^{C}$, into a conformationally altered form called $PrP^{Sc}$. Prion propagation involves an autocatalytic process in which $PrP^{Sc}$ serves as a molecular template that converts additional molecules of $PrP^{C}$ into the $PrP^{Sc}$ form (1, 2). Although its role as a substrate for conversion into $PrP^{Sc}$ is well known, the physiological function of $PrP^{C}$, and how this function relates to the structure of the protein, have remained obscure.

$PrP^{C}$ consists of two major structural domains (Fig. 1). The N-terminal domain, comprising residues 23-121 following the signal peptide cleave site, is natively unstructured. It contains a short polybasic domain (KKRPKPGGW), a series of four histidine-containing octapeptide repeats (PHGGGWGQ), a second, positively charged cluster (KPSKPKTNLK), and a hydrophobic region (VAGAAAAGAVVGGLGGYMLG) that is highly conserved among diverse species(3, 4). The C-terminal domain (residues 121-230), whose structure has been determined by both NMR and X-ray crystallography, consists of three $\alpha$-helices (H1: 144–154; H2: 175–193; and H3: 200–219), and two short, anti-parallel $\beta$-strands flanking helix 1 (S1: 128–131; and S2: 161–164). A disulfide bond connects helices 2 and 3 (Cys178/Cys213), and there are two N-linked glycosylation sites at asparagine residues 180 and 196(3–6).

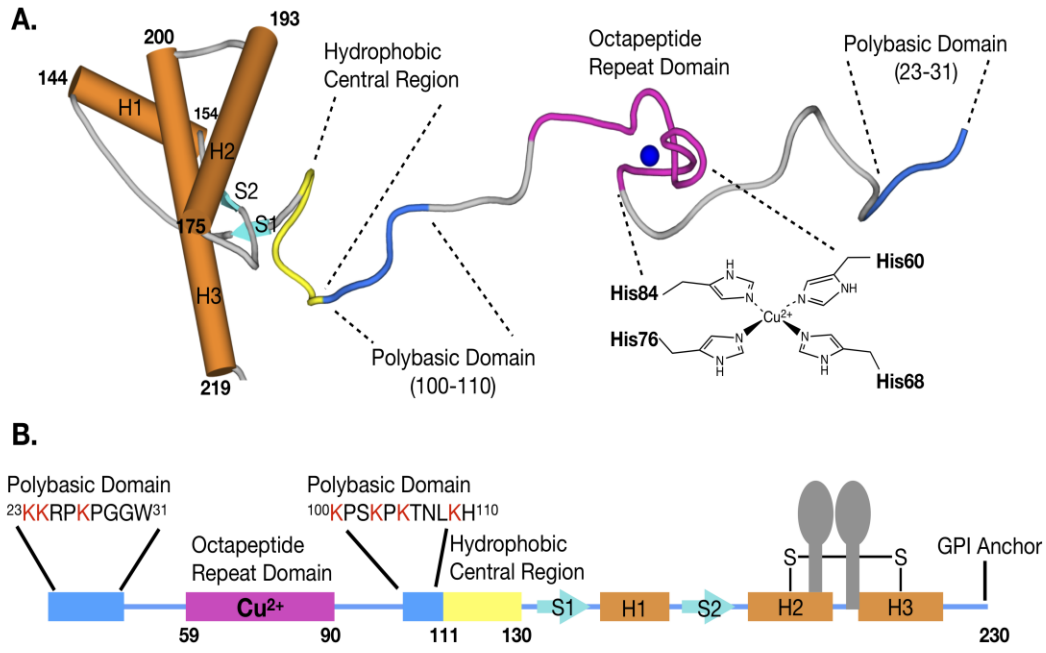


**Figure 13: Structural Overview of the Prion Protein. (Top) 3D ribbon diagram of 120-230 (PDB:1XYX) MoPrP. Modeled are the entire octarepeat(purple) and octarepeat histidine coordination chemistries (dark purple) for $Cu^{2+}$ (dark blue sphere) (component 3)(7) to show metal binding. Bottom) Linear diagram of $PrP^{C}$ (mouse sequence) numbering indicating secondary structure and post translational modifications. Wild type MoPrP linear diagram from residues 23-230. Octarepeat domain in magenta, Beta sheets in cyan, helices in orange, disulfide bond linking helices two and three in black, glycosylation sites in grey, GPI anchor at residue 230. N-terminal domain is residues 23-120 and c-terminal residues are 120-230. The N-terminal domain regions are the: octarepeat domain (purple) coordinates $Cu^{2+}$ via histidine side chains (component 3), polybasic extreme N-terminus, hydrophobic central region(yellow). All lysines at noted for the entire protein.**

$PrP^{C}$ is expressed at highest levels in neurons of the CNS, where it is concentrated along axons and at pre- and postsynaptic sites. It is localized primarily at the cell surface, where it is attached to the outer leaflet of the lipid bilayer via a glycosyl-phosphatidylinositol (GPI) anchor at its C-

terminus(8–10). Consistent with its cell-surface localization, $PrP^C$ has been suggested to function as a receptor or transporter for physiological ligands and pathological protein aggregates, and as a signal transduction component (11–13).

Perhaps the most well documented functional activity of $PrP^C$ is its ability to bind divalent metal ions via the four, tandem octapeptide repeats in the N-terminal domain. EPR and XAFS studies have revealed that the four histidines contained within the octarepeats are capable of coordinating a single $Cu^{2+}$ ion in square planar geometry with sub-nanomolar affinity(7, 14–16). Each of the individual tandem repeats is also capable of coordinating a single $Cu^{2+}$ ion (for a total of four coordinated $Cu^{2+}$ ions) with a weaker nanomolar affinity if local $Cu^{2+}$ concentrations increase (4, 14, 17). The ability of $PrP^C$ to bind $Cu^{2+}$ has led to speculation that the protein acts as a modulator for $Cu^{2+}$ ion concentration i*n vivo* (18). Consistent with a physiological role for $PrP^C$ in metal ion homeostasis, $Cu^{2+}$ causes cellular redistribution of $PrP^C$ and alters the biochemical properties of the protein. Additional clues to the physiological activities of $PrP^C$, and the role of specific structural elements, have emerged from studies of molecules harboring several kinds of deletion mutations within the N-terminal domain. Deletions spanning a 21-amino acid region (amino acids 105–125) at the end of the flexible, N-terminal domain induce a spontaneous neurodegenerative phenotype with certain similarities to natural prion diseases(19), but

without accumulation of $PrP^{Sc}$ (20–23). Importantly, these phenotypes are dose-dependently suppressed by co-expression of wild-type $PrP^{C}$, suggesting that the wild-type and deleted molecules interact with each other, or compete for binding to a common molecular target that mediates both physiological and pathological effects (19, 21). The shortest deletion, Δ105–125 (designated ΔCR, for central region), produces the most severe neurodegenerative phenotype, and requires the largest amount of wild-type $PrP^{C}$ for rescue (21). In our efforts to understand why these deleted forms of $PrP^{C}$ are so neurotoxic, we have discovered that they induce large, spontaneous ionic currents, recordable by patch clamping techniques, when expressed in a variety of cell lines (24, 25) and in primary neurons (26). These currents are silenced by co-expression of wild-type $PrP^{C}$ in the same cells, paralleling the rescuing effects of wild-type $PrP^{C}$ in transgenic mice expressing deleted $PrP^{C}$(19, 26–28).

Although the flexible, N-terminal domain of $PrP^{C}$ and its structured C-terminal domain have often been described as independent structural elements, several lines of evidence now suggest that these two domains actually interact with each other in a functionally important manner. EPR and NMR studies show that binding of divalent metal ions ($Cu^{2+}$, $Zn^{2+}$) to the octapeptide repeats drives an intramolecular contact between the N- and C-terminal domains (27, 29–31). This *cis* interaction involves a negatively charged surface patch contributed by helices 2 and 3 in the C-terminal

domain. A number of mutations linked to familial prion diseases reside in this region, and NMR experiments demonstrate that some of these mutations cause weakened the N-C interaction, possibly contributing to the disease phenotype(29–31).

Cellular experiments suggest that the N-C domain interaction plays an important functional role in the protein. The ΔCR $PrP^C$ mutant, which elicits spontaneous ionic currents, displays diminished N-C interactions based on NMR analysis, and expression of the N-terminal domain in the absence of the C-terminal domain elicits ionic currents similar to those seen with the ΔCR mutant (27). In addition, antibody ligands that bind to the outer surface of helix 3, potentially disrupting interdomain interactions, induce spontaneous currents, and cause degeneration of the dendrites of cultured neurons (27). Finally, the toxic activities of ΔCR $PrP^C$ are abolished by deletion or mutation of the polybasic sequence KKRPKPGGW at the N-terminus of $PrP^C$, and by ligands ($Cu^{2+}$ ions, glycosaminoglycans, antibodies) that bind to several different regions within the N-terminal domain (27). Taken together, these results have led us to propose a model in which the N-terminal domain of $PrP^C$, including the polybasic sequence, acts toxic effector whose activity is normally auto-inhibited by intramolecular association with the C-terminal domain(28, 31).

Although it is now clear that the N- and C-terminal domains of $PrP^C$ interact, and that this interaction has functional consequences, several

important structural features of the docking phenomenon remained uncertain. First, because the N-terminal is flexibly disordered, NMR experiments could not define which specific amino acid residues within this domain engaged in contact with the C-terminal domain. Moreover, the NMR experiments depended on metal ion-induced changes in $^{15}N$ HSQC cross-peak intensities, so they did not permit analysis of $PrP^C$ conformation in the absence of metal ions, and they did not reveal the location of N-terminal residues distant from the octapeptide repeats (29–31). Finally, since binding interactions between the two domains are likely to be weak and transient, previous spectroscopic studies may not have fully captured all of the relevant contacts. These limitations pose challenges for developing structural models for the critical interdomain docking interactions in $PrP^C$. In this paper, we have overcome these limitations by the combined use of chemical cross-linking/mass spectrometry and multi-dimensional NMR. We have used the distance constraints provided by these techniques, in conjunction with molecular dynamics simulations, to arrive at a refined structural model for N-C domain interactions in $PrP^C$, and the effect of several structurally and functionally relevant mutations. We have tested the functional predictions of our models using patch-clamp recording of ionic currents associated with the different $PrP^C$ mutants. Taken together, our results provide important new insights into the physiological and

pathological activities of $PrP^C$, and their relationship to the domain structure of the protein.

## RESULTS

### Mass Spectrometry Analysis of $PrP^C$'s cis Interaction

Using a cleavable heterobifunctional crosslinker, APDC4, allows for accurate determination of N-C terminal contact points (32). With a total of 11 lysine residues in wild-type and 7 in the N-terminus alone, ADPC4 preferentially cross-links lysines in the unstructured N-terminal domain that flank either end of the octarepeat domain, $^{22}$M**KK**RP**K**PGGW$^{31}$, $^{99}$N**K**PS**K**P**K**TNL$^{108}$, and $^{109}$**K**HVAGAAAAGAVVGGLGGY$^{127}$. Thus, providing an excellent structural complement to NMR $Cu^{2+}$ studies, which depended on the presence of $Cu^{2+}$ ions bound to the octapeptide repeats.

The N-hydroxysuccinimide (NHS) ester conjugates lysines on the N-terminus the while diazirine moiety reacts non-specifically with C-terminal side chains and backbone, where location and amount of crosslink alters upon the addition of $Cu^{2+}$(32). Prior to $Cu^{2+}$ addition but after treatment with APDC4 and UV exposure, we observed that the three lysine-containing peptides in the N-terminal domain of $PrP^C$. Afterwards, the UV reactive end cross-linked to several peptides derived from the C-terminal domain, which implies a structural interaction between the two domains prior to the addition of $Cu^{2+}$(32). The polybasic extreme N-terminus crosslinked with the

C-terminal end of helix α3; Where the central region reacted with two different peptides located between helices α1 and α2 (155-162 and 163-174). Additionally, central region lysines cross-linked with the C-terminal end of α3. This interaction was not measurable by NMR, which indicates a transient interdomain contact prior to the addition of $Cu^{2+}$ that could be on an unobservable timescale for certain spectroscopic methods.

By performing cross-linking with APDC4 in the presence of $Cu^{2+}$, we could determine how binding of this metal altered the N-C interaction. We observed peptides produced in the presence of $Cu^{2+}$ as in its absence, and that the same residues participated in the interaction. However, $Cu^{2+}$ also induced major changes in the relative amounts of several of the cross-linked peptides. Most notably, there was a decrease in cross-links of the polybasic extreme N-terminal and central region to the C-terminal end of helix α3. Conversely, $Cu^{2+}$ substantially increased cross-links of the central region to the C-terminal region between helices α1 and α2. Figure 14A shows the $Cu^{2+}$-induced changes in cross-linking of N-terminal peptides mapped onto the surface structure of the C-terminal domain. The fact that the same cross-linked peptide pairs were observed in the both, suggests that the $Cu^{2+}$-bound and apo conformations of $PrP^C$ normally exist in equilibrium, and $Cu^{2+}$ being responsible for these changes.

To further our characterization of the interaction seen in wild-type, we tested a multitude of disease conferring and designed mutations with

ADPC4. Mutations tested show a substantial decrease of cross-links being formed prior and post addition of $Cu^{2+}$. Deletion mutation, ΔCR, in the presence of $Cu^{2+}$ has a decrease in cross- links formed with the poly basic extreme N-terminus. However, cross-links with the central region were non-existent. This suggests that the residues 105-125 of wild-type $PrP^C$ are critical for maintenance of the normal *cis* interaction between the N- and C-terminal domains. Furthermore, disruption of these critical contact points

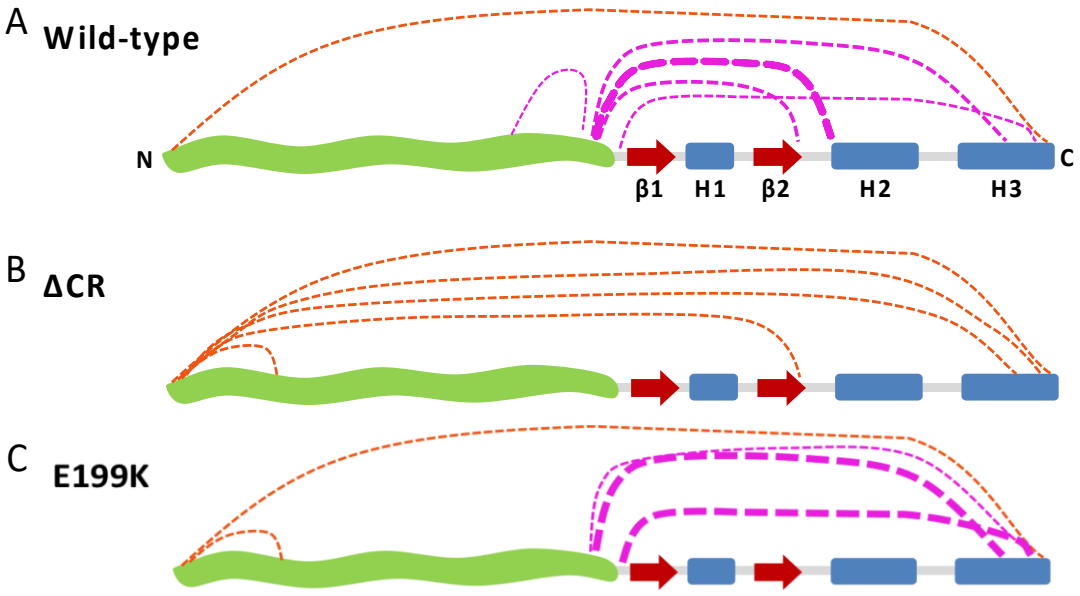


**Figure 14: Linear Diagram of Cross-Linking Sites. C-terminal residues which cross-linked to the peptides $^{23}$MKKRPKPGGW$^{31}$ (orange) and $^{99}$NKPSKPKTNL$^{108}$ (magenta) upon the addition of $Cu^{2+}$ to wild-type and subsequent mutations. The unstructured N-terminus is indicated in green. The C-terminal domain is indicated by red beta strands (1 and 2) and blue α Helices (1,2 and 3).**

E199K, human mutation (E200K), causes familial Creutzfeldt-Jakob disease(33, 34). E199 MoPrP contributes to an electronegative patch on the surface of helices $\alpha$2 and $\alpha$3, and previous NMR studies have demonstrated that this patch represents a docking site for $Cu^{2+}$ and $Zn^{2+}$ ions bound the octapeptide repeats (29, 31, 35). We found that, the most notable difference between E199K and wild-type $PrP^C$ was the absence of cross-links between the 99-127 region in the central domain and the 155-174 region between helices $\alpha$1 and $\alpha$2, a feature also seen in ΔCR $PrP^C$. These results suggest that toxicity from ΔCR $PrP^C$ and mutation E199K due to a lack of proper *cis* interaction maintenance.

NMR analysis of N-C domain interactions in $PrP^C$

The cross-linking experiments just described depended on the presence of lysine residues in the N-terminal domain for attachment to one end of the APDC4 cross-linker(32). Therefore, these experiments could provide structural information only for inter-domain interactions that involved peptides flanking the octapeptide repeats (22-31, 99-108, and 109-127), but not for those involving the octapeptide region itself (51-90), which lacks lysine residues. To address this gap, we turned to multi-dimensional NMR experiments, in which $Cu^{2+}$ ions bound to the octapeptide repeats served as a probe for the location of the N-terminal domain in its interactions with the C-terminal domain. Previous work demonstrated that both $Cu^{2+}$ and $Zn^{2+}$

coordination to the OR domain promotes a *cis* interaction between this segment and an electronegative surface patch formed primarily by helices $\alpha$2 and $\alpha$3 in the C-terminal domain of $PrP^C$ (29–31).

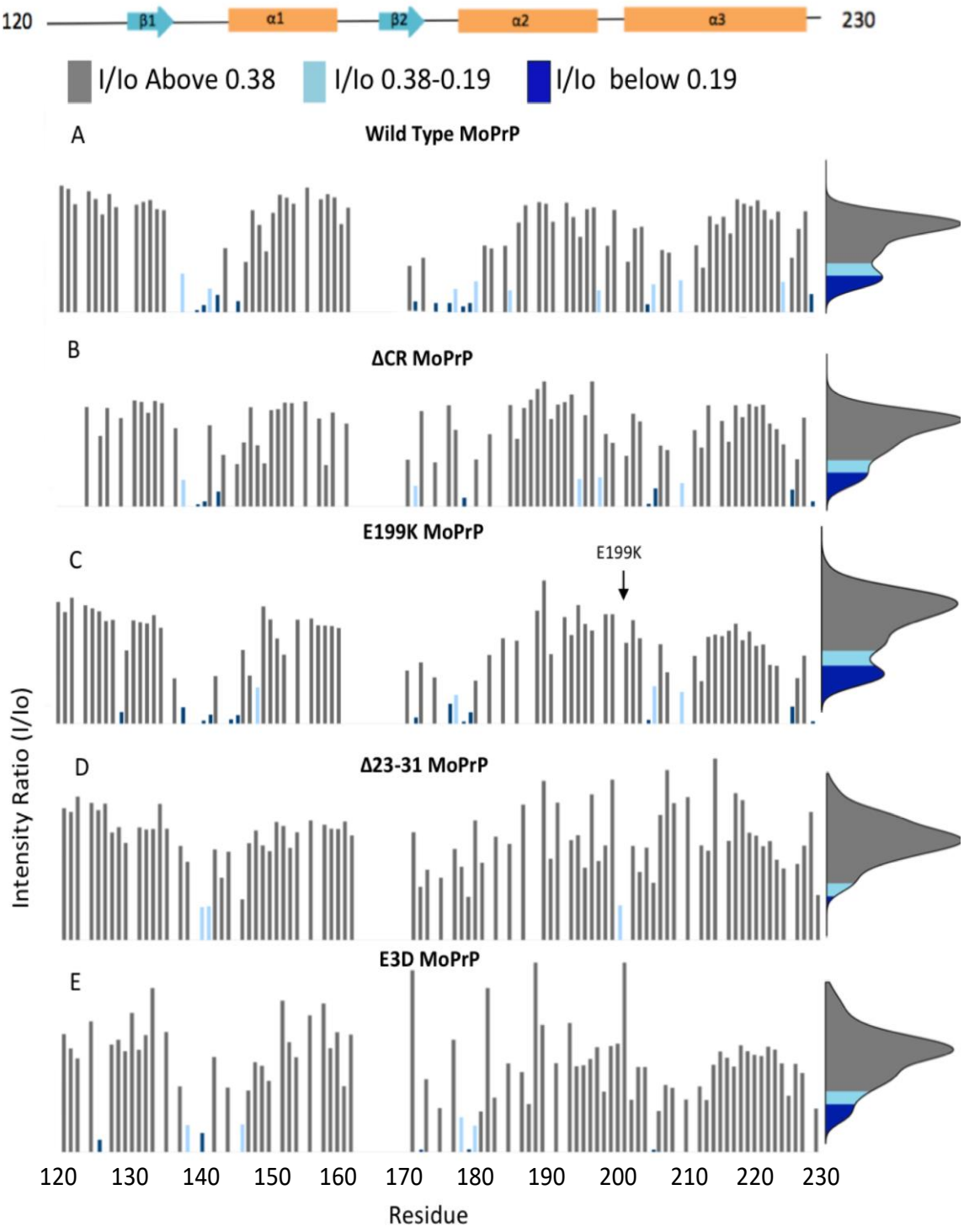


**Figure 15 Intensity ratios $I/I_o$ as a function of position along the C-terminal globular domain. Relevant secondary structural elements are indicated along the top; associated kernel density distributions are on the right. Wild type $PrP^C$ , in the presence of 1.0 eq. $Cu^{2+}$ gives the greatest population of strongly affected**

**residues, as indicated by low $I/I_o$ (blue). The majority of these residues are along helices 2 and 3, and several residues at the N-terminal end of helix 1. The mutant forms of $PrP^C$ show, without exception, fewer affected residues consistent with a weaker cis interaction.**

To determine how mutations and N-terminal deletions in $PrP^C$ affected this *cis* interaction, we performed $^1H$-$^{15}N$ HSQC NMR on uniformly $^{15}N$,$^{13}C$-labeled $PrP^C$ in the presence and absence of 300 μM $Cu^{2+}$ at pH 6. Backbone resonance assignments were obtained using a suite of triple-resonance NMR experiments. Paramagnetism of the $d^9$ center of $Cu^{2+}$ broadens the NMR signals of proximal residues through distance-dependent paramagnetic relaxation enhancement (PRE) (30, 36). Therefore, broadening of specific peaks in the structured, C-terminal domain can be used as an indicator of the proximity of the corresponding residues to $Cu^{2+}$ ions bound to the octapeptide repeats.

In these experiments, the extent of N-C interaction was quantitated by calculation of intensity ratios, $I/I_o$, where I and $I_o$ are the cross peak amplitudes from $^1H$-$^{15}N$ HSQC NMR spectra in the presence and absence of $Cu^{2+}$, respectively. The bar graphs in Fig. 15 show the $I/I_0$ ratios plotted for each residue in the C-terminal domain of wild type $PrP^C$ and all five of the $PrP^C$ mutants tested here. The intensity ratios were categorized into three groups (>0.62, black; 0.62-0.31, light blue; and <0.31, dark blue), reflecting weak, medium, and strong PRE values, respectively. The intensity ratios were also transformed to kernel density distributions, using Gaussian-weighted sliding windows, to provide an unbiased metric of the relative

number of C-terminal residues affected by the $Cu^{2+}$-occupied octapeptide repeats (Fig. 15, traces to the right of each bar graph). Finally, to visualize these $Cu^{2+}$-induced effects in terms of the three-dimensional structure of $PrP^C$, the $I/I_0$ ratios for each residue were mapped onto the crystal structure of the C-terminal domain (Fig. 16), using the same color scheme as in Fig. 15 to indicate weak, medium, and strong PRE effects.

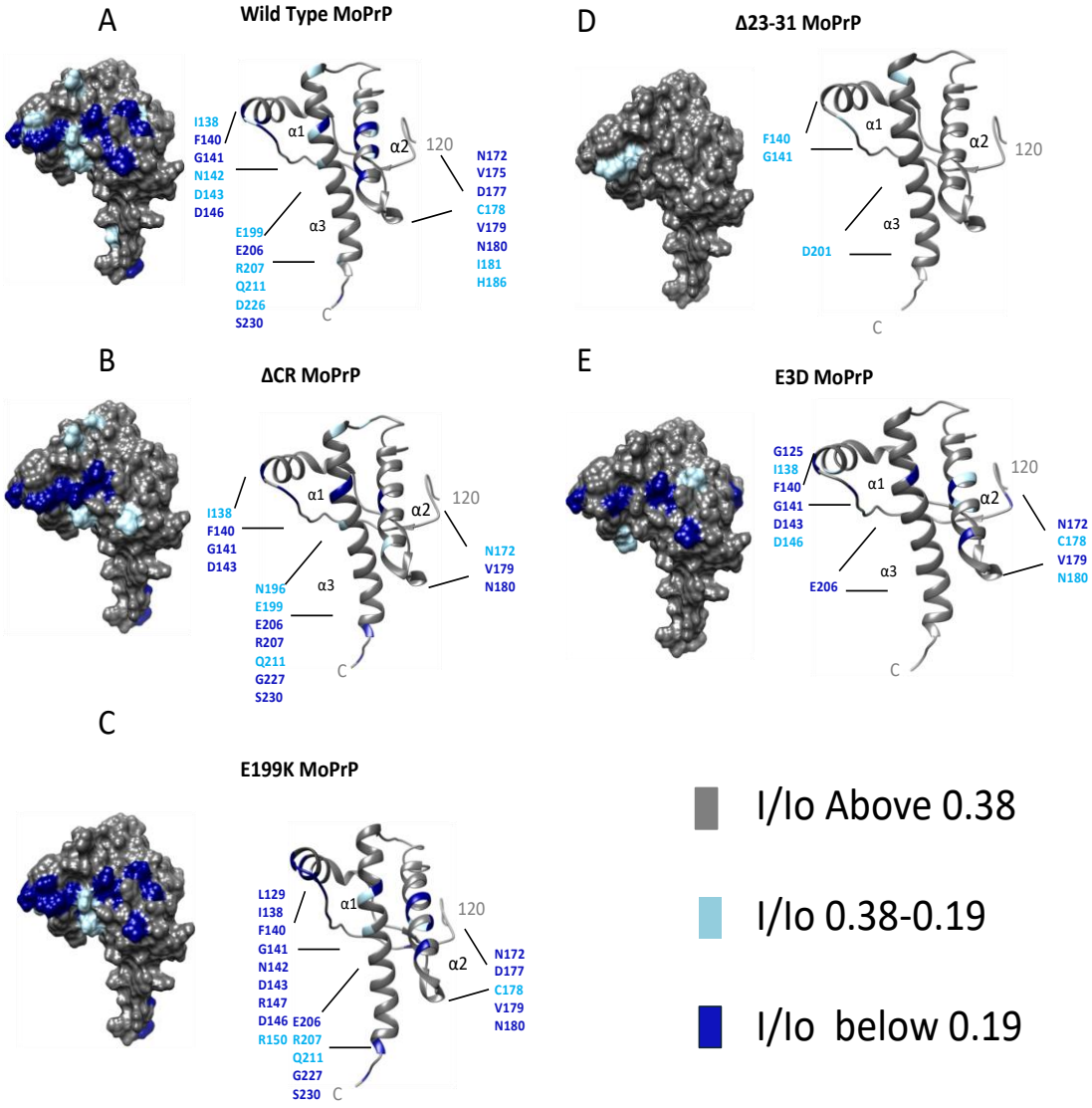


**Figure 16 Surface plots of the $PrP^C$ C-terminal domain displaying residue positions weakly affected (light blue) and strongly affected (dark blue) by PRE from the $Cu^{2+}$-occupied OR domain. The shown patches identify the docking surface for the interdomain cis interaction. Consistent with Figure 15, wild type $PrP^C$ exhibits the most pronounced docking patch, whereas $PrP^C$ Δ23-31 is almost devoid of a docking surface. The other mutants are in between these two**

**extremes. Note that broadened resonances from buried residues are not visible in these surface plots.**

For wild-type $PrP^C$, these data confirm our previously published results indicating that octapeptide-bound $Cu^{2+}$ interacts with most strongly ($I/I_0$ <0.31) with three different regions in the C-terminal domain (Figs. 15A and 116A): the N-terminal end of the $\beta$1-$\alpha$1 loop, extending to the beginning of helix 1; the N-terminal half of helix $\alpha$2; and the N-terminal half of helix $\alpha$3. The strength of these interactions is reflected in the kernel density distribution for wild-type $PrP^C$ (Fig. 15A), which shows two distinct maxima, one near $I/I_o = 1$, representing unaffected residues, and another at approximately 0.2, arising from strong, $Cu^{2+}$-induced PRE.

We next used the same techniques to analyze $PrP^C$ to characterize two mutations we studied using cross-linking (ΔCR, and E199K), as well as two additional mutations (Δ23-31 and E3D). The latter mutations encompass functionally important polybasic residues at the extreme N-terminus. To facilitate comparison of the wild-type and mutant proteins, Fig. 17 shows surface structures onto which are mapped those residues in the mutant protein that are no longer affected by $Cu^{2+}$ in comparison with the wild-type protein.

In previous experiments, performed at pH 5.5, we showed that the ΔCR mutation caused a significant reduction in $Cu^{2+}$-induced N-C interactions (27, 37), a result confirmed here at pH 6.0. The surface map (Figs. 16B,

17B) shows a loss of strong PRE values (dark blue) along helices 2 and 3, and the kernel density plot (Fig. 15B) shows a global reduction in the peak centered on 0.2 with a corresponding increase in the peak centered on 1. The E199K mutant shows a subtle decrease in the population of both weakly and strongly affected residues, consistent with a weakening of the *cis* interaction (Figs. 15D, 16D, 17D). Interestingly, the affected residues, showing a loss of PRE broadening, are dispersed throughout the C-terminal domain, as opposed to being localized to a specific C-terminal patch.

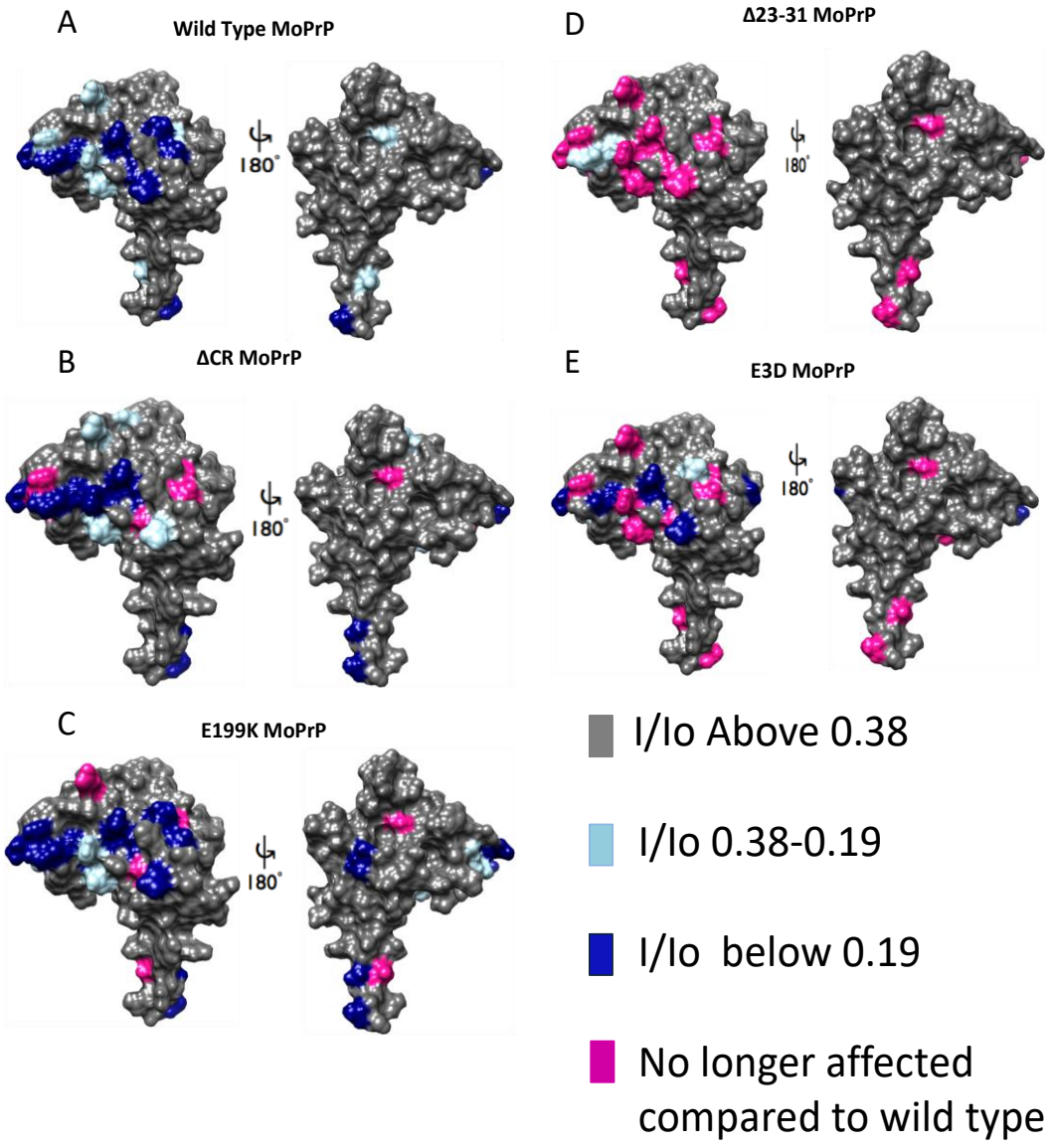


**FIGURE 17: Surface map of PRE-differences between mutant & wild-type $PrP^C$.**

Finally, we examined the role of the polybasic N-terminal segment, residues 23-31, in the $Cu^{2+}$-dependent *cis* interaction. This region is functionally important, since deletion of this segment eliminates the spontaneous ionic currents induced by ΔCR, and abrogates the ability of wild-type $PrP^C$ to suppress these currents in a dose-dependent fashion (11). This region is also essential for the neurodegenerative phenotype of certain deleted forms of $PrP^C$ in transgenic mice. Mutations affecting the 23-31 region had the most dramatic effect of all the ones we analyzed. As shown in Figs. 15E, 16E, and 17E, deletion of this region in Δ23-31 led to a nearly complete loss of $Cu^{2+}$-induced line broadening. To test the role of the positively charged residues within this segment, we generated a new mutant (E3D) in which the basic residues were replaced with acidic residues (K23E, K24E, R25D, K27E). These mutations also abrogate the ionic currents associated with ΔCR (27, 28). As seen in Figs. 15F, 16F, and 17F, this mutant was also impaired in its N-C interactions, although not as much as the Δ23-31 mutant. We conclude from these data that residues 23-31 play a significant role in stabilizing the *cis* interaction of copper-bound $PrP^C$, and this effect depends on the intrinsic positive charge of this segment.

**Electrophysiology**

We wanted to correlate our cross-linking and NMR analysis of the $PrP^C$ mutants with their functional activity based on electrophysiological measurements. We showed previously that cultured cells expressing $PrP^C$

molecules harboring the ΔCR deletion, as well as several point mutations associated with familial prion diseases, display spontaneous, inward currents that can be recorded by patch-clamping techniques (11, 27). We did not detect any current activity in cells expressing E199K, similar to cells expressing wild-type $PrP^C$. The lack of current activity associated with E199K correlates with the fact that N-C domain interactions are less perturbed in this mutant compared to either ΔCR, based on cross-linking and NMR experiments.

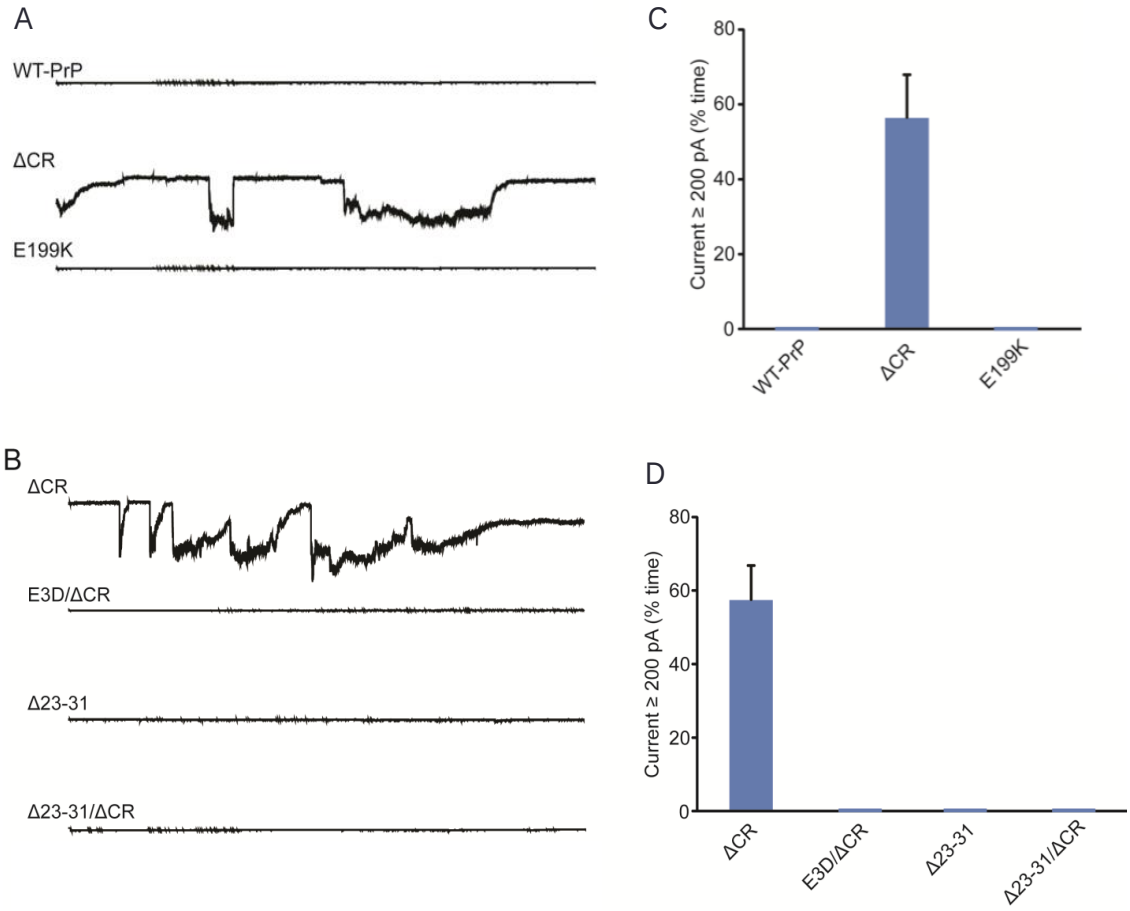


**Figure 18 Electrophysiological Studies of MoPrP Constructs. (A) Left, representative traces of currents recorded from N2a cells expressing wild-type**

**$PrP^C$, ΔCR, or E199K. Right, quantitation of the currents, plotted as the percentage of the total time the cells exhibited inward current ≥ 200 pA (mean ± S.E.M., n=10). B) Left, representative traces of currents recorded from N2a cells expressing ΔCR, E3D/ΔCR, Δ23-31 or Δ23-31/ ΔCR. Right, quantitation of the currents, plotted as the percentage of the total time the cells exhibited inward current ≥ 200 pA (mean ± S.E.M., n=10). Scale bars in all panels: 1 nA, 30 s.**

Given the importance of the 23-31 region in stabilizing N-C domain interactions, as indicated by the NMR experiments, we wished to test its role in induction of ionic currents. We confirmed our previous observations that deletion of the N-terminal polybasic region (Δ23-31) or reversal of positive charges within this region (E3D) abolished the current activity associated with the ΔCR mutant (Fig. 18B). Moreover, removal of the 23-31 region in the context of the wild-type protein did not produce currents. Thus, although the 23-31 region is essential for stabilization of N-C interactions in $PrP^C$, it is also required for the membrane perturbations that are responsible for abnormal ionic current activity.

## DISCUSSION

In this study, we have utilized chemical cross-linking/mass spectrometry, in combination with NMR, to define, on an individual residue level, points of contact between the N- and C-terminal domains of $PrP^C$ in the presence and absence of metal ligands. In addition, we have analyzed how several kinds of $PrP^C$ mutations affect N-C domain interactions, and have characterized how these structural effects correlate with the behavior of the mutants in a cellular assay for $PrP^C$ physiological activity. Taken together, our results provide a detailed structural model for the docking interactions of the N-

and C-terminal domains of $PrP^C$, and lead to hypotheses about the role of this intramolecular switch in the physiological and pathological functions of the protein. Our results also illustrate the power of chemical cross-linking to define molecular interactions of flexibly disordered protein regions.

In the absence of $Cu^{2+}$ or $Zn^{2+}$, $PrP^C$ consists of a flexibly disordered N-terminal domain linked to a structured, C-terminal domain consisting of three $\alpha$-helices ($\alpha$1-$\alpha$3) and two short $\beta$-strands flanking helix $\alpha$1. Historically, the N- and C-terminal domains have been treated as structurally independent. Considerable evidence now indicates, however, that these two domains interact with each other in a highly regulated way that plays an important role in the physiological and pathological functions of protein. The N-terminal domain includes a series of four, histidine-containing octapeptide repeats that bind $Cu^{2+}$ and $Zn^{2+}$, and these ions have been shown to induce a specific interaction between the two halves of the molecule. This phenomenon has been previously characterized using NMR and EPR, leading to identification of a negatively charge surface patch encompassing helices $\alpha$2 and $\alpha$3 upon which the N-terminal domain docks when bound to $Cu^{2+}$ and $Zn^{2+}$ ions in the octapeptide repeat region. However, these experiments did not determine whether other regions of the N-terminal domain flanking the octapeptide repeats participated in the N-C interaction, and they did not address whether intramolecular docking occurred in the absence of metals (38).

Our combined cross-linking and NMR experiments identify three critical regions within the N-terminal domain of $PrP^C$ that associate with the C-terminal domain: the N-terminal, polybasic tail (23-31), the octarepeats (59-90), and the central region (99-127). The locations of the polybasic tail and central region in the docked structure were identified by cross-linking, and the location of the octapeptide repeat by virtue of $Cu^{2+}$-induced paramagnetic relaxation in the NMR spectra. In the absence of $Cu^{2+}$, the N-terminal, polybasic tail cross-linked to the end of helix 3, suggesting an important docking association between the extreme ends of the polypeptide chain. In addition, there were cross-links between the central region and the region between helices $\alpha$1 and $\alpha$2 (encompassing strand S2), as well as the end of helix $\alpha$3. Addition of $Cu^{2+}$ ions induced major changes in the interdomain conformation of the protein. $Cu^{2+}$ binding forced the octapeptide repeats into an interaction with a negatively charged patch on the face of helices $\alpha$2 and $\alpha$3 (as evidenced increased PRE), coincident with increased cross-linking between part of the central region and the $\alpha$1/$\alpha$2 linker, and loss of cross-linking between the polybasic tail and helix $\alpha$3.

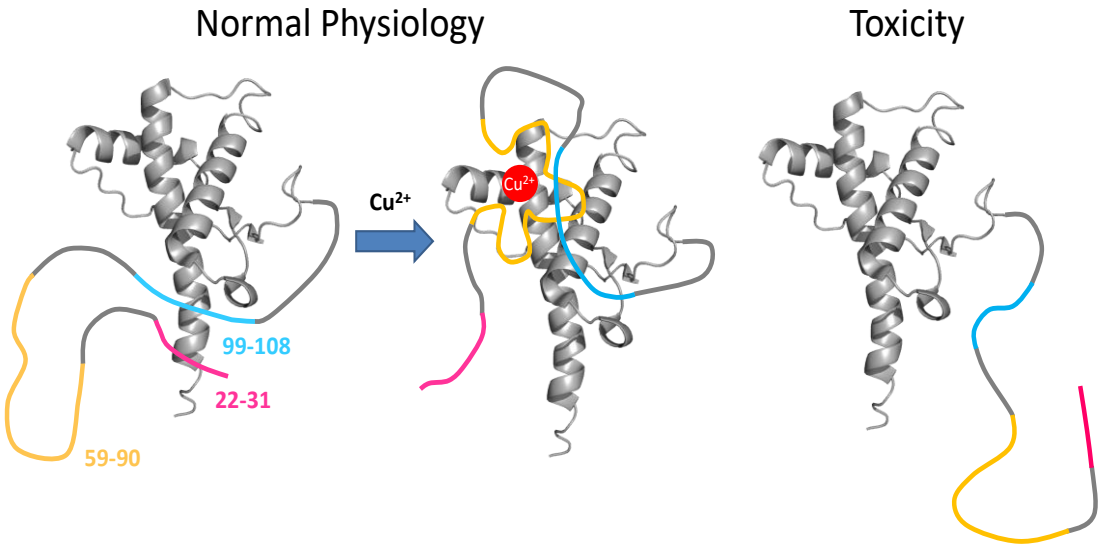


**Figure 19 Model of MoPrP$^{C}$ in the absence and presence of $Cu^{2+}$. In the absence of $Cu^{2+}$, both the N-terminus (magenta) and central region (blue) associate with the end of α-helix 3 (left). $Cu^{2+}$ coordination to the octarepeat domain (gold) promotes association with the beginning of α-helix 3 (middle). When mutations or other events cause the N-terminus to become completely dislodged from the C-terminus, toxicity ensues (right).**

Our results also allowed us to determine how several functionally and structurally important mutations affect the interdomain conformation of PrP$^{C}$. The highly toxic ΔCR deletion completely disrupted cross-linking between the central region (adjacent to the deletion) and the C-terminal domain, leaving only cross-links involving the 22-31 peptide, several of which were not present in the wild-type protein, possibly reflecting relaxation of the normal constraints on the position of this region. The ΔCR deletion also dramatically reduced PRE interactions between octapeptide repeat-bound $Cu^{2+}$ and helices α2 and α3. Overall, consistent with our previous report, the ΔCR deletion diminished the extent of N-C interdomain association, in both the presence and absence of $Cu^{2+}$. The human

pathogenic mutation E199K had effects that were similar to those of the ΔCR deletion, but more subtle. Like the ΔCR deletion, the E199K mutation disrupted cross-links between the central domain and the α1-α2 loop, although other cross-links involving the central region and the C-terminal domain were preserved, as were cross-links involving the N-terminal polybasic region. Similarly, E199K caused diminished PRE interactions between octapeptide repeat-bound $Cu^{2+}$ and helices α2 and α3, although fewer residues comprising this interaction surface were affected compared to ΔCR.

The two mutations with the most dramatic effects were those affecting the N-terminal, polybasic domain (22-31), which we analyzed by NMR. Deletion of the polybasic region in Δ22-31 almost completely abolished $Cu^{2+}$-induced interaction between the N- and C-terminal domains, and mutating the four positive residues in this region to negative ones greatly diminished the interaction. These experiments demonstrate that the N-terminal, polybasic region plays a crucial role in mediating interdomain interactions in $PrP^C$. Since this region is separated from the octapeptide repeat region by approximately 30 residues, and is not involved in $Cu^{2+}$ binding, it is remarkable that deletion or mutation of the polybasic region has such a dramatic effect on the $Cu^{2+}$-driven conformation of $PrP^C$ (7, 27, 31, 37). A likely explanation is that the polybasic region plays an important role in stabilizing N-C domain interactions independent of $Cu^{2+}$ binding, a

conclusion consistent with our detection of cross-links between the 22-31 peptide and C-terminal domain peptides in the wild-type and all mutant versions of $PrP^C$ in both the presence and absence of $Cu^{2+}$.

An important structural role for the polybasic region is consistent with evidence that this region is essential for several kinds of $PrP^C$-related functional activities and molecular interactions. These include clathrin-mediated endocytosis, $Zn^{2+}$ transport, and APP proteolytic cleavage, which are dependent upon $PrP^C$ interactions with LRP1, AMPA receptors, and BACE1, respectively (39–42). Moreover, deletion or mutation of the polybasic domain abolishes the aberrant ion channel activity associated with the ΔCR $PrP^C$ mutant, as well as the ability of wild-type $PrP^C$ to rescue ΔCR $PrP^C$ -related toxic activities (27, 43, 44). Neurons expressing $PrP^C$ harboring a Δ23-31 deletion are resistant to the synaptotoxic effects of exogenously applied $PrP^{Sc}$. Finally, the 23-31 region is important for efficient conversion of $PrP^C$ to $PrP^{Sc}$ (Turnbaugh et al., 2011). Taken together, these data suggest that the N-terminal, polybasic region of $PrP^C$ may, by virtue of its interactions with the C-terminal domain, promote or stabilize an interdomain conformation that is essential for various physiological and toxic activities of the protein and for its ability to associate with other cell-surface receptors.

The structural studies reported here strongly support the interdomain regulatory model we have developed to explain the toxic activity of $PrP^C$.

We have proposed that the flexible N-terminal domain of $PrP^C$ can act as a toxic effector whose activity is normally inhibited by a *cis* interaction with the structured C-terminal domain (27). Manipulations that perturb this interaction, including deletion of the central region (in ΔCR $PrP^C$), substitution of the C-terminal domain with an unrelated protein (GFP), or binding of antibodies targeting the N-C interaction surface, unleash several kinds of toxic processes, including abnormal ion channel activity, dendritic degeneration, and neurological disease in transgenic mouse models. The altered cross-linking pattern and diminished $Cu^{2+}$-induced PRE effects described here for ΔCR $PrP^C$, which imply decreased N-C interactions, are consistent with this model. The more subtle effect of E199K, and other mutations that weaken N-C interactions (27, 29), might explain the pathogenicity of these mutations in human beings, in which the mutant proteins are expressed over many years. The electrophysiology experiments reported here, in which ΔCR produced strong ionic current activity, while E199K has weaker effects, is also consistent with the model.

There is evidence that $PrP^C$ serves as a cell-surface receptor for several kinds of neurotoxic protein aggregates, including $PrP^{Sc}$, Aβ, α-synucelin, and tau (45, 46). Some of these aggregates bind to the N-terminal domain of $PrP^C$, and it is possible that this disrupts normal N-C domain interactions, thereby contributing to neurotoxic signaling. Interdomain interactions may play a role in $PrP^C$/$PrP^{Sc}$ conversion.

Our results raise the possibility that interdomain interactions may also play an important role in the physiological activity of $PrP^C$. The most obvious potential connection would be in the realm of copper metabolism. The fact that $Cu^{2+}$ promotes reversible formation of specific molecular contacts between the N- and C-terminal domains of $PrP^C$(30, 31) would be consistent with a role for the protein as a transporter or sensor of $Cu^{2+}$ ions. For example, it has been reported that $Cu^{2+}$ ions, which are released during neurotransmission (47), drive $PrP^C$ to associate with NMDA receptors, facilitating their desensitization to glycine (40). Thus, the structural rearrangement of $PrP^C$ in response to $Cu^{2+}$ provides a mechanism by which $PrP^C$ can selectively regulate excitotoxic effects of the NMDA receptor. Many multi-domain proteins undergo conformational rearrangements as a feature of their functional activity. Particularly relevant to the case of $PrP^C$ are examples where a posttranslational modification or ligand binding relieve or enhance an inhibitory interaction between two protein domains, resulting in altered catalytic activity (48). Interdomain rearrangements in proteins have been studied by several different techniques, including, NMR (49, 50). However, characterizing these conformational changes is particularly challenging when the protein domains involved are flexibly disordered, and the interactions are weak or transient, as is the case for $PrP^C$. By using covalent cross-linking in combination with NMR and molecular dynamics simulations, we have been able to overcome this limitation. We

have generated a new molecular model for the interactions between the two halves of the $PrP^C$ molecule and connected these with the physiological and pathological activities of the protein.

**METHODS**

Synthesis of APDC4

DABCO was obtained from commercial suppliers and used without further purification. A mixture of DABCO (**1**; 0.58 g, 5.1 mmol) in ethyl acetate (15 mL) was stirred at room temperature until all solids had dissolved and was then cooled in an ice bath. To this was added dropwise a freshly prepared ethyl acetate solution (10 mL) of 3-(2-iodoethyl)-3-methyl-3*H*-diazirine (Shigdel e al., 2008 ) (**2**; 0.90 g, 4.3 mmol), derived from the alcohol made by the method of Kambe (Kambe e al., 2014). After addition was complete (~ 8 min), the bath was removed and the solution was stirred at room temperature for 6 days during which a white solid precipitated. The solids were collected by filtration, washed with 1:3 ethyl acetate:hexanes (4 x 20 mL), and dried to give **3** (1.12 g, 81 %) as an off-white powder. $^1$H NMR (400 MHz, DMSO-$d_6$): $\delta$ 3.22 (m, 6H), 3.00 (s, 8H), 1.78 (m, 2H), 1.08 (s, 3H).

*Conjugation of $PrP^C$ with APDC4, cross-linking, and preparation for MS analysis*

Lyophilized recombinant $PrP^C$ was resuspended in 0.2 µm filtered $H_2O$ to generate 200 µM samples. After waiting >10 minutes to let the lyophilized peptide redissolve, samples were diluted by 50% in 50 mM MOPS pH 7.4 to a

protein concentration of 100 μM and a MOPS concentration of 25 mM. APDC4 cross-linker ($M_r$ 586.26) was dissolved in sterile filtered $H_2O$ to generate a 10 mM stock solution. Two Molar equivalents of APDC4 were added to each protein sample: *i.e.* 2 μL of APDC4 per 100 μL of protein sample. Samples were conjugated with APDC4 by incubation at 4 °C for at least 2 hrs. Excess APDC4 was removed from samples by Amicon Ultra 0.5 mL centrifugal filters, Ultracel-10K cutoff (Millipore). Samples were centrifuged in the spin filters, then resuspended in 400 μL of nitrogen-degassed 25 mM MOPS pH 7.4. The dilution/concentration steps were repeated two times. Samples retained in the spin filter were the collected, and their absorption at 280 nm was determined using a Nanodrop 2000c (Thermo Scientific) and used to calculate the protein concentration.

Samples were then diluted in nitrogen-degassed 25 mM MOPS pH 7.4 in order to achieve a final protein concentration of 10 μM. Samples were divided into 100-μL aliquots in low-binding 1.5 mL tubes (Fisherbrand). Four separate replicates were prepared for each $PrP^C$ construct (wild-type, ΔCR and E199K) and each condition (+/- Cu2+). For samples in which the effects of $Cu^{2+}$ were being tested, two-equivalents of 1 mM copper(II) acetate was added to each sample (2 μL of $Cu^{2+}$ per 100 μL protein sample). Samples were then given at least 10 minutes to incubate at 25 °C in the dark in order to allow the $Cu^{2+}$ to coordinate to the protein. Samples were then placed in a metal block pre-chilled to 4 °C, and exposed to UV A light (360

nm) for six hours in a Crosslinker Select (Spectroline) kept in a 4 °C cold room. The metal block holding the samples was swapped with another pre-chilled block every hour in order to prevent the UV light from excessively heating the samples and causing the protein to denature.

After cross-linking, samples were reduced with dithiothreitol (DTT) (5 mM final concentration) and incubated at 50 °C for one hour. Samples were then alkylated by adding iodacetamide (10 mM final concentration) and incubating at 37 °C for one hour. The pH of the samples was adjusted with 1 M Tris pH 9 to achieve a final pH of 8. Excess iodacetamide was quenched by adding additional DTT (5 mM more DTT added). The pH of the samples was verified to be 7.5-8, and then 1 µg of sequencing grade chymotrypsin (Promega) was added per sample. Samples were then subjected to clean-up using Pierce C-18 Tips, 100 µL (Thermo Scientific) following the manufacturer's recommendations, and dried in a SPD1010 Speedvac System (Thermo Scientific). Finally samples were resuspended in 40 µL of HPLC grade $H_2O$ containing 1% acetonitrile (ACN)/0.1% formic acid, and transferred to 100-µL autosampler vials (Thermo Scientific) for MS analysis.

nUPLC-MS/MS data acquisition and analysis

Three different types of MS experiments were performed, all using the same chromatography methodology and system: (1) Survey; (2) Targeted; and (3) $MS^1$-only. Two-µL aliquots were analyzed in each MS experiment. The

aliquots were injected into a nanoAcquity-UPLC (Waters) equipped with reversed phase columns: 5-µm Symmetry C18, 180 µm x 20 mm, trap column and 1.7 µm BEH130 C18, 150 µm x 100 mm, analytical column (Waters). The nano-UPLC was connected online to a Q Exactive HF Hybrid Quadrupole Orbitrap Mass Spectrometer (Thermo Scientific) equipped with a Triversa NanoMate (Advion) electrospray ionization (ESI) source operated at 1.7 kV, in order to generate a constant nanoESI plume. The sample was loaded onto the precolumn, washed for 4 min at a flow of 4 µL/min with 100% Mobile Phase A/% (1% ACN/0.1% FA/Water). After the trapping event, the peptides were eluted to the analytical column and resolved by a gradient of 3-40% mobile phase B (1% $H_2O$/0.1% FA/ACN) delivered over 90 min at a flow rate of 500 nL/min. For all acquisitions, the MS was operated in positive ion mode. The sample ions were introduced through a heated capillary ion transfer tube (250 °C) and a stacked ring ion guide (RF Lens (S-lens)) operated at 55 V. The $MS^1$ scan was set at a resolution of 60,000 @ *m/z* 200, to cover the scan range *m/z* 370-1800, 1 µscan/spectrum, maximum injection time (ion accumulation time) of 100 ms with a target automatic gain control (AGC) of 1 x $10^6$ ion population. Solvent background ions at *m/z* 371.1012, 391.2843, and 455.1200 were used as Lock Masses to calibrate the $MS^1$ mass spectra, which were acquired in the profile mode.

<u>nUPLC-MS/MS survey</u>

The experiment was performed in automatic Data Dependent Acquisition "top 20" mode. Ions with charge state ≥3 in the survey MS scan were selected, using a 1.6-Da isolation window, and were fragmented in the HCD cell with a normalized collision energy (NCE) of 15 V. The $MS^2$ scan events were acquired at 15,000 resolution @ *m/z* 200, AGC target 1 x $10^5$, 50 ms maximum injection time, 3 μscan/spectrum;the scan started at *m/z* 100. The dynamic exclusion feature was set to 8 s. The minimal AGC target for $MS^2$ was 1 x $10^4$ with a signal threshold of 2 x $10^5$. The peptide recognition feature was enabled and charge states of < 3+ or ≥ 8+ were rejected for $MS^2$. To identify potential APDC4 cross-linked precursors, the Thermo RAW files were converted to mzML using Proteome Discoverer 1.4. These mzML files were then processed using software developed in-house. The protein sequences for wild-type and mutant $PrP^C$ were digested *in-silico*, and the resulting peptides were categorized according to their potential cross-linker binding site. Each pair of peptides whose combination contained both binding sites, and whose combined mass plus the mass of the reacted cross linker was within 5 ppm of the precursor mass, was considered a potential match. The list of potential matches was filtered to include only pairs that corresponded to intact peptides with the expected XL-marks (i.e., 68.0262 Da for the NHS-ester reactive peptide and 166.1470 Da for the diazarine generated.

Protein expression, purification, and isotope labeling

Plasmids encoding *Mus musculus* $PrP^C$ in the pJ414 vector (DNA 2.0) were expressed in *E. coli* (BL21 (DE3); Invitrogen). Codon mutations were introduced using PCR-based site-directed mutagenesis with mutagenic primers (Invitrogen) and Phusion DNA Polymerase (Finnzymes). All constructs were confirmed by DNA sequencing. For NMR experiments, bacteria were grown in M9 minimal media supplemented with $^{15}NH_4Cl$ (1 g/L) or $^{15}NH_4Cl$ and $^{13}C_6$-glucose (2.5 g/L) (Cambridge Isotopes). Cells were grown at 37 °C until they reached an $OD_{600}$ of 0.6, at which they were then transferred to the M9 minimal media and protein expression was induced with 1 mM isopropyl-1-thio-D-galactopyranoside (IPTG) for 3 hours.
All $PrP^C$ constructs were purified as previously described (Spevacek et al. 2013). Briefly, proteins were extracted from inclusion bodies with 8 M guanidium chloride (GdnHCl) (pH 8) at room temperature and were purified by $Ni^{2+}$ immobilized metal-ion chromatography (IMAC). Proteins were eluted from the IMAC column in 5 M GdnHCl (pH 4.5) and were brought to pH 8 with KOH and left at 4°C for 2 days to oxidize the native disulfide bond. Proteins were then desalted into 10 mM KOAc buffer (pH 4.5) and purified by reversed-phase high performance liquid chromatography (HPLC) on a C4 column. The purity and identity of all constructs were verified by analytical HPLC and mass spectrometry (ESI-MS). Disulfide oxidation was confirmed by reaction with *N*-ethylmaleimide and subsequent ESI-MS analysis.

Nuclear magnetic resonance spectroscopy

All samples were prepared at 300 μM PrP in a buffer containing 10 mM MES (Fisher) and 10% D2O, at pH 6.0. Copper containing samples also contained 300 μM $CuCl_2$. $^{1}H$-$^{15}N$ HSQC spectra were recorded at 37 °C on a Varian INOVA 600-MHz spectrometer at UCSC NMR facility (Santa Cruz, CA). NMR spectra were analyzed with NMR Pipe and Sparky. Structural analysis was done with Chimera using protein assignments from Evans et al. (2016).

In order to separate the residues involved in the *cis*-interaction from the rest of the protein, we performed a kernel density estimation on the data using a Gaussian smoothing kernel in R. We observed a bimodal distribution of intensity ratios ($I/I_0$), representing peaks involved and uninvolved in the *cis*-interaction. To eliminate the effects of differential unspecific broadening across mutants, the data were scaled so that the center values of each mutant's uninvolved mode were aligned. The local minimum between the two modes ($I/I_0 = 0.38$) was used as a cutoff to discriminate involved from uninvolved residues, and uninvolved residues were plotted on the protein in grey. We further divided the residues involved in the *cis*-interaction into two categories based on the broadening of their peaks: strongly broadened ($I/I_0$ = 0 to 0.19, plotted on the protein as dark blue), and weakly broadened ($I/I_0 = 0.19$ to 0.38, plotted on the protein as light blue). The cutoff values derived from WT PrP were used as cutoffs for all mutants.

Electrophysiological analysis

pcDNA3.1(+)Hygro plasmids (Invitrogen) encoding wild-type, ΔCR, ΔCR/Δ23-31, Δ23-31, or ΔCR/E3D PrP have been described previously {Solomon et al., 2010; Solomon et al., 2011;Turnbaugh et al., 2011 }.

N2a cells (ATCC Cat. #CCL-131, RRID: CVCL 0470) were maintained in DMEM supplemented with nonessential amino acids, 10% fetal bovine serum, and penicillin/streptomycin. The N2a cell line we used in this study is mycoplasma free. Cells were transiently co-transfected using PureFection (System Biosciences, Cat. # LV750A-1) with pEGFP-N1 (Clontech), along with empty pcDNA3.1(+)Hygro vector, or vector encoding wild-type or mutant $PrP^C$. Cell-surface expression of all $PrP^C$ constructs was confirmed by immunofluorescence staining.

Recordings were made from N2a cells 24-48 hrs after transfection. Transfected cells were recognized by green fluorescence resulting from co-transfection with pEGFP-N1. Whole-cell patch clamp recordings were collected using standard techniques. Pipettes were pulled from borosilicate glass and polished to an open resistance of 2–5 megaohms. Experiments were conducted at room temperature with the following solutions: internal, 140 mM Cs-glucuronate, 5 mM CsCl, 4 mM MgATP, 1 mM $Na_2GTP$, 10 mM EGTA, and 10 mM HEPES (pH 7.4 with CsOH); external, 150 mM NaCl, 4 mM KCl, 2 mM $CaCl_2$, 2 mM $MgCl_2$, 10 mM glucose, and 10 mM HEPES (pH 7.4 with NaOH). Current signals were collected from a Multiclamp 700B

amplifier (Molecular Devices), digitized with a Digidata 1440 interface (Axon Instruments), and saved to disc for analysis with PClamp 10 software.

## REFERENCES


1. Prusiner, S. 1982. Novel proteinaceous infectious particles cause scrapie. Science (80-. ). 216: 136–144.

2. Prusiner, S.B. 1997. Prion Diseases and the BSE Crisis. Science (80-. ). 278: 245–251.

3. Zahn, R., A. Liu, T. Lührs, R. Riek, C. von Schroetter, F.L. García, M. Billeter, L. Calzolai, G. Wider, and K. Wüthrich. 2000. NMR solution structure of the human prion protein. Proc. Natl. Acad. Sci. 97: 145–150.

4. Riek, R., S. Hornemann, G. Wider, R. Glockshuber, and K. Wüthrich. 1997. NMR characterization of the full-length recombinant murine prion protein, mPrP(23-231). FEBS Lett. 413: 282–8.

5. Donne, D.G., J.H. Viles, D. Groth, I. Mehlhorn, T.L. James, F.E. Cohen, S.B. Prusiner, P.E. Wright, and H.J. Dyson. 1997. Structure of the recombinant full-length hamster prion protein PrP(29-231): the N terminus is highly flexible. Proc. Natl. Acad. Sci. U. S. A. 94: 13452–7.

6. Zahn, R., C. von Schroetter, and K. Wüthrich. 1997. Human prion proteins expressed in Escherichia coli and purified by high-affinity column refolding. FEBS Lett. 417: 400–4.

7. Walter, E.D., D.J. Stevens, A.R. Spevacek, M.P. Visconte, A. Dei Rossi, and G.L. Millhauser. 2009. Copper binding extrinsic to the octarepeat region in the prion protein. Curr. Protein Pept. Sci. 10: 529–35.

8. Herms, J., T. Tings, S. Gall, A. Madlung, A. Giese, H. Siebert, P. Schürmann, O. Windl, N. Brose, and H. Kretzschmar. 1999. Evidence of presynaptic location and function of the prion protein. J. Neurosci. 19: 8866–75.

9. Steele, A.D., S. Lindquist, and A. Aguzzi. The prion protein knockout mouse: a phenotype under challenge. Prion. 1: 83–93.

10. Millhauser, G.L. 2007. Copper and the prion protein: methods, structures, function, and disease. Annu. Rev. Phys. Chem. 58: 299–320.

11. Solomon, I.H., N. Khatri, E. Biasini, T. Massignan, J.E. Huettner, and D.A. Harris. 2011. An N-terminal polybasic domain and cell surface localization are required for mutant prion protein toxicity. J. Biol. Chem. 286: 14724–14736.

12. Biasini, E., J.A. Turnbaugh, U. Unterberger, and D.A. Harris. 2012. Prion protein at the crossroads of physiology and disease. Trends Neurosci.

13. Biasini, E., U. Unterberger, I.H. Solomon, T. Massignan, A. Senatore, H. Bian, T. Voigtlaender, F.P. Bowman, V. Bonetto, R. Chiesa, J. Luebke, P. Toselli, and D.A. Harris. 2013. A Mutant Prion Protein Sensitizes Neurons to Glutamate-Induced Excitotoxicity. J. Neurosci. 33: 2408–2418.

14. Walter, E.D., D.J. Stevens, M.P. Visconte, and G.L. Millhauser. 2007. The prion protein is a combined zinc and copper binding protein: Zn2+ alters the distribution of Cu2+ coordination modes. J. Am. Chem. Soc. 129: 15440–15441.

15. Pushie, M.J., K.H. Nienaber, A. McDonald, G.L. Millhauser, and G.N. George. 2014. Combined EXAFS and DFT structure calculations provide structural insights into the 1:1 multi-histidine complexes of Cu(II) , Cu(I) , and Zn(II) with the tandem octarepeats of the mammalian prion protein. Chemistry. 20: 9770–83.

16. Stellato, F., V. Minicozzi, G.L. Millhauser, M. Pascucci, O. Proux, G.C. Rossi, A. Spevacek, and S. Morante. 2014. Copper–zinc cross-modulation in prion protein binding. Eur. Biophys. J. 43: 631–642.

17. Chattopadhyay, M., E.D. Walter, D.J. Newell, P.J. Jackson, E. Aronoff-Spencer, J. Peisach, G.J. Gerfen, B. Bennett, W.E. Antholine, and G.L. Millhauser. 2005. The Octarepeat Domain of the Prion Protein Binds Cu(II) with Three Distinct Coordination Modes at pH 7.4. J. Am. Chem. Soc. 127: 12647–12656.

18. Pushie, M.J., I.J. Pickering, G.R. Martin, S. Tsutsui, F.R. Jirik, and G.N. George. 2011. Prion protein expression level alters regional copper, iron and zinc content in the mouse brain. Metallomics. 3: 206.

19. Solomon, I.H., E. Biasini, and D.A. Harris. Ion channels induced by the prion protein Mediators of neurotoxicity. Prion. 61: 40–45.

20. Baumann, F., M. Tolnay, C. Brabeck, J. Pahnke, U. Kloz, H.H. Niemann, M. Heikenwalder, T. Rülicke, A. Bürkle, and A. Aguzzi. 2007. Lethal recessive myelin toxicity of prion protein lacking its central domain. EMBO J. 26: 538–547.

21. Li, A., H.M. Christensen, L.R. Stewart, K. a Roth, R. Chiesa, and D. a Harris. 2007. Neonatal lethality in transgenic mice expressing prion protein with a deletion of residues 105-125. EMBO J. 26: 548–58.

22. Shmerling, D., I. Hegyi, M. Fischer, T. Blättler, S. Brandner, J. Götz, T. Rülicke, E. Flechsig, A. Cozzio, C. von Mering, C. Hangartner, A. Aguzzi, and C. Weissmann. 1998. Expression of amino-terminally truncated PrP in the mouse leading to ataxia and specific cerebellar lesions. Cell. 93: 203–14.

23. Weissmann, C., M. Fischer, A. Raeber, H. Büeler, A. Sailer, D. Shmerling, T. Rülicke, S. Brandner, and A. Aguzzi. 1998. The use of transgenic mice in the investigation of transmissible spongiform encephalopathies. Rev. Sci. Tech. 17: 278–90.

24. Solomon, I.H., N. Khatri, E. Biasini, T. Massignan, J.E. Huettner, and D.A. Harris. 2011. An N-terminal Polybasic Domain and Cell Surface Localization Are Required for Mutant Prion Protein Toxicity .

25. Solomon, I.H., J.E. Huettner, and D.A. Harris. 2010. Neurotoxic mutants of the prion protein induce spontaneous ionic currents in cultured cells. J. Biol. Chem. 285: 26719–26726.

26. Biasini, E., U. Unterberger, I.H. Solomon, T. Massignan, A. Senatore, H. Bian, T. Voigtlaender, F.P. Bowman, V. Bonetto, R. Chiesa, J. Luebke, P. Toselli, and D. a Harris. 2013. A mutant prion protein sensitizes neurons to glutamate-induced excitotoxicity. J. Neurosci. 33: 2408–18.

27. Wu, B., A.J. McDonald, K. Markham, C.B. Rich, K.P. McHugh, J. Tatzelt, D.W. Colby, G.L. Millhauser, and D.A. Harris. 2017. The N-terminus of the prion protein is a toxic effector regulated by the C-terminus. Elife. 6.

28. McDonald, A.J., B. Wu, and D.A. Harris. 2017. An inter-domain regulatory mechanism controls toxic activities of PrP $^{C}$. Prion. : 1–10.

29. Spevacek, A.R., E.G.B. Evans, J.L. Miller, H.C. Meyer, J.G. Pelton, and G.L. Millhauser. 2013. Zinc Drives a Tertiary Fold in the Prion Protein with Familial Disease Mutation Sites at the Interface. Structure. 21: 236–246.

30. Evans, E.G.B., M.J. Pushie, K.A. Markham, H.-W. Lee, and G.L. Millhauser. 2016. Interaction between Prion Protein's Copper-Bound Octarepeat Domain and a Charged C-Terminal Pocket Suggests a Mechanism for N-Terminal Regulation. Structure. 24: 1057–1067.

31. Evans, E.G.B., and G.L. Millhauser. 2017. Copper- and Zinc-Promoted Interdomain Structure in the Prion Protein: A Mechanism for Autoinhibition of the Neurotoxic N-Terminus. . pp. 35–56.

32. Clifford-Nunn, B., H.D.H. Showalter, and P.C. Andrews. 2012. Quaternary Diamines as Mass Spectrometry Cleavable Crosslinkers for Protein Interactions. J. Am. Soc. Mass Spectrom. 23: 201–212.

33. Mead, S. 2006. Prion disease genetics. Eur. J. Hum. Genet. 14: 273–281.

34. Minikel, E.V., S.M. Vallabh, M. Lek, K. Estrada, K.E. Samocha, J.F. Sathirapongsasuti, C.Y. McLean, J.Y. Tung, L.P.C. Yu, P. Gambetti, J. Blevins, S. Zhang, Y. Cohen, W. Chen, M. Yamada, T. Hamaguchi, N. Sanjo, H. Mizusawa, Y. Nakamura, T. Kitamoto, S.J. Collins, A. Boyd, R.G. Will, R. Knight, C. Ponto, I. Zerr, T.F.J. Kraus, S. Eigenbrod, A. Giese, M. Calero, J. de Pedro-Cuesta, S. Haïk, J.-L. Laplanche, E. Bouaziz-Amar, J.-P. Brandel, S. Capellari, P. Parchi, A. Poleggi, A. Ladogana, A.H. O'Donnell-Luria, K.J. Karczewski, J.L. Marshall, M. Boehnke, M. Laakso, K.L. Mohlke, A. Kähler, K. Chambert, S. McCarroll, P.F. Sullivan, C.M. Hultman, S.M. Purcell, P. Sklar, S.J. van der Lee, A. Rozemuller, C. Jansen, A. Hofman, R. Kraaij, J.G.J. van Rooij, M.A. Ikram, A.G. Uitterlinden, C.M. van Duijn, M.J. Daly, D.G. MacArthur, and D.G. MacArthur. 2016. Quantifying prion disease penetrance using large population control cohorts. Sci. Transl. Med. 8: 322ra9-322ra9.

35. Evans, E.G.B., M.J. Pushie, K.A. Markham, H.-W. Lee, and G.L. Millhauser. 2016. Interaction between Prion Protein's Copper-Bound Octarepeat Domain and a Charged C-Terminal Pocket Suggests a Mechanism for N-Terminal Regulation. Structure. 24: 1057–67.

36. Evans, E.G.B., and G.L. Millhauser. 2017. Copper- and Zinc-Promoted Interdomain Structure in the Prion Protein: A Mechanism for Autoinhibition of the Neurotoxic N-Terminus. In: Progress in molecular biology and translational science. . pp. 35–56.

37. Evans, E.G.B., M.J. Pushie, K.A. Markham, H.-W. Lee, and G.L. Millhauser. 2016. Interaction between Prion Protein's Copper-Bound Octarepeat Domain

and a Charged C-Terminal Pocket Suggests a Mechanism for N-Terminal Regulation. Structure. 24: 1057–67.

38. Narayanan, S.P., D.G. Nair, D. Schaal, M.B. De Aguiar, S. Wenzel, W. Kremer, S. Schwarzinger, and H.R. Kalbitzer. 2016. Structural transitions in full-length human prion protein detected by xenon as probe and spin labeling of the N-terminal domain. Nat. Publ. Gr. 6: 1–17.

39. Taylor, D.R., and N.M. Hooper. 2007. The low-density lipoprotein receptor-related protein 1 (LRP1) mediates the endocytosis of the cellular prion protein. Biochem. J. 402: 17–23.

40. Khosravani, H., Y. Zhang, S. Tsutsui, S. Hameed, C. Altier, J. Hamid, L. Chen, M. Villemaire, Z. Ali, F.R. Jirik, and G.W. Zamponi. 2008. Prion protein attenuates excitotoxicity by inhibiting NMDA receptors. J. Cell Biol. 181: 551–565.

41. Watt, N.T., D.R. Taylor, T.L. Kerrigan, H.H. Griffiths, J. V Rushworth, I.J. Whitehouse, and N.M. Hooper. 2012. Prion protein facilitates uptake of zinc into neuronal cells. Nat. Commun. 3: 1134.

42. Slapšak, U., G. Salzano, L. Amin, R.N.N. Abskharon, G. Ilc, B. Zupančič, I. Biljan, J. Plavec, G. Giachin, and G. Legname. 2016. The N Terminus of the Prion Protein Mediates Functional Interactions with the Neuronal Cell Adhesion Molecule (NCAM) Fibronectin Domain. J. Biol. Chem. 291: 21857–21868.

43. Aronoff-Spencer, E., C.S. Burns, N.I. Avdievich, G.J. Gerfen, J. Peisach, W.E. Antholine, H.L. Ball, F.E. Cohen, S.B. Prusiner, and G.L. Millhauser. 2000. Identification of the Cu2+ binding sites in the N-terminal domain of the prion protein by EPR and CD spectroscopy. Biochemistry. 39: 13760–71.

44. Westergard, L., J.A. Turnbaugh, and D.A. Harris. 2011. A nine amino acid domain is essential for mutant prion protein toxicity. J. Neurosci. 31: 14005–17.

45. Brody, A.H., and S.M. Strittmatter. 2018. Synaptotoxic Signaling by Amyloid Beta Oligomers in Alzheimer's Disease Through Prion Protein and mGluR5. In: Advances in pharmacology (San Diego, Calif.). . pp. 293–323.

46. De Cecco, E., and G. Legname. 2018. The role of the prion protein in the internalization of α-synuclein amyloids. Prion. 12: 23–27.

47. Kardos, J., I. Kovács, F. Hajós, M. Kálmán, and M. Simonyi. 1989. Nerve endings from rat brain tissue release copper upon depolarization. A possible role in regulating neuronal excitability. Neurosci. Lett. 103: 139–44.

48. Zamaraev, A. V., G.S. Kopeina, E.A. Prokhorova, B. Zhivotovsky, and I.N. Lavrik. 2017. Post-translational Modification of Caspases: The Other Side of Apoptosis Regulation. Trends Cell Biol. 27: 322–339.

49. Kay, L.E. 2005. NMR studies of protein structure and dynamics. J. Magn. Reson. 173: 193–207.

50. Venditti, V., V. Tugarinov, C.D. Schwieters, A. Grishaev, and G.M. Clore. 2015. Large interdomain rearrangement triggered by suppression of micro- to millisecond dynamics in bacterial Enzyme I. Nat. Commun. 6: 5960.

**CHAPTER 3**

# Molecular Features of the $Zn^{2+}$ Binding Site in the Prion Protein Probed by $^{113}Cd$ NMR

Kate A. Markham[1], Richard B. Linsley[1], Hsiau-Wei Lee[1], and Glenn L. Millhauser[1*]

[1] Department of Chemistry and Biochemistry, University of California, Santa Cruz, Santa
Cruz, CA 95064, USA

[*] Corresponding Author: glennm@ucsc.edu

**Abstract**

The cellular prion protein ($PrP^C$) is a zinc binding protein that contributes to the regulation of $Zn^{2+}$ and other divalent species of the central nervous system. $Zn^{2+}$ coordinates to the flexible, N-terminal repeat region of $PrP^C$ and drives a tertiary contact between this repeat region and a well-defined cleft of the C-terminal domain. The tertiary structure promoted by $Zn^{2+}$ is thought to regulate inherent $PrP^C$ toxicity. Despite the emerging consensus regarding the interaction between $Zn^{2+}$ and $PrP^C$, there is little direct spectroscopic confirmation of the metal ion's coordination details. Here we address this conceptual gap by using $Cd^{2+}$ as a surrogate for $Zn^{2+}$. NMR finds that $Cd^{2+}$ binds exclusively to the His imidazole side chains of the repeat segment, with a dissociation constant of approximately 1.2 mM, and promotes an N-terminal—C-terminal *cis* interaction very similar to that observed with $Zn^{2+}$. Analysis of $^{113}Cd$ NMR spectra of $PrP^C$, along with relevant control proteins and peptides, suggests that coordination of $Cd^{2+}$ in the full-length protein is consistent with a planar, four-His geometry. Examination of the mutation E199K in mouse $PrP^C$ (E200K in humans), responsible for inherited Creutzfeldt-Jakob disease, finds that the mutation lowers $Cd^{2+}$ affinity and weakens the metal ion-promoted *cis* interaction. These findings not only provide deeper insight into $PrP^C$ metal ion coordination, they also suggest new perspectives on the role of familial mutations in prion disease.

**Introduction**

Transmissible Spongiform Encephalopathies (TSEs), also known as prion diseases, are a class of fatal neurodegenerative diseases for which there is no cure or treatment (1) . Examples of prion diseases are Kuru and Creutzfeldt-Jakob (CJD)

in humans, scrapie in sheep, chronic wasting disease in cervids and mad cow disease(2) . Prion diseases originate from genetic, sporadic, or infectious routes and involve misfolding of the predominately helical cellular prion protein ($PrP^{C}$) to the beta sheet rich scrapie form ($PrP^{SC}$)(2) . Similar to Alzheimer's disease, sporadic disease accounts for the majority prion cases in humans.

$PrP^{C}$ is expressed throughout the body but appears to be concentrated primarily at pre- and post-synaptic neuronal membranes(3–5). The precise physiological function of $PrP^{C}$ is largely unknown, however, the protein's well documented ability to coordinate $Cu^{2+}$ and $Zn^{2+}$ suggests a role in metal ion homeostasis (6–10). Structurally, mature, human $PrP^{C}$ is a 208 amino acid protein with two N-linked glycans and a glycophosphatidylinositol (GPI) moiety that anchors the protein to the extracellular membrane surface. The protein has two distinct domains: the C-terminal domain (residues 126-230) composed of three alpha helices, two short antiparallel beta strands, and a disulfide bond linking helices two and three, and the N-terminal domain (residues 23-125), a flexible segment that coordinates both $Cu^{2+}$ and $Zn^{2+}$ *in vivo* (7, 11–14).

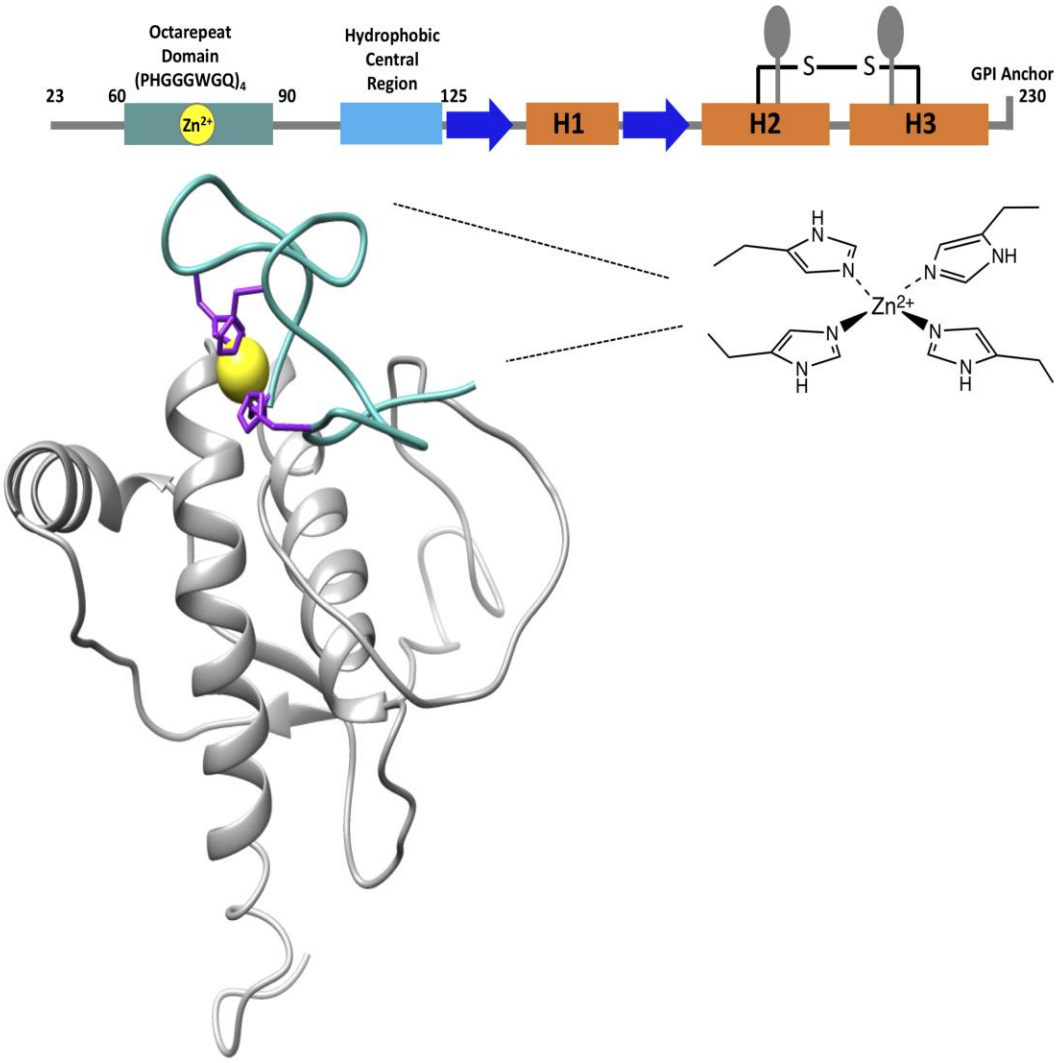


**Figure 20: Sequence and Structural Model of Mouse $PrP^C$-$Zn^{2+}$ Complex**
**A) Linear sequence diagram of $PrP^C$(23-230) (mouse sequence) with numbering indicating important N-terminal segments, along with secondary structure and post translational modifications of the folded C-terminal domain. Coloring shows the octarepeat (OR) domain (light green) that coordinates $Zn^{2+}$, beta sheets (blue), helices (orange), disulfide bond linking helices two and three and GPI anchor at residue 230. B) Three-dimensional ribbon model of $PrP^C$ with $Zn^{2+}$ coordinated to the octarepeat domain His residues and docked against a C-terminal cleft formed by helices 1-3 (15).**

$Zn^{2+}$ is the most abundant trace metal in the brain with roles in diverse functions, including structural support in certain transcription factors, as catalytic

elements in zinc metalloenzymes and as an abundant counter ion in presynaptic glutamate vesicles(14, 16). Glutamate release results in a synaptic [$Zn^{2+}$] spike and recent findings suggest that $Zn^{2+}$ binding to $PrP^C$ stimulates $Zn^{2+}$ transport back into neurons through AMPA receptors, thereby restoring normal synaptic metal ion concentrations (16). Our lab demonstrated previously that $Zn^{2+}$ binds to a $PrP^C$ N-terminal segment composed of the sequence $(PHGGGWGQ)_4$ (residues 60-91 in human $PrP^C$), termed the octarepeat (OR) domain, with a dissociation constant ($K_d$) of approximately 200 μM (Figure 20)(13). This OR segment is essential for $Zn^{2+}$ binding and subsequent transport of the ion through AMPA receptors.

Although once thought to be non-interacting, we recently demonstrated that $PrP^C$'s N-terminal and C-terminal domains have an important interdomain interaction driven by the addition of physiologic metal ions (6, 7, 17) . Evidence for this *cis* interaction came from detailed double electron-electron resonance (DEER) EPR and $^1H$-$^{15}N$ HSQC NMR. Specifically, Spevacek et al. (17) demonstrated that the addition of $Zn^{2+}$ drives the N-terminal OR to make a direct contact with a negatively charged patch on C-terminal surface composed of residues from helices two and three, as well as the N-terminal end of the $\beta1$-$\alpha1$ loop extending to the beginning of helix 1. Interestingly, a significant number of pathological mutations responsible for inherited prion disease reside on this surface and those tested systematically weakened the observed *cis* interaction (17). Therefore, it was hypothesized that $PrP^C$'s *cis* interaction plays a role in regulating the prion protein, with a decrease in this *cis* interaction promoting prion-mediated toxicity.

In addition to $Zn^{2+}$, $Cu^{2+}$ also drives a *cis* interaction, as shown by Evans et al.(6). This was demonstrated using paramagnetic relaxation enhancement (PRE)

NMR and Double Electron-Electron Resonance (DEER) Electron Paramagnetic Resonance (EPR). PRE-broadening of $PrP^C$ $^1H$-$^{15}N$ HSQC NMR cross peaks with 1.0 equivalent of $Cu^{2+}$ localized the *cis* interaction to the same C-terminal $PrP^C$ surface identified in the $Zn^{2+}$ studies. The specific location of the $Cu^{2+}$ ion was further refined using DEER EPR, along with trilateration calculation(6). These structural data suggest that physiologically relevent metal ions are essential for stabilizing higher order structure in $PrP^C$. Recent monoclonal antibody (mAb) and electrophysiology experiments underscore the importance of this newly discovered *cis* interaction (18). These experiments show consistently that the $PrP^C$ C-terminal domain regulates the othwerwise toxic N-terminal executive domain. Using mutagenesis and select $PrP^C$ constructs, we have provided strong evidence that this regulatory function requires the $Zn^{2+}$/$Cu^{2+}$-promoted *cis* interaction identified by our magnetic resonance experiments(6, 7, 17–19).

$Cu^{2+}$ is a paramagnetic species, which enables EPR experiments for assessing details of the metal ion's coordination environment. Using EPR with 1.0 eq. of $Cu^{2+}$, we showed that the copper ion is bound to the four imidazole side chains of the OR histidines (9). This coordination environment is preserved in both the OR domain alone, when expressed as a polypeptide, as well as in the full-length protein. This information was essential in developing a structural model of $Cu^{2+}$-occupied $PrP^C$.

Unlike $Cu^{2+}$, there is no convenient magnetic resonance method for probing the coordination environment of $Zn^{2+}$. However, given the essential role of $Zn^{2+}$ in $PrP^C$ physiology, as evidenced by the ion's ability to trigger divalent ion transport through the AMPA receptor (16), it is very important to evaluate the precise details

of how this physiologic ion coordinates within the prion protein. We have shown previously with indirect methods such as mass spectrometry mapping applied to OR peptides that, much like $Cu^{2+}$, $Zn^{2+}$ binds to the OR through imidazole coordination (13). However, this has yet to be demonstrated in the full-length prion protein. As such, it is unclear whether $Zn^{2+}$ remains confined solely by the histidine residues of the OR segment or, alternatively, forms a direct bond to the C-terminal residue side chains.

To investigate the molecular details, we report here the application of $^{113}Cd$ NMR spectroscopy to probe $Zn^{2+}$ coordination in $PrP^{C}$. $Cd^{2+}$, like $Zn^{2+}$, is a transition metal in group 12 of the periodic table, and therefore forms a stable divalent ion with a diamagnetic $d^{10}$ configuration(20). Being separated by just one period, the ionic radii of $Cd^{2+}$ and $Zn^{2+}$ are similar at 0.98 Å and 0.74 Å, respectively (20). As demonstrated in the context of other proteins, $Cd^{2+}$ is an excellent $Zn^{2+}$ surrogate recapitulating zinc's coordination properties (21). For example, the zinc metalloenzymes carbonic anhydrase B and C were studied using $^{113}Cd$ NMR spectroscopy (22, 23). The enzymes retained activity with $Cd^{2+}$ at the catalytic center and analysis of the $^{113}Cd$ NMR spectra distinguished between competing coordination models by identifying an exchangeable water molecule at the active site (24).

Cd has two spin ½ isotopes – $^{111}Cd$ and $^{113}Cd$. Of these, $^{113}Cd$ is somewhat more sensitive and thus more desirable for NMR studies(25). $^{113}Cd$ NMR offers several advantages for probing metal ion binding sites(24, 26, 27). $^{113}Cd$ NMR signals are spread over a remarkably wide chemical shift range, approximately 900 ppm, with specific resonances sensitive to coordination geometry and specific

coordinating atoms (25). $^{113}$Cd chemical shifts are predictable with deshielding following S > N > O (28–30). Consequently, $^{113}$Cd NMR provides a sensitive probe for assessing the metal ion coordination environment. Although $^{113}$Cd is a low sensitivity nucleus, enrichment to 94.8% (natural abundance of $^{113}$Cd is 12.26%) allows for acquisition of high quality spectra in approximately 12 hours using a broad band probe on an $^{1}$H 500 MHz instrument (corresponding to a $^{113}$Cd resonance frequency of approximately 111 MHz)(31). Finally, because of the uniqueness of $^{113}$Cd, spectra are devoid of background signals.

In this study, we use $^{1}$H-$^{15}$N NSQC NMR to compare the interactions of $Zn^{2+}$ and $Cd^{2+}$ with $PrP^{C}$. Titration studies and $^{2}J_{NH}$ couplings from HSQC experiments are used to assess the $Cd^{2+}$-$PrP^{C}$ dissociation constant(32, 33). Next, using $^{113}$Cd NMR, we compare binding in the isolated OR domain and in the full-length protein. Finally, we evaluate several $PrP^{C}$ mutants relevant to prion toxicity and disease. Together, these data provide a more refined view of $Cd^{2+}$, and hence $Zn^{2+}$, binding in $PrP^{C}$.

**Results**

Cadmium Induces a *cis* Interaction Between $PrP^{C}$ N-terminal and C-terminal Domains

Previous $^{1}$H-$^{15}$N HSQC NMR experiments performed on uniformly $^{15}$N-labeled $PrP^{C}$ with one to three equivalents of $Zn^{2+}$ identified a collection of C-terminal residues that exhibited both linewidth broadening and/or changes in chemical shift of select cross peaks. The affected residues, when mapped to the 3D structure of C-terminal domain of $PrP^{C}$, identified a shallow cavity localized primarily to a surface patch composed of adjacent sides of helices 2 and 3 (α2 and α3), along

with the residues corresponding to the β1-α1 loop. When combined with EPR DEER experiments and suitable controls, these NMR data demonstrated that the $Zn^{2+}$-OR segment docks to a well-defined, negatively-charged patch on the $PrP^C$ C-terminal domain (Fig. 20) (17). Divalent Zn is diamagnetic; we therefore attributed changes in the lineshapes and chemical shifts of the affected C-terminal residues to intermediate exchange molecular dynamics at the interface between the interacting N-terminal and C-terminal domains. To confirm the use of $Cd^{2+}$ as a viable $Zn^{2+}$ surrogate, we performed parallel $^1H$-$^{15}N$ HSQC NMR experiments at 25°C on $^{15}N$-labeled wild type MoPrP(23-230) (300 μM) in the presence of 1 mM $Cd^{2+}$ (added as $CdCl_2$) at pH 6.0 and pH 7.0.

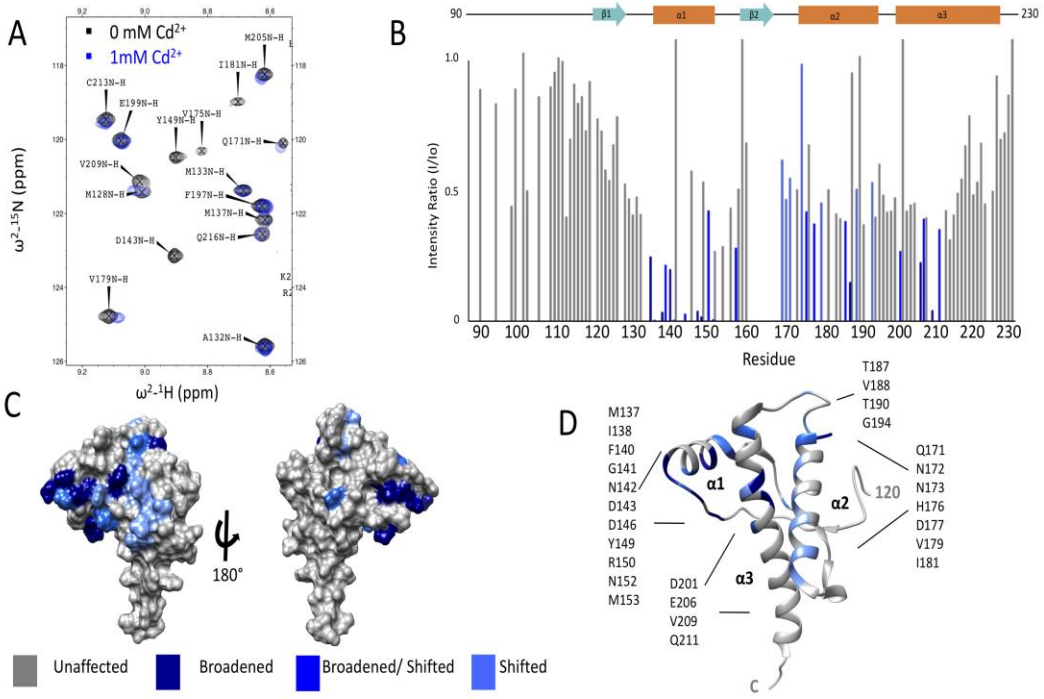


**Figure 21: $Cd^{2+}$ Promotes an Interdomain Interaction Wild Type MoPrP at pH6.0 A) Selected Region of the $^1H$-$^{15}N$ HSQC of wild type MoPrP in the absence of metal (black) and in the presence of 1mM of $Cd^{2+}$ (blue). B) Bar graph of $I/I_o$ for residues 90-23 of $PrP^C$ in the presence of $Cd^{2+}$. C) and D) Surface and ribbon plots, respectively, of C-terminal residues affected by the presence of $Cd^{2+}$**

**(coordinates from PDB:1XYX). Affected residues are noted specifically on the ribbon diagram**

Figure 21A shows a segment of the 800 MHz $^{1}H$-$^{15}N$ HSQC NMR spectrum. As with $Zn^{2+}$, we find that select cross peaks exhibit changes in linewidth and chemical shift(17). To evaluate these spectral changes, intensity ratios ($I/I_0$) were calculated for all assigned C-terminal resonances. These ratios are obtained by dividing the cross-peak intensity in the presence of $Cd^{2+}$ by the intensity of the cross-peak before addition of $Cd^{2+}$. The average and standard deviation of the $I/I_0$ values were calculated, and standard Z-score analysis(6) was performed to determine a threshold residues broadened more than 1 STD from the mean by the presence of $Cd^{2+}$. In addition, cross-peaks exhibiting changes in chemical shift greater than 0.1 ppm were deemed to be significantly affected by the addition of $Cd^{2+}$. The results are summarized in Fig. 21B, which shows $I/I_0$ vs residue position for the C-terminal domain. Affected residue cross-peaks exceeding statistical significance are noted by dark blue ($I/I_0$ exceeding one standard deviation from the mean), medium blue ($I/I_0$ greater than 0.5 standard deviation with a chemical shift greater than 0.1 ppm), and in light blue (0.1 ppm or greater change in chemical shift)(6, 37). When plotted onto surface (Fig. 21C) or ribbon (Fig. 21D) diagrams, the data identify a patch of affected residues similar to those observed by the addition of $Zn^{2+}$. Specifically, the $Cd^{2+}$ caused either broadening, shifting or broadening+shifting of proximal residues on α2, α3, and the ß1-α1 loop. The 27 affected residues are all proximal to each other and, of these, 12 are equivalent to those affected by $Zn^{2+}$ (Supporting Information). Spectra acquired at pH 6.0 and 7.0 gave similar results, however, for experiments that follow, we standardized on

the lower pH value as it was found to give narrower $^{113}Cd$ lineshapes (see below, Figure 26). Given that neither $Zn^{2+}$ or $Cd^{2+}$ bind directly PrP(90-230), these results show that, like $Zn^{2+}$, $Cd^{2+}$ drives a well-defined *cis* interaction between the $PrP^C$ $Cd^{2+}$-occupied N-terminal domain and the shallow cavity of the C-terminal domain.

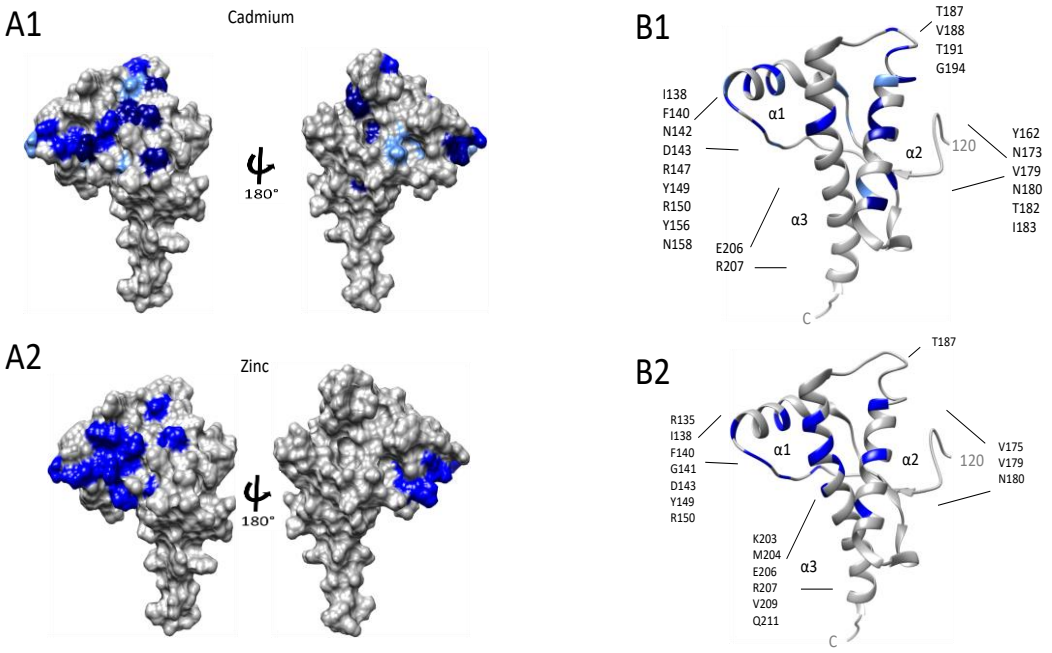


**Figure 22: $Zn^{2+}$ and $Cd^{2+}$ Promoted cis Interaction Wild-Type MoPrP is Localized to the Same C-terminal Surface. Both samples were run with 300μM protein in a buffer containing 10mM MES (Sigma), 10% $D_2O$, at pH 7.0 for solubility purposes. Subsequent to the addition of 500μM $ZnCl_2$ or 1mM $CdCl_2$, the pH was measured and adjusted, if necessary. Residues that are broadened (dark blue), broadened+shifted (medium blue), and shifted (light blue) in the presence of the respective metal ion are indicated in the surface diagrams, A1 and A2, and ribbon diagrams, B1 and B2. Coordinates for the C-terminal $PrP^C$ structure are from PDB:1XYX.**

<u>$Cd^{2+}$ Coordinates to Imidazole Groups of Octarepeat Histidines</u>

We previously used chemical mapping to show that $Zn^{2+}$ coordinates specifically to His imidazole residues in the PrP OR segment with a dissociation constant of approximately 200 μM (10). To examine $Cd^{2+}$ coordination details and

measure its binding affinity, we applied $^{1}H$-$^{15}N$ HSQC with pulse sequence modifications to highlight $^{2}J_{NH}$ scalar couplings (32). With this pulse sequence, His side chains give characteristic patterns depending on the protonation state of the imidazole ring. Spectra of full-length $PrP^{C}$ and PrP(23-125), both in the absence of $Cd^{2+}$, are compared in Figure 23. $PrP^{C}$ contains nine His residues, six of which are in the flexible region 23-125. Examination of Fig. 23 shows that Hε1 cross-peaks with $^{1}H$ chemical shifts above 8.1 ppm are readily assigned to this N-terminal segment. In addition, prominence of the specific cross-peak pattern of Nδ1-Hε1, Nε2-Hε1, Nε2-Hδ2 for each imidazole is consistent with protonation of the ε2 nitrogen of the imidazole ring. Three separate patterns are observed for PrP(23-125) with approximate volume ratios of 4:1:1. We therefore assigned the four OR His residues to more intense set cross-peaks.

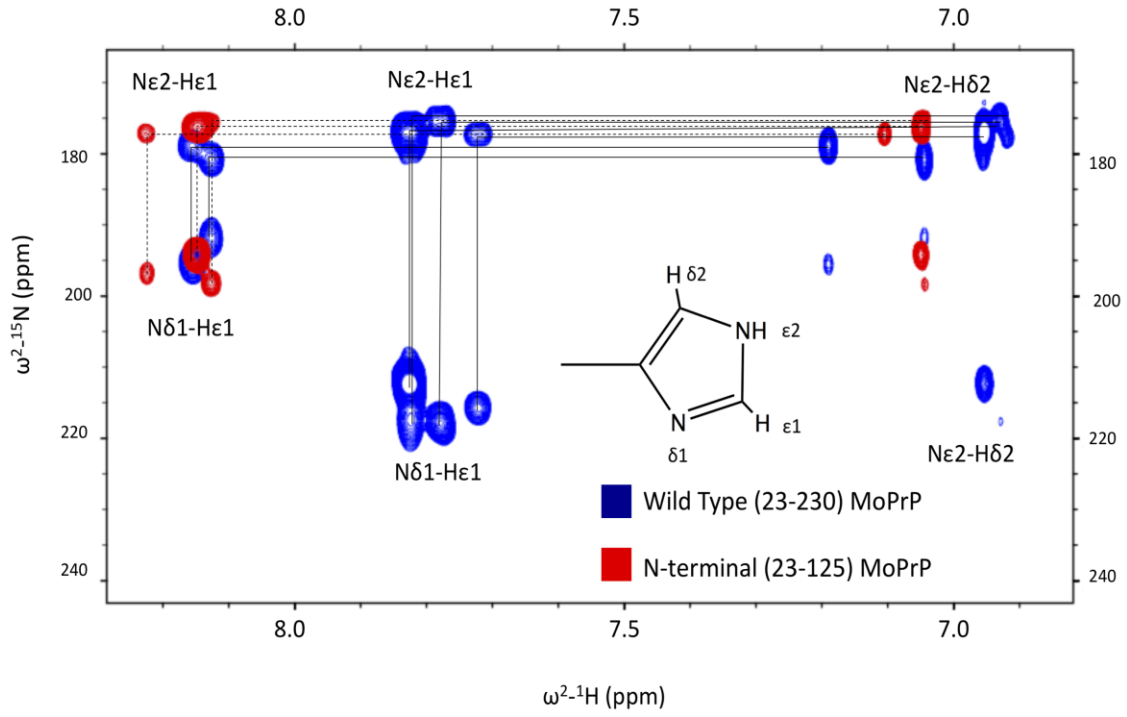


***Figure 23: $^{2}J_{NH}$-HSQC of $^{15}N$-Labeled N-terminal PrP and $PrP^{C}$***

***$^{1}H$-$^{15}N$-HSQC spectra with pulse sequence modified to highlight $^{2}J_{NH}$ couplings showing the imidazole region of the spectrum for PrP(23-125) (red, correlated cross peaks connected by dashed lines) and full-length MoPrP (blue, peaks connected by solid lines). The pattern of connections from Nδ1-Hε1 → Nε2-Hε1 → Nε2-Hδ2 is characteristic of the protonation at Nε2.***

Next, we added increasing concentrations of $Cd^{2+}$ to a solution of 300 μM PrP(23-125) and observed a progressive chemical shift changes of the Nε2-Hε1 and Nε2-Hδ2 cross-peaks, assigned to the OR His residues (Fig. 24). The peaks exhibited only slight broadening with increasing [$Cd^{2+}$], consistent with fast exchange. These data suggest that $Cd^{2+}$ coordinates preferentially to the ε2 nitrogen, perhaps displacing the exchangeable proton. Plotting the Nε2 chemical shifts derived from the Nε2-Hε1 and Nε2-Hδ2 cross-peaks gave saturable binding curves, which we fit independently to a standard model for equilibrium fast-exchange (37).

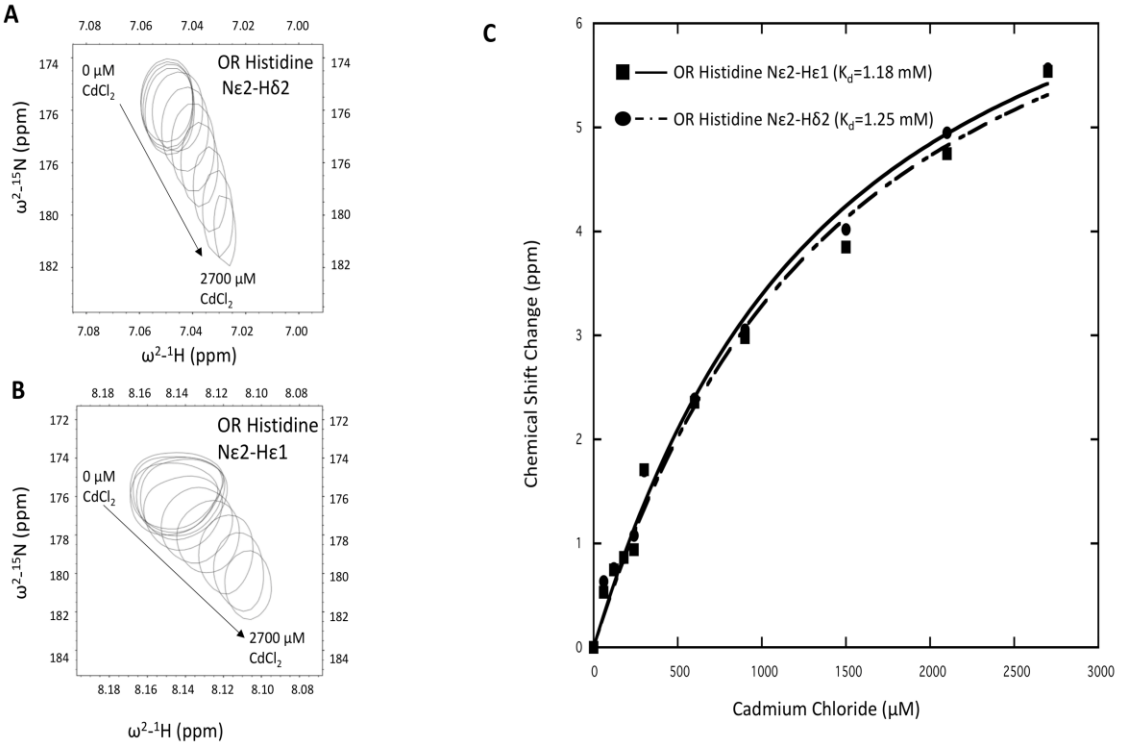


**Figure 24: Determination of $K_d$ from $^{2}J_{NH}$ HSQC Chemical Shifts vs $Cd^{2+}$**

**A) Nε2-Hδ2 and B) Nε2-Hε1 $^{2}J_{NH}$ HSQC cross peak shifts of $N^{15}$-labeled MoPrP(23-125) as a function of added cadmium chloride. C) Plot of $^{15}N$ chemical shift change vs $CdCl_2$. Data were fitted to $K_d$ the expression derived for fast chemical exchange (Material and Methods) to determine binding constant for $Cd^{2+}$ to the OR domain (Table 1). Resulting Kd values derived from the Nε2-Hδ2 and Nε2-Hε1 cross peaks are approximately 1254 μM and 1187 μM, respectively.**

Both curves gave similar results with an approximate $K_d$ of 1.2 mM. We also attempted titration with full-length $PrP^C$, however, the relevant $^{2}J_{NH}$ cross-peaks exhibited significant broadening, likely due to intermediate exchange, and were therefore not amenable to fast exchange binding analysis. Taken together, these NMR experiments demonstrate that $Cd^{2+}$, like $Zn^{2+}$, binds to the OR His residues but with an approximate six-fold reduction in affinity.

**Table 1: Dissociation Constants for Octarepeat Histidine Epsilon Nitrogen**
**Top is OR Histidine Nε2-Hε1 and bottom is OR Histidine Nε2-Hδ2**

| | Kd (μM) | Error (μM) |
|---|---|---|
| OR Histidine Nε2-Hε1 | 1187 | +/- 200.89 |
| OR Histidine Nε2-Hδ2 | 1253.8 | +/- 245.34 |

<u>$^{113}Cd$ NMR of Wild-Type $PrP^C$ and Relevant Mutants</u>

With the goal of assessing the $Cd^{2+}$ coordination environment, we carried out direct NMR measurements on $^{113}Cd$ combined with $PrP^C$ and various relevant constructs. With an 11.7 T magnetic field (500 MHz for $^{1}H$), the $^{113}Cd$ resonance frequency is 110.9 MHz (31). All spectra were referenced to the chemical shift of 0.10 M $Cd(ClO_4)_2$ (aq), which places the chemical shift of aquo $^{113}Cd$ at zero ppm

(31). Given the low gyromagnetic ratio of $^{113}Cd$, it was essential to adjust sample conditions to give the best possible spectra. Consequently, we prepared peptides and proteins to concentrations of 300 μM, which is near the $PrP^C$ solubility limit, along with 1.0 mM $^{113}CdCl_2$. Under these conditions, a spectrometer fitted with a cryoprobe was capable of acquiring resolvable spectra in eight to twelve hours.

Resulting spectra are shown in Fig. 26. As shown in the insert, nitrogen coordination leads to deshielding of the $^{113}Cd$ center, with concomitant resonances of higher chemical shift values. Oxygen coordination produces resonance signals of lower chemical shifts (25). The differences between nitrogen and oxygen coordination are reflected in the comparison of imidazole (175 ppm) and EDTA (108 ppm).

All peptide and protein samples gave only a single resonance line consistent with fast exchange between the coordinated species and free $Cd^{2+}$ in buffered solution, as seen with the $^1H$-$^{15}N$ HSQC above (Figure 21). A peptide containing the isolated OR segment (KKRPKP-PrP(56-90)-$NH_2$) produces a single line with a $^{113}Cd$ chemical shift close to that of imidazole, consistent with our findings above that $Cd^{2+}$ coordinates primarily through His side chains. Full-length murine $PrP^C$ (MoPrP) is further deshielded relative to the isolated OR by approximately 5 ppm. Consequently, either the *cis* interaction described above further stabilizes OR-$Cd^{2+}$ coordination or the $Cd^{2+}$ coordination shell is additionally enhanced by C-terminal His residues. To test for this latter case, we prepared PrP(H139Y, H176Y), which replaces two C-terminal His residues at the $Cd^{2+}$-OR docking interface, specifically, H139 on the ß1-α1 loop and H176 on α2. The resulting $^{113}Cd$ spectrum is equivalent to that of wild-type $PrP^C$ suggesting that either $Cd^{2+}$ remains fully confined by

coordination to the OR His residues or that one or two of the C-terminal His residues replace OR His residues thereby maintaining a four-His coordination environment.

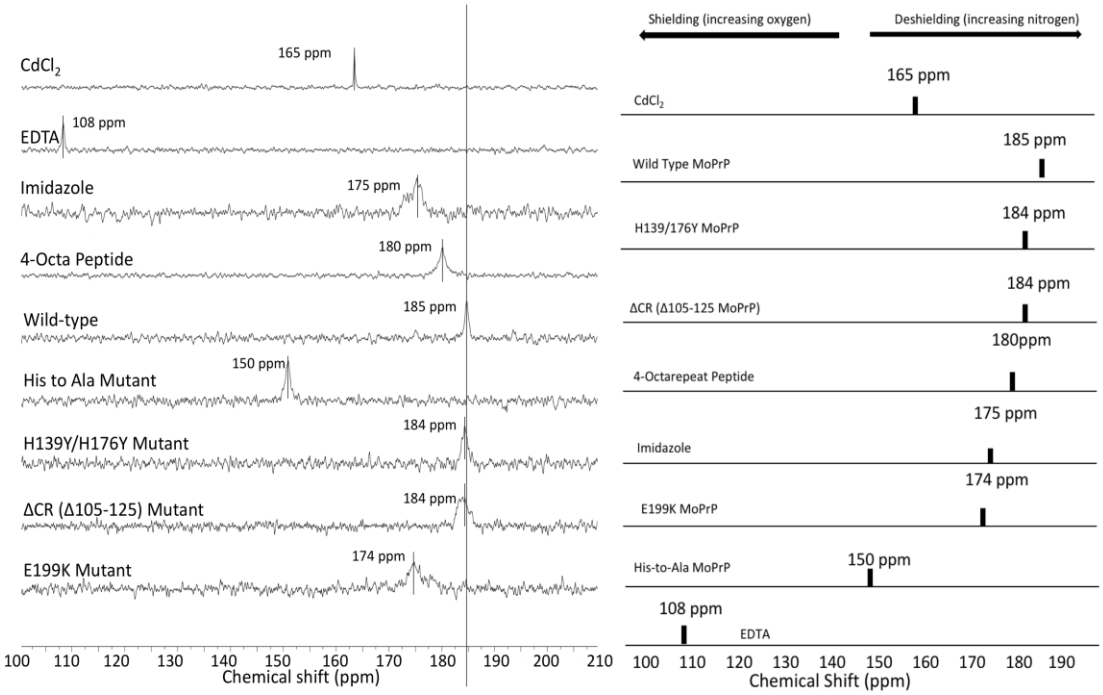


**Figure 25: $^{113}Cd$ NMR Spectra of Controls, Octarepeat Segment, Full-Length $PrP^C$ and Relevant Mutants Left) $^{113}Cd$ NMR spectra with chemical shifts referenced against to 0.1 M $Cd(ClO_4)_2$ (aq). Spectra for the OR peptide and all proteins were acquired with 300 μM peptide/protein and 1.0 mM $^{113}Cd^{2+}$. The vertical line is drawn as a reference against wild-type protein. Right) A stick diagram of the $^{113}Cd$ NMR spectra ordered by chemical shift from high to low (with reference $CdCl_2$ at the top). As noted at the top, nitrogen coordination decreases chemical shielding, leading to higher chemical shift values, while oxygen coordination shifts in the opposite direction**

To directly test the involvement of $Cd^{2+}$ binding to the flexible N-terminal $PrP^C$ domain, we prepared a mutant in which all OR His residues, His95 and His110 were mutated to Ala. This construct shows a strong shift towards a more shielded $^{113}Cd$ signal of approximately 35 ppm, close to that of $CdCl_2$ in aqueous solution. We therefore conclude that indeed the N-terminal segment provides the primary

coordination environment for $Cd^{2+}$ with a four-His coordination shell, as previously found for $Zn^{2+}$.

The fast exchange conditions observed for $^{113}Cd$ provide an opportunity to estimate the chemical shift of the $PrP^C$-$^{113}Cd^{2+}$ species. Under fast exchange, the observed signal is a weighted average of the free and fully $PrP^C$ bound $^{113}Cd$ chemical shifts. Using a $K_d$ = 1.2 mM, [$PrP^C$] = 300 μM and [$Cd^{2+}$] = 1.0 mM, we calculate that the concentration of the bound $PrP^C$-$Cd^{2+}$ species is 126 μM, or 12.6% of the total $^{113}Cd^{2+}$ in solution. Given the free $^{113}Cd^{2+}$ signal of 165 ppm (from $CdCl_2$), and exchanged average signal of 185 ppm, the fully bound species is determined to be approximate 318 ppm. This value aligns well with published data of other four-N coordination environments such as myoglobin and superoxide dismutase (SOD), both of which coordinate $Cd^{2+}$ with a square planar environment(38–40).

Next, we evaluated two important mutants than link directly to prion disease. ΔCR $PrP^C$ is a designed deletion mutant in which residues 105-125, corresponding to the Central Region, are eliminated. Surprisingly, loss of this 21-residue segment between the OR and globular C-terminal domain drives severe cerebellar degeneration and neonatal lethality in laboratory mice(41). Electrophysiological experiments performed on cells transfected with the ΔCR $PrP^C$ gene show spontaneous cationic currents associated with the early stages of prion disease (42, 43). In culture, these currents are inhibited by the addition of $Cu^{2+}$, which binds with high affinity to the OR (18). Similar to $Zn^{2+}$, $Cu^{2+}$ drives a *cis* interaction and previous work from our lab showed a loss of this copper promoted interaction in ΔCR $PrP^C$. Fig. 25 shows that ΔCR $PrP^C$ gives a $^{113}Cd$ spectrum

approximately equivalent to that of wild-type $PrP^C$. Consequently, there is no loss of $Cd^{2+}$ coordination in ΔCR $PrP^C$, however, we cannot rule out a potential loss of the metal ion promoted cis interaction.

Finally, we examined murine $PrP^C$(E199K), a mutation that corresponds to familial E200K in humans (44, 45). Families that carry this fully penetrant E200K mutation develop mid-life CJD (46). Spevacek et al. demonstrated that the E199K mutation exhibits a weakened *cis* interaction, relative to wild-type, upon the addition of $Zn^{2+}$(17). They postulated that, because E199 is located on the N-terminal end of helix 3 contributing to a large concentration of negatively charge C-terminal residues, the mutation to a Lys confers toxicity by reducing the localized negative charge thereby weakening electrostatic contributions to the *cis* interaction(17). The $^{113}Cd$ spectrum of $PrP^C$(E199K) shows a significant shift relative to that obtained from wild-type $PrP^C$, with a chemical shift reflecting a partial loss of nitrogen coordination. Consistent with the findings of Spevacek et al. these data suggest partial release of the metal ion(17).

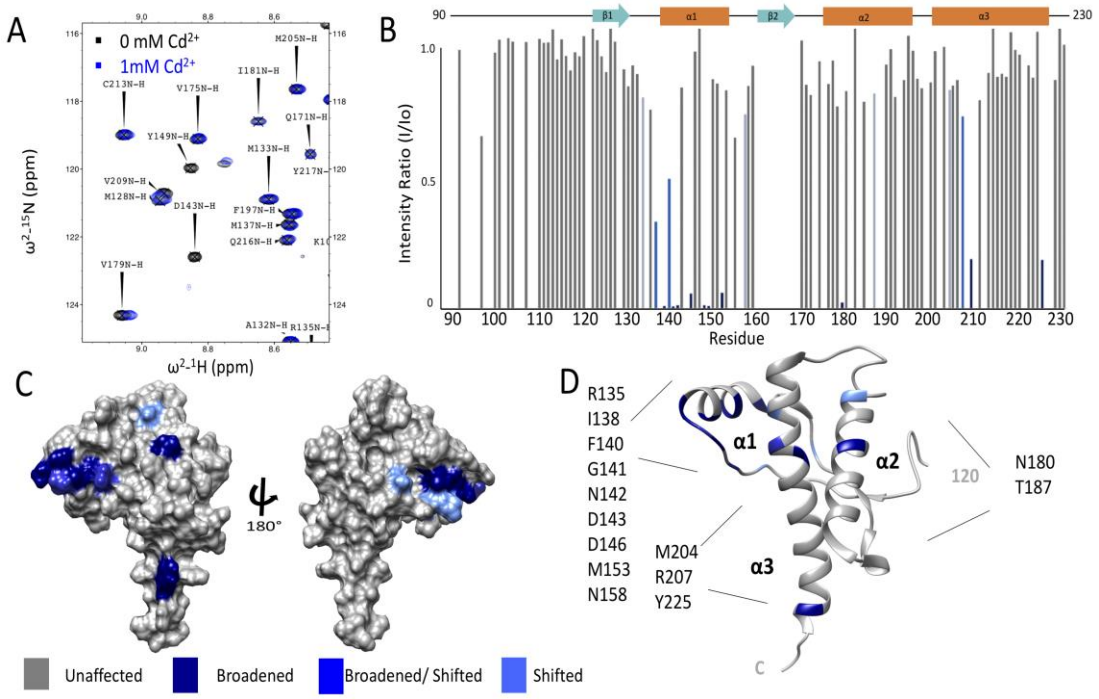


**Figure 26: $Cd^{2+}$ Promoted Interdomain Interaction $PrP^C$(E199K) is Significantly Weakened Relative to Wild-Type. The $PrP^C$ mutation E200K (E199K in mouse) correlates with the human prion disease CJD. A) Selected region of the $^1H$-$^{15}N$ HSQC of wild type MoPrP in the absence of metal (black) and in the presence of 1mM of $Cd^{2+}$ (blue). B) Bar graph of $I/I_o$ for residues 90-23 of $PrP^C$ in the presence of $Cd^{2+}$. C) and D) Surface and ribbon plots, respectively, of C-terminal residues affected by the presence of $Cd^{2+}$ (coordinates from PDB:1XYX). Affected residues are noted specifically on the ribbon diagram.**

To further explore the consequence of the E199K mutation, we performed $^{15}N$-$^1H$ HSQC NMR in the presence of 1.0 mM $CdCl_2$. Figure 26 shows that the E199K mutation significantly weakens the observed *cis* interaction relative to wild-type, similar to our previous observations with $Zn^{2+}$. The majority of the remaining broadened residues are localized to helix 1; lineshape broadening of cross-peaks from residues at the respective N-termini of helices 2 and 3 is much less pronounced. These data suggest that electrostatic repulsion between the Lys

residue at position 199 and $Cd^{2+}$ lowers reduces affinity for the metal ion with concomitant loss of the interdomain *cis* interaction.

**Discussion**

$PrP^C$ is a $Zn^{2+}$ binding protein, and emerging evidence suggests that uptake of this essential metal ion of the CNS drives an intramolecular *cis* interaction that is critical for regulating $PrP^C$ function and arresting inherent toxicity. Previous to this current study, we used chemical mapping performed on an OR peptide to suggest that $Zn^{2+}$ coordinates exclusively to OR His side chain imidazole groups(13). Here we used $Cd^{2+}$ as a $Zn^{2+}$ surrogate to more carefully investigate the metal ion coordination features and the resulting *cis* interaction. As with $Zn^{2+}$, $^1H$-$^{15}N$ HSQC NMR experiments show that the binding of $Cd^{2+}$ to the N-terminal OR segment of $PrP^C$ leads to broadening of select C-terminal residues located to a shallow, negatively-charged cleft formed primarily by three α-helices. Next, we used a modified $^1H$-$^{15}N$ HSQC NMR sequence that selects for $^2J_{NH}$ scalar couplings to assess the $Cd^{2+}$-$PrP^C$ dissociation constant, in turn establishing optimal conditions for $^{113}Cd$ NMR studies (25, 32, 33). Finally, $^{113}Cd$ NMR studies allowed us to compare $Cd^{2+}$ complexation features among the isolated OR, the full-length $PrP^C$ protein, as well as important mutants.

Given the remarkable chemical shift sensitivity of $^{113}Cd$, the agreement between the isolated OR and the full-length protein provides strong evidence that the OR alone is responsible for $Cd^{2+}$ uptake(25). Consistent with this proposal, elimination of N-terminal His residues leads to a significant change in $^{113}Cd$ chemical shift. Moreover, analysis of the fast exchange signal finds a calculated

chemical shift of the $Cd^{2+}$-$PrP^C$ species to be consistent with coordination by four nitrogen atoms in a planar configuration (37, 47). Together, these findings firmly support our previous proposal that $PrP^C$ takes up $Cd^{2+}$ with four-His coordination in the repeat domain.

Following our chemical mapping studies (13), several EXAFS and related X-ray studies investigated $Zn^{2+}$ coordination to $PrP^C$ (48, 49). Stellato et al. probed the competition between $Zn^{2+}$ and $Cu^{2+}$ coordination and showed that, at low $Cu^{2+}$ occupancy, $Zn^{2+}$ partially displaces His side chains from the copper centers (50). In a separate study, this group found that $Zn^{2+}$ does not fully coordinate to all OR His residues but, instead, may facilitate OR peptide clustering(49). Given that this work was performed exclusively on OR peptides, it is not clear whether this type of metal ion-assisted cross-linking applies to full-length $PrP^C$. Pushie et al. (48) combined Density Functional Theory (DFT) and EXAFS to carefully examine $Zn^{2+}$ occupation of the OR. Interestingly, their calculations found little energy difference between $Zn^{2+}$ coordinated to three imidazole groups and a single water vs $Zn^{2+}$ coordinated to four imidazoles. This finding was supported by analysis of the EXAFS data, which was well fit with a model of only three imidazole groups (48). Although our findings here suggest four-His coordination, this is determined by extrapolation from the fast exchange signal and comparison of the estimated chemical shift to that of know four-His $Zn^{2+}$ complexes. As such, our result is an approximation and therefore cannot rule out a coordination environment of three-His and one water.

A surprising finding of our study is the dramatic change in chemical shift associated with the E199K mutation. In humans, the parallel E200K mutation

potently confers familial CJD (46, 51). Residue 200 is located near the N-terminal end of α3 so it is therefore reasonable to hypothesize that this mutation destabilizes the protein thereby promoting aggregation(6). However, biophysical studies with NMR and Circular Dichroism find that $PrP^C$(E200K) maintains the same fold and stability as the wild-type protein (17, 52, 53). Residue E200 contributes to a highly conserved, negatively charged electrostatic patch on the $PrP^C$ C-terminal domain(17). In our previous investigations with $PrP^C$-$Zn^{2+}$ binding, we noted that all C-terminal disease promoting mutations involving acidic or basic residues result in a reduction of the patch's negative charge character. Using $^1H$-$^{15}N$ HSQC NMR, we directly tested the influence of the Glu→Lys mutation and found a significant loss of the $Zn^{2+}$ promoted *cis* interaction, especially in the vicinity of α3 (17). This finding led to the proposal of a new paradigm for understanding the E200K and related mutations in which alteration of the protein's electrostatics results in a weakening of the regulatory *cis* interaction. Our findings here take this concept further by suggesting a loss of metal ion affinity. Specifically, the dramatic change in $^{113}Cd$ chemical shift found for $MoPrP^C$(E199K) is consistent with a loss of nitrogen coordination likely arising from an equilibrium shift to the free $Cd^{2+}$ species.

In summary, $^{113}Cd$ NMR has provided new and important insights into metal ion coordination in the prion protein. Our studies continue to support the concept of an interdomain *cis* interaction promoted by coordination of $Zn^{2+}$ to the OR; mutations that weaken this interaction correlate with inherited prion disease. This concept may prove useful in the continued study of $PrP^C$ function and treatment of prion diseases.

**Materials and Methods**

$^{15}$N- Labeled Protein Expression

MoPrP variants were constructed using the template plasmid pJexpress 414 MoPrP (DNA 2.0) containing full-length *Mus musculus* PrP(23–230). All constructs and mutations were confirmed by DNA sequencing. Protein expression was executed in *Escherichia coli* BL21Star (DE3) (Invitrogen). For For $^{1}$H-$^{15}$N HSQC NMR experiments, $^{15}$N-labeled proteins were grown per the protocols reported by Evans et al. (6). N-terminal PrP(23-125) was produced by introducing a TEV cleavage site to remove the C-terminal (126-230) domain(34).

Peptide Synthesis

The linear peptide KKRPKPWGQPHGGGWGQPHGGSWGQPHGGSWGQPHGGGWGQ-$NH_2$, corresponding to KKRPKP-PrP(56-90)-$NH_2$, (MW= 4291.66, ε= 28450 $cm^{-1}M^{-1}$) was prepared by solid phase peptide synthesis using standard Fmoc chemistry protocols on a Liberty 1 Microwave Peptide Synthesizer (CEM). 4-octa peptide was cleaved from ChemMatrix ® Rink amide resin (Sigma Aldrich) and purified by reverse phase C18 HPLC and lyophilized for long term storage once reaching analytical purity.

Nuclear Magnetic Resonance Spectroscopy

$PrP^{C}$ and PrP-derived peptide samples for $^{1}$H-$^{15}$N NMR experiments were prepared at 300μM protein or peptide in a buffer containing 10mM MES (Sigma), 10% $D_2O$, at pH 6.0 or 7.0, depending on specific experiment. Subsequent to the addition of 1mM $CdCl_2$, the pH was measured and adjusted, if necessary. $^{1}$H-$^{15}$N HSQC spectra were recorded at 25°C on an 800-MHz spectrometer (Bruker) at UCSC

NMR facility (Santa Cruz, CA). NMR spectra were analyzed with NMR Pipe(35) and Sparky. Structural analysis was performed with Chimera(36). Protein assignments were achieved using previously determined values from Evans et al (6).

The $Cd^{2+}$ dissociation constant $K_d$ was determined from $^{1}H$-$^{15}N$-HSQC spectra using non-linear least-squares fitting to the following equation(37):

$$\Delta\delta_{obs} = \Delta\delta_{max}\{([P]_t + [L]_t + K_d) - [([P]_t + [L]_t + K_d)^2 - 4[P]_t[L]_t]^{\frac{1}{2}}\}/2[P]_t$$

where $[P]_t$ and $[L]_t$ are the total protein and ligand ($Cd^{2+}$) concentrations, respectively, and $\Delta\delta_{max}$, determined from the fitting procedure, is the difference in chemical shift between the free and fully bound protein.

For $^{113}Cd$ NMR experiments, all samples were prepared in buffer containing 10mM MES buffer (sigma), 10% $D_2O$ at pH 6.0 and 25°C, with either 300 μM protein, EDTA or 1.8 mM imidazole, and 1mM $^{113}CdCl_2$ (Cambridge Isotopes, 95% isotopically labeled). $^{113}Cd$ NMR was performed on a Bruker-500MHz spectrometer tuned to 110.9MHz. All samples were externally referenced to 0.1 M $Cd(ClO_4)_2$ (aq).

Analysis leading to the conclusion of fast exchange in the $^{113}Cd$ specta utilized the following relations:

$$P + L \underset{k_{off}}{\overset{k_{on}}{\rightleftharpoons}} P{:}L$$

$$K_d = \frac{k_{off}}{k_{on}}$$

$$k_{ex} = [P]k_{on} + k_{off}$$

$$\Delta\omega = 2\pi\Delta\delta\nu_o$$

where $\Delta\delta$ is the difference in $^{113}$Cd chemical shift between free $Cd^{2+}$ and the fully bound metal ion, and $v_o$ is the spectrometer frequency. $k_{on}$ is estimated to be diffusion controlled and approximately $10^9$ $M^{-1}s^{-1}$. With a protein concentration of 300 μM, $k_{ex}$ >> Δω thereby satisfying fast exchange consistent with a single $^{113}$Cd NMR line.

**Author Contributions**

K.A.M and G.L.M designed the experiments; K.A.M, R.B.L and H-W L. performed the experiments; K.A.M and G.L.M wrote the manuscript.

**Acknowledgements**

The authors extend their sincere gratitude to Professor Ian M. Armitage, University of Minnesota, for helpful advice on the use of $^{113}$Cd as an NMR probe of metal ion coordination centers. Also, to Graham Roseman and Kevin Schilling who generously contributed protein for $^{113}$Cd NMR studies. This work was funded by NIH instrumentation grant S10OD018455, which supported acquisition of the UC Santa Cruz 800 MHz NMR spectrometer, and NIH research grant R01GM065790 (awarded to G.L.M.).

**References**


1. Prusiner, S. 1982. Novel proteinaceous infectious particles cause scrapie. Science (80-. ). 216: 136–144.

2. Prusiner, S.B. 1997. Prion Diseases and the BSE Crisis. Science (80-. ). 278: 245–251.

3. Herms, J., T. Tings, S. Gall, A. Madlung, A. Giese, H. Siebert, P. Schürmann, O. Windl, N. Brose, and H. Kretzschmar. 1999. Evidence of presynaptic location and function of the prion protein. J. Neurosci. 19: 8866–75.

4. Steele, A.D., S. Lindquist, and A. Aguzzi. The prion protein knockout mouse: a phenotype under challenge. Prion. 1: 83–93.

5. Millhauser, G.L. 2007. Copper and the Prion Protein: Methods, Structures, Function, and Disease. Annu. Rev. Phys. Chem. 58: 299–320.

6. Evans, E.G.B., M.J. Pushie, K.A. Markham, H.-W. Lee, and G.L. Millhauser. 2016. Interaction between Prion Protein's Copper-Bound Octarepeat Domain and a Charged C-Terminal Pocket Suggests a Mechanism for N-Terminal Regulation. Structure. 24: 1057–67.

7. Evans, E.G.B., and G.L. Millhauser. 2017. Copper- and Zinc-Promoted Interdomain Structure in the Prion Protein: A Mechanism for Autoinhibition of the Neurotoxic N-Terminus. . pp. 35–56.

8. Aronoff-Spencer, E., C.S. Burns, N.I. Avdievich, G.J. Gerfen, J. Peisach, W.E. Antholine, H.L. Ball, F.E. Cohen, S.B. Prusiner, and G.L. Millhauser. 2000. Identification of the Cu2+ binding sites in the N-terminal domain of the prion protein by EPR and CD spectroscopy. Biochemistry. 39: 13760–71.

9. Chattopadhyay, M., E.D. Walter, D.J. Newell, P.J. Jackson, E. Aronoff-Spencer, J. Peisach, G.J. Gerfen, B. Bennett, W.E. Antholine, and G.L. Millhauser. 2005. The Octarepeat Domain of the Prion Protein Binds Cu(II) with Three Distinct Coordination Modes at pH 7.4. J. Am. Chem. Soc. 127: 12647–12656.

10. Walter, E.D., D.J. Stevens, M.P. Visconte, and G.L. Millhauser. 2007. The prion protein is a combined zinc and copper binding protein: Zn2+ alters the distribution of Cu2+ coordination modes. J. Am. Chem. Soc. 129: 15440–1.

11. Donne, D.G., J.H. Viles, D. Groth, I. Mehlhorn, T.L. James, F.E. Cohen, S.B. Prusiner, P.E. Wright, and H.J. Dyson. 1997. Structure of the recombinant full-length hamster prion protein PrP(29-231): the N terminus is highly flexible. Proc. Natl. Acad. Sci. U. S. A. 94: 13452–7.

12. Brown, L.R., and D.A. Harris. 2003. Copper and zinc cause delivery of the prion protein from the plasma membrane to a subset of early endosomes and the Golgi.

J. Neurochem. 87: 353–63.

13. Walter, E.D., D.J. Stevens, M.P. Visconte, and G.L. Millhauser. 2007. The prion protein is a combined zinc and copper binding protein: Zn2+ alters the distribution of Cu2+ coordination modes. J. Am. Chem. Soc. 129: 15440–15441.

14. Watt, N.T., H.H. Griffiths, and N.M. Hooper. 2013. Neuronal zinc regulation and the prion protein. Prion. 7: 203–8.

15. Spevacek, A.R., E.G.B. Evans, J.L. Miller, H.C. Meyer, J.G. Pelton, and G.L. Millhauser. 2013. Zinc Drives a Tertiary Fold in the Prion Protein with Familial Disease Mutation Sites at the Interface. Structure. 21: 236–246.

16. Watt, N.T., D.R. Taylor, T.L. Kerrigan, H.H. Griffiths, J. V. Rushworth, I.J. Whitehouse, and N.M. Hooper. 2012. Prion protein facilitates uptake of zinc into neuronal cells. Nat. Commun.

17. Spevacek, A.R., E.G.B. Evans, J.L. Miller, H.C. Meyer, J.G. Pelton, and G.L. Millhauser. 2013. Zinc drives a tertiary fold in the prion protein with familial disease mutation sites at the interface. Structure. 21: 236–46.

18. Wu, B., A.J. McDonald, K. Markham, C.B. Rich, K.P. McHugh, J. Tatzelt, D.W. Colby, G.L. Millhauser, and D.A. Harris. 2017. The N-terminus of the prion protein is a toxic effector regulated by the C-terminus. Elife. 6: e23473.

19. McDonald, A.J., B. Wu, and D.A. Harris. 2017. An inter-domain regulatory mechanism controls toxic activities of PrP $^{C}$. Prion. 11: 388–397.

20. Cotton FA, W.G. 1988. Advanced Inorganic Chemistry: A Comprehensive Text. New York: Wiley.

21. Otvos, J.D., I.M. Armitage, J.F. Chlebowski, and J.E. Coleman. 1979. 31P NMR of alkaline phosphatase. Dependence of phosphate binding stoichiometry on metal ion content. J. Biol. Chem. 254: 4707–13.

22. Ian M. Armitage, R.T.P. 1976. Cadmium- 113 Fourier Transform Nuclear Magnetic Resonance of Cadmium(I1) Carbonic Anhydrases and Cadmium(I1) Alkaline Phosphatase. J. Am. Chem. Soc. . : 18.

23. Jonsson, N.B., L. a Tibell, J.L. Evelhoch, S.J. Bell, and J.L. Sudmeier. 1980. Cadmium-113 NMR of carbonic anhydrases: effect of pH, bicarbonate, and cyanide. Proc. Natl. Acad. Sci. U. S. A. 77: 3269–72.

24. Armitage, I.M., A.J.. Schoot Uiterkamp, J.F. Chlebowski, and J.E. Coleman. 1978. 113Cd NMR as a probe of the active sites of metalloenzymes. J. Magn. Reson. 29: 375–392.

25. Armitage, I.M., T. Drakenberg, and B. Reilly. 2013. Use of 113Cd NMR to Probe the Native Metal Binding Sites in Metalloproteins: An Overview. In: Metal ions in life sciences. . pp. 117–144.

26. Armitage, Ian M.; Otvos, James D.; Briggs, Richard W.; Boulanger, Y. 1982. Structure elucidation of the metal-binding sites in metallothionein by cadmium - 113 NMR. Biophys. Biochem. 13: 2974–80.

27. I. M. Armitage and Y. Boulanger. 1983. Cadmium-113 NMR. NMR New. Access. Nucl. 2: 337–365.

28. Maciel, G.E., and M. Borzo. High Resolution l13Cd Nuclear Magnetic Resonance by Pulse Fourier Transform. 19.

29. Kostelnik$, R.J., and A.A. Bothner-By. 1974. Cadmium-113 Nuclear Magnetic Resonance Studies of Cadmium(II)- Ligand Binding in Aqueous Solutions. I. The Effect of Diverse Ligands on the Cadmium-113 Chemical Shift*? J. Magn. Reson. 14: 141–51.

30. Cardin, A.D., P.D. Ellis, J.D. Odom, and J.W. Howard. 1975. Cadmium-113 Fourier transform nuclear magnetic resonance spectroscopy. J. Am. Chem. Soc. 97: 1672–1679.

31. Lambert, J.B., and F.G. Riddell. 1982. The Multinuclear approach to NMR spectroscopy. Hingham, MA: D. Reidel Publishing Company .

32. Pelton, Jeffrey G.;Torchia, D.A..;Meadow; Roseman, S. 1993. Tautomeric states of the active-site histidines of phosphorylated a signal-transducing protein and unphosphorylated from Escherichia III Glc , coli, using two-dimensional heteronuclear NMR techniques. Protein Sci. : 543–558.

33. Tettamanzi, M.C., C. Keeler, S. Meshack, and M.E. Hodsdon. 2008. Analysis of site-specific histidine protonation in human prolactin. Biochemistry. 47: 8638–47.

34. Raran-Kurussi, S., S. Cherry, D. Zhang, and D.S. Waugh. 2017. Removal of Affinity Tags with TEV Protease. In: Methods in molecular biology (Clifton, N.J.). . pp. 221–230.

35. Frank Delaglio, Stephan Grzesiek, Geerten. W. Vuister, Guang Zhu, John. Pfeifer, and A.B. 1995. NMRPiper. : 6, 277–293.

36. Pettersen EF, Goddard TD, Huang CC, Couch GS, Greenblatt DM, Meng EC, F. TE. 2004. UCSF Chimera--a visualization system for exploratory research and analysis. : (13)1605-12.

37. Williamson, M.P. 2013. Using chemical shift perturbation to characterise ligand binding. Prog. Nucl. Magn. Reson. Spectrosc. 73: 1–16.

38. Marchetti, P.S., M.A. Kennedy, P.D. Ellis, S. Bank, and T.W. Bell. 1989. Cadmium-113 NMR Spectroscopy. Long Bond Interactions and Chemical Shielding in the Cadmium Complex of an Unsaturated Nitrogen Analogue of 18-Crown-6. J. Am. Chem. Soc. .

39. Bailey, D.B., P.D. Ellis, and J.A. Fee. 1980. Cadmium-113 nuclear magnetic resonance studies of cadmium-substituted derivatives of bovine superoxide dismutase. Biochemistry. 19: 591–6.

40. Kofod ', H., R. Bauer ', E. Danielsen ', E. Larsen ', M.J. Bjerrum ', and M.J. Bjerrum. 1991. 3Cd-NMR investigation of a cadmium-substituted copper, zinc-containing superoxide dismutase from yeast. Eur. J. Biochem. 8: 607–611.

41. Li, A., H.M. Christensen, L.R. Stewart, K.A. Roth, R. Chiesa, and D.A. Harris. 2007. Neonatal lethality in transgenic mice expressing prion protein with a deletion of residues 105–125. EMBO J. 26: 548–558.

42. Solomon, I.H., N. Khatri, E. Biasini, T. Massignan, J.E. Huettner, and D.A. Harris. 2011. An N-terminal polybasic domain and cell surface localization are required for mutant prion protein toxicity. J. Biol. Chem.

43. Biasini, E., J.A. Turnbaugh, T. Massignan, P. Veglianese, G. Forloni, V. Bonetto, R. Chiesa, and D.A. Harris. 2012. The toxicity of a mutant prion protein is cell-autonomous, and can be suppressed by wild-type prion protein on adjacent cells. PLoS One.

44. Bell, J.E., and J.W. Ironside. 1993. Neuropathology of spongiform encephalopathies in humans. Br. Med. Bull. 49: 738–77.

45. Kong, Q., Surewicz, W.K., Peterson, R.B., Zou, W., Chen, S.G., Gambetti, P., Parchi, P., Capellari, S., Goldfarb, L., Montagna, P. 2008. Prion Diseases and Biology. Inherited Prion Diseases. .

46. Mead, S. 2006. Prion disease genetics. Eur. J. Hum. Genet. 14: 273–281.

47. Borsari, M., Borsari, and Marco. 2014. Cadmium: Coordination Chemistry. In: Encyclopedia of Inorganic and Bioinorganic Chemistry. Chichester, UK: John Wiley & Sons, Ltd. pp. 1–16.

48. Pushie, M.J., K.H. Nienaber, A. McDonald, G.L. Millhauser, and G.N. George. 2014. Combined EXAFS and DFT structure calculations provide structural insights into the 1:1 multi-histidine complexes of Cu(II) , Cu(I) , and Zn(II) with the tandem octarepeats of the mammalian prion protein. Chemistry. 20: 9770–83.

49. Stellato, F., V. Minicozzi, G.L. Millhauser, M. Pascucci, O. Proux, G.C. Rossi, A. Spevacek, and S. Morante. 2014. Copper–zinc cross-modulation in prion protein binding. Eur. Biophys. J. 43: 631–642.

50. Stellato, F., A. Spevacek, O. Proux, V. Minicozzi, G. Millhauser, and S. Morante. 2011. Zinc modulates copper coordination mode in prion protein octa-repeat subdomains. Eur. Biophys. J. 40: 1259–1270.

51. Minikel, E.V., S.M. Vallabh, M. Lek, K. Estrada, K.E. Samocha, J.F. Sathirapongsasuti, C.Y. McLean, J.Y. Tung, L.P.C. Yu, P. Gambetti, J. Blevins, S. Zhang, Y. Cohen, W. Chen, M. Yamada, T. Hamaguchi, N. Sanjo, H. Mizusawa, Y. Nakamura, T. Kitamoto, S.J. Collins, A. Boyd, R.G. Will, R. Knight, C. Ponto, I. Zerr, T.F.J. Kraus, S. Eigenbrod, A. Giese, M. Calero, J. de Pedro-Cuesta, S. Haïk, J.-L. Laplanche, E. Bouaziz-Amar, J.-P. Brandel, S. Capellari, P. Parchi, A. Poleggi, A. Ladogana, A.H. O'Donnell-Luria, K.J. Karczewski, J.L. Marshall, M. Boehnke, M. Laakso, K.L. Mohlke, A. Kähler, K. Chambert, S. McCarroll, P.F. Sullivan, C.M. Hultman, S.M. Purcell, P. Sklar, S.J. van der Lee, A. Rozemuller, C. Jansen, A. Hofman, R. Kraaij, J.G.J. van Rooij, M.A. Ikram, A.G. Uitterlinden, C.M. van Duijn, M.J. Daly, D.G. MacArthur, and D.G. MacArthur. 2016. Quantifying prion disease penetrance using large population control cohorts. Sci. Transl. Med. 8: 322ra9-322ra9.

52. Bae, S.-H., G. Legname, A. Serban, S.B. Prusiner, P.E. Wright, and H.J. Dyson. 2009. Prion proteins with pathogenic and protective mutations show similar structure and dynamics. Biochemistry. 48: 8120–8.

53. Liemann, S., and R. Glockshuber. 1999. Influence of amino acid substitutions related to inherited human prion diseases on the thermodynamic stability of the cellular prion protein. Biochemistry. 38: 3258–67.

# CHAPTER 4
# CONCLUSIONS

It has been well established that the prion protein is the infectious element in TSEs, however, there is still a considerable amount of debate on $PrP^C$'s endogenous function. Until recently, rigorous biophysical characterization of mature full length $PrP^C$ in the presence and absence of metal ions had been lacking. Historically, the N and C terminal domains were treated independently of each other, but our knowledge has been significantly advanced by spectroscopic studies of $PrP^C$'s $Cu^{2+}/Zn^{2+}$ driven *cis* interaction(1–3). This interdomain contact provides insight into how $PrP^C$ potentially regulates metal ion concentrations in the brain. Furthermore, these results add a deeper level of understanding to how prion disease toxicity could be transduced.

The studies conducted in this dissertation identified relevant contact points between the N- and C-terminal domains that may not have been previously captured. The use of multidimensional NMR and mass-spectrometry to characterize functionally disruptive mutations resulted in a refined molecular model of $PrP^C$'s *cis* interaction. Utilizing PRE cross-peak broadening through the addition of $Cu^{2+}$, $^1H$-$^{15}N$ HSQC NMR identified key components of the N-terminal domain essential for $PrP^C$'s *cis* interaction. The first region examined was the polybasic tail that has been implicated in physiological processes, such as the rate of scrapie conversion, ΔCR toxicity, and association with ion channels(4–7). The second region of interest was the deletion mutation Δ105-125 (ΔCR) PrP, which confers massive

neurodegeneration and neonatal lethality(10). The final region that was tested was the negatively charge surface potential of helices α2 and α3 through pathological mutation E199K. Since the N-terminal domains of these regions are both structurally and functionally relevant, we aimed to investigate the molecular details of these segments upon the addition of $Cu^{2+}$.

Deletion of the polybasic tail resulted in an almost entirely suppressed *cis* interaction, which is consistent with the hypothesis that the metal driven *cis* interaction are assisted through electrostatics(1, 3, 11). However, it was unclear if deletion of the polybasic tail weakened the *cis* interaction due to elimination of the tail or positive charge the KKRPK motif. Polybasic tail charge reversal mutation, E3D, showed diminished contacts along the well-defined cleft of the C-terminal domain; however, the effects observed were not as drastic as elimination of the polybasic tail. These results indicate that the positive charge of the poly basic tail contributes to $PrP^C$'s $Cu^{2+}$ - induced *cis* interaction (8). The central region is primarily a hydrophobic domain of alanines, glycines, and valines, and is not implicated in what drives electrostatics (13). Despite this, when ΔCR $PrP^C$ was tested by $^1H$-$^{15}N$ HSQC NMR, it was observed that ΔCR still weakened $PrP^C$'s $Cu^{2+}$ - induced *cis* interaction. This behavior could be due to the linker region being too short to physically reach the contact points or could also be due to the deletion of significant sequences. Future

experimentation to investigate the sequence pattern versus linker length would help to further define how $PrP^C$'s $Cu^{2+}$ - induced *cis* interaction is modulated by the central region.

In addition to $^1H$-$^{15}N$ HSQC NMR, LC-MS/MS was performed using a heterobifunctional cross-linker (14). These heterobifunctional cross-linking studies identified key contact points for the central region and polybasic tail to dock to the C-terminus. These data are consistent with the $^1H$-$^{15}N$ HSQC NMR results that both the central region and polybasic tail are essential components to $PrP^C$'s $Cu^{2+}$ - induced *cis* interaction. Previous biophysical characterization hypothesized that only the $Cu^{2+}/Zn^{2+}$ occupied OR domain(1, 13, 15) was involved in $PrP^C$'s *cis* interaction . However, studies reported in this dissertation have demonstrate that the cis interaction not only depends on metal coordination to the OR, but also relies on the polybasic tail and central region. These results explain how the C-terminus potentially regulates the polybasic tail and, if left unregulated, how toxicity could occur as seen in ΔCR PrP.

$PrP^C$ has been demonstrated to be essential for facilitating uptake of $Zn^{2+}$ in the CNS (9, 16).Previous studies have demonstrated that both $Cu^{2+}$ and $Zn^{2+}$ induce a *cis* interaction with $^1H$-$^{15}N$ HSQC NMR(15, 17). DEER EPR studies along with trilateration calculations located $Cu^{2+}$'s position on $PrP^C$'s C-terminal domain, thereby providing information about the *cis* interaction from the metal ion's perspective (15). Since $Zn^{2+}$ is diamagnetic, EPR is not

an applicable method to spectroscopically investigate the molecular details of its coordination environment. Instead $^{113}Cd$ NMR is utilized to biophysically characterize the $Zn^{2+}$ ion coordination environment with $Cd^{2+}$ being used as a surrogate(18). Using $^{1}H$-$^{15}N$ HSQC NMR, we demonstrated that $Cd^{2+}$ induced a *cis* interaction along the C-terminal negatively charged cleft that also was previously identified with $Zn^{2+}$(1). Further characterization using $^{2}J_{NH}$ HSQC NMR(19, 20) localized $Cd^{2+}$ to the most distal nitrogen of the four histidine imidazole rings within the OR (21–23). Additionally, titrating $CdCl_2$ allowed us to determine the approximate affinity of $Cd^{2+}$ to the OR (24). These results demonstrated that $Cd^{2+}$ was a viable surrogate for $Zn^{2+}$, and thus provided a solid foundation for the use of $^{113}Cd$ NMR.

$^{113}Cd$ NMR is a powerful tool because of its 900 ppm chemical shift scale, which allows for measurement of subtle changes in $Cd^{2+}$'s coordination environment (25). The use of $^{113}Cd$ NMR provided the molecular details for $Zn^{2+}$'s metal coordination sphere, which had not been previously measured. When compared with $N_4$ square planar coordinated superoxide dismutase, the chemical shifts observed with wild-type $PrP^{C}$ are consistent with $Cd^{2+}$ coordination to nitrogen ligands (26). Our results demonstrated that $Cd^{2+}$ chemical shifts were able to distinguish between $Cd^{2+}$ -OR and $Cd^{2+}$ -wild type, resulting from $PrP^{C}$'s *cis* interaction. Furthermore, pathological mutation, E199K (mouse numbering) has been

documented to have a weakened *cis* interaction(27), and the $^{113}Cd$ chemical shifts are consistent with those reports. Specifically, the $^{113}Cd$ chemical shift found for $MoPrP^{C}$(E199K) is substantially shielded in the uncoordinated $Cd^{2+}$ species direction, which is consistent with a loss of nitrogen coordination.

This study establishes $^{113}Cd$ NMR as a spectroscopic technique that is sensitive enough to measure changes in $Cd^{2+}$'s coordination environment. This powerful tool used in tandem with $^{1}H$-$^{15}N$ HSQC NMR furthers our understanding of $Zn^{2+}$'s coordination environment and resulting *cis* interaction. With a variety of biophysical techniques, we are able to establish a path of how toxicity is transduced. Once we establish how $PrP^{C}$ transmits toxicity, we can then start developing highly targeted therapeutics to help treat prion diseases.

References


1. Spevacek, A.R., E.G.B. Evans, J.L. Miller, H.C. Meyer, J.G. Pelton, and G.L. Millhauser. 2013. Zinc drives a tertiary fold in the prion protein with familial disease mutation sites at the interface. Structure. 21: 236–246.

2. Evans, E.G.B., M.J. Pushie, K.A. Markham, H.-W. Lee, and G.L. Millhauser. 2016. Interaction between Prion Protein's Copper-Bound Octarepeat Domain and a Charged C-Terminal Pocket Suggests a Mechanism for N-Terminal Regulation. Structure. 24: 1057–1067.

3. Evans, E.G.B., and G.L. Millhauser. 2017. Copper- and Zinc-Promoted Interdomain Structure in the Prion Protein: A Mechanism for Autoinhibition of the Neurotoxic N-Terminus. . pp. 35–56.

4. Watt, N.T., D.R. Taylor, T.L. Kerrigan, H.H. Griffiths, J. V. Rushworth, I.J. Whitehouse, and N.M. Hooper. 2012. Prion protein facilitates uptake of zinc

into neuronal cells. Nat. Commun. 3: 1134.

5. Watt, N.T., H.H. Griffiths, and N.M. Hooper. 2013. Neuronal zinc regulation and the prion protein. Prion. 7: 203–8.

6. Westergard, L., J.A. Turnbaugh, and D.A. Harris. 2011. A nine amino acid domain is essential for mutant prion protein toxicity. J. Neurosci. 31: 14005–17.

7. Solomon, I.H., N. Khatri, E. Biasini, T. Massignan, J.E. Huettner, and D.A. Harris. 2011. An N-terminal polybasic domain and cell surface localization are required for mutant prion protein toxicity. J. Biol. Chem.

8. Wu, B., A.J. McDonald, K. Markham, C.B. Rich, K.P. McHugh, J. Tatzelt, D.W. Colby, G.L. Millhauser, and D.A. Harris. 2017. The N-terminus of the prion protein is a toxic effector regulated by the C-terminus. Elife. 6.

9. Biasini, E., J.A. Turnbaugh, T. Massignan, P. Veglianese, G. Forloni, V. Bonetto, R. Chiesa, and D.A. Harris. 2012. The toxicity of a mutant prion protein is cell-autonomous, and can be suppressed by wild-type prion protein on adjacent cells. PLoS One.

10. Li, A., H.M. Christensen, L.R. Stewart, K.A. Roth, R. Chiesa, and D.A. Harris. 2007. Neonatal lethality in transgenic mice expressing prion protein with a deletion of residues 105–125. EMBO J. 26: 548–558.
11. Evans, E.G.B., M.J. Pushie, K.A. Markham, H.-W. Lee, and G.L. Millhauser. 2016. Interaction between Prion Protein's Copper-Bound Octarepeat Domain and a Charged C-Terminal Pocket Suggests a Mechanism for N-Terminal Regulation. Structure. 24: 1057–67.
12. McDonald, A.J., B. Wu, and D.A. Harris. 2017. An Inter-Domain Regulatory Mechanism Controls Toxic Activities of PrP $^{C}$. Prion. : 00–00.

13. Zahn, R., A. Liu, T. Lührs, R. Riek, C. von Schroetter, F.L. García, M. Billeter, L. Calzolai, G. Wider, and K. Wüthrich. 2000. NMR solution structure of the human prion protein. Proc. Natl. Acad. Sci. 97: 145–150.

14. Clifford-Nunn, B., H.D.H. Showalter, and P.C. Andrews. 2012. Quaternary Diamines as Mass Spectrometry Cleavable Crosslinkers for Protein Interactions. J. Am. Soc. Mass Spectrom. 23: 201–212.

15. Evans, E.G.B., M.J. Pushie, K.A. Markham, H.-W. Lee, and G.L. Millhauser. 2016. Interaction between Prion Protein's Copper-Bound Octarepeat Domain and a Charged C-Terminal Pocket Suggests a Mechanism for N-Terminal

Regulation. Structure. 24: 1057–67.

16. Watt, N.T., D.R. Taylor, T.L. Kerrigan, H.H. Griffiths, J. V Rushworth, I.J. Whitehouse, and N.M. Hooper. 2012. Prion protein facilitates uptake of zinc into neuronal cells. Nat. Commun. 3: 1134.

17. Spevacek, A.R., E.G.B. Evans, J.L. Miller, H.C. Meyer, J.G. Pelton, and G.L. Millhauser. 2013. Article Zinc Drives a Tertiary Fold in the Prion Protein with Familial Disease Mutation Sites at the Interface. 111: 236–246.

18. Bailey, D.B., P.D. Ellis, and J.A. Fee. 1980. Cadmium-113 nuclear magnetic resonance studies of cadmium-substituted derivatives of bovine superoxide dismutase. Biochemistry. 19: 591–6.

19. Pelton, Jeffrey G.;Torchia, D.A..;Meadow; Roseman, S. 1993. Tautomeric states of the active-site histidines of phosphorylated a signal-transducing protein and unphosphorylated from Escherichia III Glc , coli, using two-dimensional heteronuclear NMR techniques. Protein Sci. : 543–558.

20. Tettamanzi, M.C., C. Keeler, S. Meshack, and M.E. Hodsdon. 2008. Analysis of site-specific histidine protonation in human prolactin. Biochemistry. 47: 8638–47.

21. Walter, E.D., D.J. Stevens, M.P. Visconte, and G.L. Millhauser. 2007. The prion protein is a combined zinc and copper binding protein: Zn2+ alters the distribution of Cu2+ coordination modes. J. Am. Chem. Soc. 129: 15440–1.

22. Pushie, M.J., K.H. Nienaber, A. McDonald, G.L. Millhauser, and G.N. George. 2014. Combined EXAFS and DFT structure calculations provide structural insights into the 1:1 multi-histidine complexes of Cu(II) , Cu(I) , and Zn(II) with the tandem octarepeats of the mammalian prion protein. Chemistry. 20: 9770–83.

23. Stellato, F., V. Minicozzi, G.L. Millhauser, M. Pascucci, O. Proux, G.C. Rossi, A. Spevacek, and S. Morante. 2014. Copper–zinc cross-modulation in prion protein binding. Eur. Biophys. J. 43: 631–642.

24. Williamson, M.P. 2013. Using chemical shift perturbation to characterise ligand binding. Prog. Nucl. Magn. Reson. Spectrosc. 73: 1–16.

25. Armitage, I.M., T. Drakenberg, and B. Reilly. 2013. Use of 113Cd NMR to Probe the Native Metal Binding Sites in Metalloproteins: An Overview. In: Metal ions in life sciences. . pp. 117–144.

26. Kofod, P., R. Bauer, E. Danielsen, E. Larsen, and M.J. Bjerrum. 1991. 113Cd-NMR investigation of a cadmium-substituted copper, zinc-containing superoxide dismutase from yeast. Eur. J. Biochem. 198: 607–11.

27. Spevacek, A.R., E.G.B. Evans, J.L. Miller, H.C. Meyer, J.G. Pelton, and G.L. Millhauser. 2013. Zinc Drives a Tertiary Fold in the Prion Protein with Familial Disease Mutation Sites at the Interface. Structure. 21: 236–246.